University of Groningen

Dynamics and observational signatures from multi-field inflation

Christodoulidis, Perseas

DOI:
10.33612/diss.173751374

IMPORTANT NOTE: You are advised to consult the publisher's version (publisher's PDF) if you wish to cite from it. Please check the document version below.

Document Version
Publisher's PDF, also known as Version of record

Publication date:
2021

Link to publication in University of Groningen/UMCG research database

Dynamics and observational signatures from multi-field inflation

Perseas Christodoulidis

Front cover and bookmark: Three snapshots of the universe: the inflationary stage (caused by a scalar field as it slowly rolls down the slope of its potential), the generation of the Cosmic Microwave Background radiation (as we observe it today) and the late-time observable universe (consisting of e.g. galaxies, stars and planets).

Cover and bookmark realized by Peggy Rapti.

Printed by Ipskamp Printing, The Netherlands.

Dynamics and observational signatures from multi-field inflation

PhD thesis

to obtain the degree of PhD at the
University of Groningen
on the authority of the
Rector Magnificus Prof. C. Wijmenga
and in accordance with
the decision by the College of Deans.

This thesis will be defended in public on

Friday 9 July 2021 at 9.00 hours

by

Perseas Christodoulidis

born on 14 February 1991
in Athens, Greece

Supervisors
Prof. D. Roest
Prof. E. A. Bergshoeff

Assessment committee
Prof. A. Mazumdar
Prof. A. Achúcarro
Prof. D. Wands

Contents

1
Introduction

This chapter offers a non-technical introduction to modern cosmology with emphasis on the cosmological milestones of the last century. We also provide an outline of the thesis and set the notation.

1.1   From ancient times to the era of relativity

Where do we come from? How was the world created? Is the age of the universe finite or is it infinitely old? Since the dawn of civilization, humankind has been preoccupied with these questions and several individuals have attempted to answer them in the context of theology and philosophy. As early as in Mesopotamian, Rigveda and Babylonian scripts, one finds people's beliefs of the universe consisting of a flat earth surrounded by an ocean [1]. Later, with the progression of astronomical observations the Earth started to be depicted as a sphere with stars and planets revolving around it. The heliocentric universe of Aristarchus was the first qualitatively correct model for our solar system, that was abandoned a few centuries later in favour of a geocentric system by e.g. Aristoteles and Ptolemy, only to be established again by N. Copernicus, in a more sophisticated version, during the renaissance [2–5]. J. Bruno pushed that idea further by postulating that our solar system is one of infinitely many similar systems in the universe [6]. In a similar spirit, I. Kant argued that nebulae in the night sky were separated "island universes" that extended beyond the Milky Way [7].

In the meantime, many different theories have been proposed for the beginning and evolution of the universe. In the 18$^{\text{th}}$ century H. W. Olbers proposed the "night sky paradox", an argument that disfavours an infinitely large and old universe [8, 9]. It is formulated as follows: if the universe extends indefinitely in space, then it will be populated by infinitely many stars and the total luminosity would be infinite; the night sky should be bright instead. Though many resolutions have been proposed without requiring a beginning for the universe, the simplest explanation is that the universe is finitely old and thus the light from distant stars has not reached us yet, explaining why the night sky is dark. These arguments became more solid after the introduction of general relativity by A. Einstein in 1916. Studying the dynamics of the new theory for a universe with only usual forms of matter and energy (such as atoms and photons) but without any preferred point or direction A. Friedmann derived the first cosmological model [10]. Using these equations G. Lemaître showed that they yield a universe with a beginning [11] that comes into existence from a singularity, dubbed the *Big Bang*.[1]

---

[1]The presence of the singularity implies that general relativity can not be applied arbitrarily close to the beginning of time and a complete theory of quantum gravity is necessary to investigate how the universe came into existence.

1.2   Expansion of the Universe

Around 1920, a "Great Debate" took place amongst astronomers regarding the size of the universe [12]. On one side, astronomers such as H. Shapley argued for a small universe of the size of the Milky Way, while the opposing side represented by H. Curtis claimed that distant nebulae were distinct galaxies located at large distances from Earth. The debate was finally settled by E. Hubble in 1927 [13]. Analysing data from stars with variable luminosity, known as Cepheid stars, of what appeared to be distant nebula enabled him to perform a cosmic distance calibration, that is a way to measure distances of distant objects. Those objects were shown to lie outside of our galaxy and therefore settled the Great Debate. Combining the previous results with redshift measurements of various galaxies led to his famous law relating distance to velocity. This relation had already been proposed by G. Lemaître as a solution of an expanding universe. Distant galaxies appeared to recede from us with a velocity proportional to their distance which implied that the universe is expanding.

A few decades later, A. Penzias and R. Wilson accidentally discovered a mysterious radiation in the microwave part of the spectrum that was coming from every part of the sky. The existence of this radiation was already predicted by G. Gamow in 1948 as the afterglow of the Big Bang and for this reason it became known as the *cosmic microwave background* (CMB) radiation [14]. Being one of the key predictions of the expanding universe, the Big Bang scenario was established in the cosmological community. Up to the end of the 20$^{\text{th}}$ century, the dominant view included a cold universe whose average density of matter would determine its fate; a densely enough universe would recollapse in the future leading to the "Big Crunch", whereas if its density was lower than a critical value it would expand forever, leading to the "Big Chill". In any case, the expansion of the universe would decelerate because it would be subject only to gravitational forces of attractive nature.

The situation changed in 1998 due to the first direct evidence for cosmic acceleration. S. Perlmutter, from the Supernova Cosmology Project, and B. P. Schmidt and A. G. Riess, from the High-Z Supernova Search Team, analysed data from supernovae type Ia that enabled them to measure distances in the universe, in a similar fashion to what E. Hubble had done in the past [15, 16]. These observations indicated that universe's expansion is accelerating and, hence, the universe should be filled with an unknown form of energy dubbed *dark energy*. In the simplest scenario, dark energy is represented by a cosmological constant and is associated with the energy of

the vacuum. The previous three milestones (the expansion of the universe, the observation of the CMB and the discovery of cosmic acceleration) set the foundations of modern cosmology.

1.3   Open questions in cosmology

Even though our understanding of the universe has become more solid over many years of research, there are still many questions left to be answered. For instance:

- How did the universe come into existence?

- What was the initial state of the universe?

- Why does the universe look homogeneous and isotropic at large scales?

- What is the driving force of the universe's acceleration?

- What is the ultimate fate of the universe?

In this thesis we will be concerned with the third question, namely the underlying physical mechanisms responsible for the observed homogeneity and isotropy of the universe. To this end, we will use the inflationary paradigm, which is the hypothetical period of accelerating expansion in the very early universe.

1.4   Outline of the thesis

The outline of the thesis is as follows:

- Chapters 2-3 contain an overview of modern cosmology and the inflationary theory. We discuss the standard cosmological model, the motivation for inflation and its connection to observations.

- In Chapter 4 we develop the necessary tools that will allow us to study multi-field dynamics in the subsequent chapters.

- In Chapter 5 we construct a two-field model that generalizes single-field α-attractors. We explore in detail the dynamics and predictions of this model and then discuss its viability against the latest *Planck* data.

- Chapter 6 presents two-field scaling solutions for a generic field geometry. We perform a detailed stability analysis and use several examples to highlight the stability criteria.

- In Chapter 7 we propose a classification scheme of various models in the literature based on the number of critical points of an effective potential. We also discuss the connection between hyperinflation and sidetracked inflation.

- In Chapter 8 we are interested in the limit of infinite fields. We use the horizon-crossing approximation to investigate the universality and prior dependence of predictions.

- Finally, in Chapter 9 we summarize our main findings.

1.5   Notation

- Throughout this thesis we will work in natural units $\hbar = c = 1$. After Ch. 3 we will also set $M_{\rm pl} = 1$.

- Primes ($'$) and dots ($\dot{}$) refer to derivatives with respect to the number of e-folds (N) and the cosmic time (t) respectively.

- The e-folding number will be negative during the inflationary stage and zero at the end of inflation.

- Greek letters ($\mu, \nu, \cdots$) denote spacetime indices and Latin letters ($a, b, \cdots$) field-metric indices.

- From Ch. 4 onwards G_{ij} and R will refer to the metric and the Ricci scalar associated with the field space.

- Partial derivatives with respect to spacetime indices will be represented by commas ($_{,a} \equiv \partial/\partial x^a$) and covariant derivatives with semicolons ($_{;a}$).

- The nabla operator (∇) acts on Euclidean 3-vectors or 3×3 tensors (e.g. $\vec{\nabla} f(\vec{x}) \equiv \partial_i f$ and $\vec{\nabla} \cdot \vec{A} \equiv \partial_i A^i$) .

- Up to (and including) Ch. 3 Ω will denote the normalized fluid components, whereas from Ch. 4 onwards it will refer to the turn rate of multi-field models.

2

The standard cosmological model

This chapter offers an elementary course on modern cosmology. We start with some remarks on the paradigm shift made by general relativity, followed by a discussion of observational evidence for isotropy of the universe at large scales. Next, we introduce the Lambda-Cold-Dark-Matter (ΛCDM) model and present some of its puzzling aspects.

2.1 Observational evidence for isotropy

The phenomenological successes of general relativity on the relatively small scales of our solar system (e.g. the calculation of Mercury's precession) indicated that it could also describe the universe as a whole. In addition to various formal challenges the theory introduces (see App. A.1) one has to take into account the non-linearity of differential equations for the metric coefficients. This severely limits the number of problems that can be treated fully analytically. However, when certain spacetime symmetries are considered then it is often possible to choose a special coordinate system that allows simple derivation of an exact solution by simplifying the metric. In the cosmological context such solutions were derived shortly after the introduction of general relativity, by e.g. A. Friedmann [10] and G. Lemaître [11], describing homogeneous and isotropic universes filled with some form of matter. These simple solutions turned out to adequately describe the observable universe.

Historically, the first evidence for cosmic isotropy came from the study of the galaxies' distribution (see e.g. [17] and references therein). This was noticed shortly after the discovery of the universe's expansion examining progressively larger catalogues of galaxies against isotropy. All data sets were consistent with the Friedmann-Lemaître-Robertson-Walker (FLRW) cosmology [18–20] with only some discrepancy over the scale of observed isotropy, currently set at around 150 Mpc [21].

Another evidence for isotropy is the existence of the CMB radiation. It is believed to be the remnant of photons in the early universe that formed a plasma together with free electrons and protons. As the universe expanded the temperature of the plasma decreased sufficiently (~ 3000 K) to allow hydrogen atoms to form, which, however, did not interact with the background photons. Photons essentially decoupled from electrons streaming freely into space until their present-day detection. The moment of this decoupling is now seen as a two-dimensional surface around us, called the last scattering surface. The COBE satellite performed the first accurate measurement of the temperature of the CMB radiation (~ 2.73 K) revealing at the same time small temperature fluctuations following a power law distribution [22]. The measurement of these anisotropies became progressively more accurate with the next two probes, WMAP [23] and Planck [24, 25] (see Fig. 2.1). The CMB radiation was a key prediction of the simple homogeneous and isotropic cosmological model, commonly known as the hot Big-Bang scenario.

Combining together the previous astrophysical observations it is com-
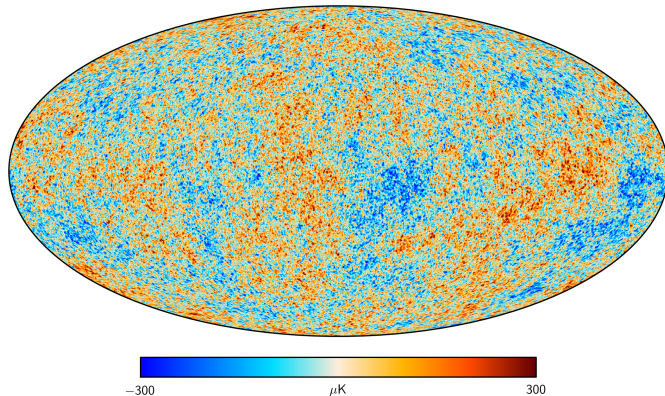
FIGURE 2.1
Picture of the infant universe created from the five years of Planck data. Credit: Planck collaboration.

monly accepted that the large-scale structure of the observable universe follows an almost isotropic distribution [26].[1] This is how far one can progress based on observations; homogeneity in particular can not be directly observed because spacetime measurements are restricted on our past light cone and not on the space-like surfaces of our current time [29]. To study the universe as a whole one needs to introduce assumptions on how it is portrayed at other points in space. It is reasonable to assume that the earth, and by extension our galaxy, is by no means a special point in space and so the universe should be seen as isotropic for every co-moving observer (special observers of the theory who will be defined later). In this way, isotropy around every point implies homogeneity. The previous assumption is called the *cosmological principle* and constitutes the pillar of modern cosmology.

2.2 The ΛCDM model

The building blocks of the standard cosmological model are the following (more details can be found e.g. in the introductory textbooks of B. Ryden [30] and S. Carroll [31]):

1. A **multicomponent perfect fluid** with energy-momentum tensor

$$T^{\mu\nu} = (\rho + P)\,u^{\mu}u^{\nu} + Pg^{\mu\nu}\,, \tag{2.1}$$

---

[1]Note that there are a few works which claim deviations from isotropy e.g. [27, 28].

whose components are **non-interacting** and satisfiy the strong energy condition

$$\left(T_{\mu\nu} - \frac{1}{2}Tg_{\mu\nu}\right)u^\mu u^\nu > 0 \,. \tag{2.2}$$

Here, u^μ is the velocity of the fluid as measured by a co-moving observer (an observer at rest with respect to the fluid), ρ is the total energy density ($\rho = \sum \rho_i$) and P is the total pressure ($P = \sum P_i$). Further, it is assumed that the two dominant forms of matter/energy are radiation and dust (or cold dark matter). We know from statistical mechanics that the equation of state for relativistic gas is $P_r = \frac{1}{3}\rho_r$ and non-relativistic matter satisfies $P_m \approx 0$. More generally, any form of matter with equation of state

$$P_i = w\rho_i \,, \tag{2.3}$$

satisfies the strong-energy condition if

$$1 + 3w > 0 \,. \tag{2.4}$$

2. A spacetime foliated with **three-dimensional maximally symmetric** surfaces orthogonal to a time-like vector $\boldsymbol{\xi}_t = a\boldsymbol{\partial}_t$.[2] These conditions fix the spacetime metric to FLRW form [18–20]

$$\mathrm{d}s^2 = -\,\mathrm{d}t^2 + a(t)^2 \left(\mathrm{d}\chi^2 + S_\kappa(\chi)\,\mathrm{d}\Omega^2\right) , \tag{2.5}$$

where the function $S_\kappa(\chi)$ takes the values

$$S_\kappa(\chi) = \begin{cases} \sin^2\chi, & \kappa = 1 \\ \chi^2, & \kappa = 0 \\ \sinh^2\chi, & \kappa = -1 \end{cases} . \tag{2.6}$$

The radial coordinate χ is called co-moving, because in this coordinate system observers at rest with the fluid perceive the universe as isotropic. The three-dimensional subspace admits the maximum number of Killing vectors, associated with the symmetries, and has constant intrinsic curvature κ. The spacetime symmetries are not independent from the assumed matter content 1; through the Einstein's field equations, properties of the energy-momentum tensor (zero shear and vorticity) correspond to symmetries (compatible with these requirements) of the spacetime metric.

---

[2]$\boldsymbol{\xi}_t$ is a conformal Killing vector because the Lie derivative of the metric along that vector satisfies $\mathcal{L}_{\boldsymbol{\xi}_t}g_{\mu\nu} = 2\dot{a}g_{\mu\nu}$.

3. A **cosmological constant** Λ which is associated with the vacuum energy. By virtue of the Einstein's field equations one can view the cosmological constant as an extra term which has either a purely geometric origin or it is a component of a perfect fluid with an equation of state $P_\Lambda = -\rho_\Lambda$. Its particle origin is still a mystery and that is why it is dubbed dark energy.

With 1, 2 and 3 one can find differential equations for the expansion rate of the universe (a) in terms of the energy density (ρ) and pressure (P)

$$3\left[\left(\frac{\dot{a}}{a}\right)^2 + \frac{\kappa}{a^2}\right] = 8\pi G_{\mathrm{N}}\rho + \Lambda \,, \tag{2.7}$$

$$3\frac{\ddot{a}}{a} = -4\pi G_{\mathrm{N}}\left(\rho + 3P\right) + \Lambda \,. \tag{2.8}$$

The first equation, also known as the Friedmann constraint, restricts evolution in the phase space on a hypersurface of three dimensions instead of four of the original problem. Combining the previous two we can express the time evolution of ρ in terms of the time derivatives of a

$$\dot{\rho} = -3\frac{\dot{a}}{a}(\rho + P) \,. \tag{2.9}$$

This is known as the continuity equation of the fluid because it is also a direct consequence of the conservation of the energy-momentum tensor $T^{\mu\nu}_{\;;\nu} = 0$.

For single-component universes with zero spatial curvature ($\kappa = 0$) the evolution of the energy density for the equation of state (2.3) can be calculated analytically by integrating (2.9)

$$\rho(a) = \rho_0 a^{-3(1+w)} \,. \tag{2.10}$$

Plugging this into the Friedmann constraint (2.7) yields the differential equation for the scale factor

$$\dot{a} = s\sqrt{\frac{8\pi G_{\mathrm{N}}\rho_0}{3}}a^{-(1+3w)/2} \,, \tag{2.11}$$

where s refers to the sign of $\dot{a}_0$ describing an initially expanding ($s > 0$) or contracting ($s < 0$) universe; in the rest of this thesis, we will only consider the expanding case. When $w \neq -1$ the solution is

$$a^{3(1+w)/2} = a_0^{3(1+w)/2} + \frac{3}{2}s\sqrt{\frac{8\pi G_{\mathrm{N}}\rho_0}{3}}(1+w)t \,, \tag{2.12}$$

while for a cosmological constant ($w = -1$) the scale factor increases exponentially with time

$$a(t) = a_0 e^{\sqrt{\Lambda/3}t} \,. \tag{2.13}$$

The latter universe is called de Sitter [32, 33]. Models with $w > -1$ (a condition known as the weak energy condition in contrast to $w > -1/3$ of the strong energy condition) have a finite age, i.e. given the solution at some time t_0 the differential equation for the scale factor becomes singular at finite time in the past, that is $a \to 0$ for $t \to t_0$. On the contrary, models with $w < -1$ have finite future, meaning the differential equation becomes singular at finite time, i.e. $a \to \infty$ for $t \to t_0$, but they have no past singularity at finite time, $a \to 0$ for $t \to -\infty$. These two singularities of the differential equation (2.7) are also curvature singularities because the Ricci scalar

$$R = 6\left[\frac{\ddot{a}}{a} + \left(\frac{\dot{a}}{a}\right)^2 + \frac{\kappa}{a^2}\right] = 8\pi G_{\mathrm{N}}(\rho - 3P) + 4\Lambda \,, \tag{2.14}$$

diverges in the past for models with $w > -1$ and in the future when $w < -1$. The de Sitter universe lies at the border between the two behaviours; it has neither finite past nor finite future.

In a similar fashion, for multi-component fluids we can define the total energy density and pressure as $\rho_t \equiv \sum \rho_i$ and $P_t \equiv \sum P_i$, which satisfy the continuity equation (2.9). The equation of state for such a fluid may not admit a simple relation of the form $P_t = w_t \rho_t$ prompting the necessity to keep each individual pressure and density as 'unknowns' and provide (by hand) relations between them. Alternatively, one can consider that the different components do not interact with each other and hence each component satisfies a separate continuity equation $\dot{\rho}_i = -3H(\rho_i + P_i)$. In this way the energy density of each fluid component is given as a function of the scale factor, and subsequently the Friedmann constraint becomes a separable differential equation for a that can always be solved.[3] The latter assumption is employed in cosmology.

To make contact with observations, it will be useful to define the Hubble parameter $H \equiv \mathrm{d}(\ln a)/\mathrm{d}t$ and re-express the Friedmann constraint as the sum of the normalized multi-component fluid densities

$$1 = \Omega - \frac{\kappa}{\dot{a}^2} \,, \tag{2.15}$$

---

[3]However, closed-form expressions can only be found for specific values of the parameters.
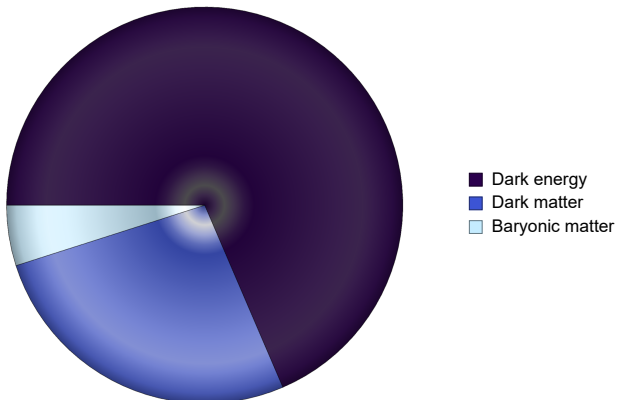
FIGURE 2.2
Pie chart illustrating the dominant ingredients of the universe.

where $\Omega \equiv \sum \Omega_i = 8\pi G_N \rho_i/(3H^2)$. These parameters are directly related to observational quantities and thus better connect dynamics to predictions of the model. For the ΛCDM model specifically it is assumed that the three species of matter are radiation, dust and dark energy resulting to $\Omega = \Omega_r + \Omega_m + \Omega_\Lambda$. The current estimates for these parameters are reported in the review of particle physics [34] and the latest *Planck* results [35]: the universe is composed of 31.5% pressureless matter (4.93% baryonic matter and 26.5% dark matter), 68.5% dark energy, while the densities of radiation and curvature are negligible (see Fig. 2.2). Light curves from distant type Ia supernovae provided distance measures and were the first solid evidence for cosmic acceleration and a cosmological constant [15,16], while the dark matter hypothesis is supported by the form of galaxy rotation curves, gravitational lensing and the dynamics of galaxy clusters (see e.g. [36,37] and references therein).

2.3   Objections to the standard picture

2.3.1   Isotropy and homogeneity

As was mentioned in Sec. 2.2, the distribution of galaxies as well as the CMB radiation appear highly isotropic. More specifically, the CMB radiation appears isotropic to one part in 10^5. If we assume that the thermal bath of photons in the early universe homogenized as a result of interactions

between them, then all photons of the universe should have overlapping past light cones. Before we estimate the size of a light cone, it is important to review the concept of horizons.

First, we introduce the notion of particle horizon [38]. The path of light follows null geodesics ($ds^2 = 0$) which for radial motion ($d\Omega = 0$) yields

$$d\chi = \frac{dt}{a} \equiv d\tau \,, \tag{2.16}$$

where τ is called the conformal time. The parametric relation $\chi_{\text{p.h.}}(t)$, found by integrating (2.16), is called the comoving particle horizon and describes the maximum distance (in co-moving radial coordinates) that light can travel between two given times, t_i and t. The physical distance is then found by multiplying with the scale factor: $d_{\text{p.h.}} = a(t)\chi_{\text{p.h.}}(t)$. For a single species of matter satisfying the inequality (2.4) the comoving particle horizon from initial time $t = 0$ to some final time t is equal to

$$\chi_{\text{p.h.}}(t) = \frac{2}{1+3w}\left[\frac{1}{a(t)H(t)} - \frac{1}{a(0)H(0)}\right] \equiv \frac{2}{1+3w}\Delta(aH)^{-1}\,. \tag{2.17}$$

Therefore, the size of $\chi_{\text{p.h.}}$ depends on the magnitude of the quantity $(aH)^{-1}$, called the co-moving Hubble radius. More specifically, points in space lying outside the Hubble radius are causally disconnected with the point in consideration.

It is also instructive to investigate the behaviour of the Hubble radius with time. Its time derivative is given by

$$\frac{d(aH)^{-1}}{dt} = \frac{1}{2a}(1+3w)\,, \tag{2.18}$$

which increases when the strong energy condition is satisfied. For sufficient time evolution the particle horizon can be dominated by the size of the Hubble radius at the time of evaluation, $\chi_{\text{p.h.}}(t) \approx \frac{2}{1+3w}(aH)^{-1}$. The above calculations are valid for single-component universes or during periods in which one component is dominant. Nevertheless, they approximate fairly well the size of causally discontinuous patches in the sky if one assumes radiation domination before the generation of the CMB.

Applying the previous reasoning on a radiation dominated universe we find that the co-moving particle horizon was around 10^{-6} of the size of the universe at the time of last scattering. In terms of what we observe from the Earth, different points separated by more than one degree of angular distance would have never been in equilibrium as the result of a thermal process, unless one assumes isotropic initial conditions for the universe. This is the *horizon problem* [26, 39] (depicted in Fig. 2.3).
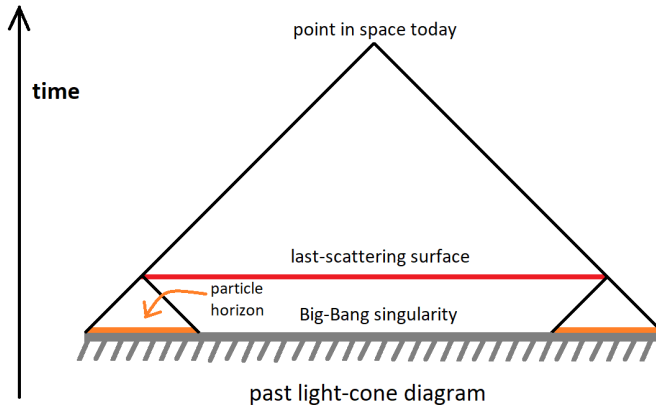
FIGURE 2.3

Diagrammatic view of the horizon problem. The past light cone of a point in space today contains regions that could have not be able to exchange information at the moment of last scattering.

2.3.2 Zero spatial curvature

We continue with what is known as *the flatness problem*, first noted by R. Dicke and subsequently popularized by him in collaboration with J. Peebles in 1979 [40]. In a nutshell, it is an argument on the improbability of measuring a vanishingly small curvature density $(\kappa/\dot{a}^2)$. It is important to note that at the time it was proposed the large-scale universe was considered to be composed of radiation, matter and (possibly) curvature. This means that measuring the energy density Ω for a universe that is successively dominated by radiation, matter and curvature, one will find at late times that $\Omega \approx \Omega_m \to 0$; a measurement with $\Omega_m \sim \mathcal{O}(1)$ seems highly improbable.

The argument was later emphasized by A. Guth as one of the primary shortcomings of the standard Big Bang model [41], providing the grounds for his new proposal. He argued that if the classical FLRW model can be used arbitrarily close to the hot Big Bang then for a radiation dominated universe the scale factor receives contribution from radiation mainly, and so $a \propto \sqrt{t}$. Hence, $\Omega - 1 \propto t$ which goes to zero as $t \to 0$. The conclusion does not change if we consider any form of matter that satisfies the strong-energy condition $1 + 3w > 0$. We see that the CDM model necessarily implies that $\Omega \approx 1$ at early times so one is in principle allowed to use this as the initial condition for Ω (or any number that is arbitrarily close to 1). However, when extrapolating back in time, the classical equations
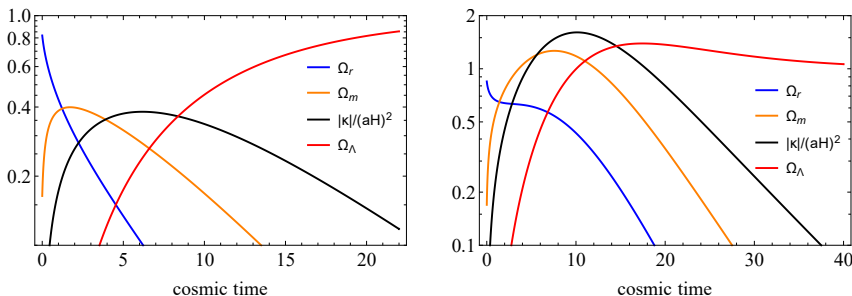
FIGURE 2.4
Evolution of normalized energy densities (in logarithmic scale) for parameter values $\rho_{r,0} = 150/(8\pi G_{\mathrm{N}})$, $\rho_{m,0} = 30/(8\pi G_{\mathrm{N}})$, $\Lambda = 0.01$, $a_0 = 1$ for $\kappa = -1$ (left panel) and $\kappa = 1$ (right panel). The used numbers do not match the observed values but are rather chosen to illustrate what one would expect from 'order one' initial conditions prior and close to radiation-matter equality.

are expected to hold up to some initial time t_0, the point when quantum effects cannot be ignored. Assuming a quantum-to-classical transition at some $t_0 \approx t_{\mathrm{Pl}}$, from this point onwards one can use the classical equations of motion to calculate the evolution of the universe. Since the Friedmann equations can not be used arbitrarily close to $t = 0$, Ω has no reason to be arbitrarily close to 1.

When a cosmological constant is included the formulation of the flatness argument requires a slight modification. The fate of a universe with $\Lambda > 0$ depends on both the curvature and the magnitude of the cosmological constant. If the spatial curvature is positive then the cosmological constant needs to exceed a certain value to avoid possible recollapsing, while a universe with $\kappa < 0$ will expand indefinitely. Excluding the former case, the rest types of universes will approach de Sitter at late times and hence $\Omega \to 1$. Therefore, $\Omega = 1$ is both the past and future attractor when the previous assumptions are satisfied. What remains unclear is the relative size of the curvature density compared to Ω_m and Ω_Λ. Using Eqs. (2.10) we can rewrite the Friedmann constraint as

$$\left(\frac{\dot{a}}{a}\right)^2 = \frac{8\pi G_{\mathrm{N}}}{3}\left(\frac{\rho_{m0}}{a^3} + \frac{\rho_{r0}}{a^4}\right) + \frac{\Lambda}{3} - \frac{\kappa}{a^2}\,, \qquad (2.19)$$

where ρ_{m0} and ρ_{r0} are the initial energy densities. Because the various fluid components fall off with a different power of the scale factor it is possible to have periods dominated by radiation, matter, curvature and cosmological constant successively (see Fig. 2.4). Under the assumption that the initial energy densities of radiation, matter and cosmological constant are "of

order one", the curvature density should succeed matter domination. The fact that we do not observe this requires less generic initial conditions for the fluid components.[4] In this way, the flatness problem is related to the "coincidence problem" [46] (the necessity for an explanation why $\Omega_m \sim \Omega_\Lambda \sim \mathcal{O}(1)$ holds today).

2.3.3 The Hubble tension

Over the last years there has been another heated debate among cosmologists regarding the value of the Hubble constant H_0 (the current value of the Hubble parameter) as measured by different methods [47]. More specifically, late-time (or low-redshift) measurements generically contradict estimates based on early-time cosmology, with a beyond 4σ discrepancy. The reported value of H_0 differs based on the probe: 74.03 ± 1.42 km/sec/Mpc from the SH0ES collaboration studying the Large Magellanic cloud cepheid standards [48]; 72.5 ± 2.3 km/sec/Mpc from the H0LiCOW collaboration based on cosmographic analysis of the doubly imaged quasar SDSS 1206+4332 [49]. On the contrary, the *Planck* collaboration, using the CMB data, predicts a Hubble constant 67.4 ± 0.5 km/sec/Mpc [35]. Finally, the Carnegie-Chicago Hubble Program has reported an intermediate value 69.8 ± 0.8 km/sec/Mpc [50], based on the Tip of the Red Giant Branch. From the above it becomes clear that the universe appears to expand faster than expected.

The arguments to alleviate the tension can be summarized in two types: it has been claimed that some systematic errors may have been overlooked in the analysis of different groups, partly because of the simplified assumptions necessary to tackle the problem (e.g. [51]), or new physics is required to match observations to existing models (see e.g. [52]). To date, the subject is an ongoing area of research.

---

[4]We should also note that the horizon and flatness puzzles are not mathematical inconsistencies of the theory (i.e. classical relativity) because given these special (or fine-tuned) initial conditions the theory works fine. Then, the formulation of the problem lies in providing arguments on why certain initial conditions are not favoured. The answer to this question usually includes some order one numbers but nevertheless overlooks the absence of the probability distribution that quantifies the probability of different initial conditions (see for instance [42–45]). This is most evident when discussing the fine tuning of the initial value of Ω where one assumes a flat prior on some interval around 1 instead of e.g. a sharply peaked distribution around one.

3

The inflationary mechanism

In this chapter we provide an overview of inflation. We start with a historical motivation of the theory and then discuss its connection to observations.

3.1   History and motivation

In the late 70s different cosmologists simultaneously and independently predicted a different expansion history before the hot Big Bang, i.e. the radiation dominated universe, based on results from high-energy theories: A. Starobinsky proposed a modified gravity scenario which evades the singularity by including a Ricci square term in the Einstein-Hilbert action [53,54]; K. Sato argued that a first-order phase transition of Grand Unified Theories would lead to a stretching of the size of CP domain walls [55]; D. Kazanas assumed a phase transition in the early universe in which energy flows from the vacuum energy to the matter altering the expansion history and solving the horizon problem [56]; A. Guth assumed a supercooling phase in the early universe that would solve the horizon, flatness and monopole relics problems [41, 57]. All previous works predicted an exponential expansion $a \propto e^{Ht}$ (de Sitter phase) before the standard Big-Bang scenario starts, and this phase was coined *inflation* (by A. Guth). The different expansion history leaves observational imprints on the structure of spacetime (such as homogeneity or isotropy).

The basic idea behind inflation is a smoothing process that will erase all significant inhomogeneities and anisotropies of the universe. By doing so, inflation solves the horizon and flatness puzzles by providing a dynamical mechanism that renders the otherwise fine-tuned conditions as the most probable instead. To better understand how to solve the horizon and flatness problems we will inverse engineer the model and assume another form of matter that yields the desired expansion history. The root of the two problems can be traced back in the behaviour of the Hubble radius. If the universe was only radiation dominated then the particle horizon today is too small to explain homogeneity. One possibility is to alter the universe's history by assuming a period that predates radiation domination and where the energy density of the universe is dominated by another fluid component. The particle horizon will then be given as

$$\chi_{\text{p.h.}}(t) \approx \chi_r + \chi_m = \frac{2}{1 + 3w_r}(aH)_r^{-1} - \frac{2}{1 + 3w_m}(aH)_m^{-1}, \qquad (3.1)$$

where the two parts refer to the radiation and the unknown form of matter period. One way to substantially increase the particle horizon is to assume that the new form of matter violates the strong energy condition and hence its contribution in Eq. (3.1) will be positive (see Fig. 3.1). Similarly, the Hubble radius shrinks during inflation which reverses the behaviour of the curvature density over time. Assuming an "order one" initial value of $\kappa/(aH)^2$ then at the end of this phase its value will be significantly smaller.

point in space today

time

last-scattering surface

Big-Bang singularity
without inflation

overlapping
past light cones

'new' Big-Bang
singularity

past light-cone diagram with inflation
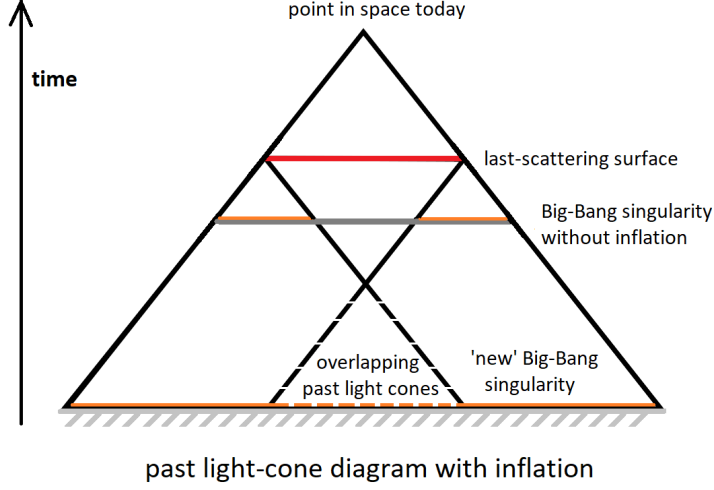
FIGURE 3.1

*Diagrammatic view of the horizon problem with inflation. In contrast to Fig. 2.3,
inflation adds enough conformal time so that the past light-cones of different points at
the moment of last scattering become overlapping.*

By tuning the duration of this phase, Ω can evolve arbitrarily close to one
which may explain its present small value.

A shrinking Hubble radius implies that the scale factor increases at an
accelerating pace

$$\frac{\mathrm{d}(aH)^{-1}}{\mathrm{d}t} = \frac{\mathrm{d}(\dot{a}^{-1})}{\mathrm{d}t} = -\frac{\ddot{a}}{\dot{a}^2} < 0 \,, \tag{3.2}$$

or in terms of the Hubble parameter

$$\frac{\dot{H}}{H^2} + 1 > 0 \,. \tag{3.3}$$

Defining the quantity

$$\epsilon \equiv -\frac{\dot{H}}{H^2} \,, \tag{3.4}$$

dubbed the slow-roll parameter (for reasons that will become clear in the
next section), the condition for accelerating expansion is $\epsilon < 1$. Because
we will be mainly interested in quasi-exponential expansion it will prove
more useful to use the e-folding number, defined as $N \equiv \ln a$, as a time
variable. Differentiating the latter with respect to time yields the relation
$\mathrm{d}N = H\,\mathrm{d}t$. Non-collapsing models preserve the sign of H and the e-folding
number can be used as an alternative variable.

Finally, we should mention that the inflationary scenario was highly promoted by the high-energy community. Various extensions of the standard model have been proposed that unify electroweak and strong interactions (e.g. $SU(3) \times SU(2) \times U(1)$) called Grand Unified Theories (GUT). A generic prediction of these theories is the existence of magnetic monopoles, supposed to be created at very high energy scales. These relic particles are stable, meaning they should have survived up to the present day with a density orders of magnitude greater than the rest of the matter [58]. These, however, are not observed in nature and hence GUT are observationally disfavoured. Inflation then provides an argument against the immediate discard of these theories by rendering the monopoles undetectable; since they were created before the ordinary standard model particles, their density (falling off as $\propto a^{-3}$) was dramatically lowered during the exponential expansion. Note that the realization of inflation rests on a new particle which violates the strong-energy condition and, therefore, inflation requires some extension of the standard model of particle physics. This hypothetical particle, called the *inflaton*, is supposed to be present at high energies and then decay to the standard model particles during reheating [59]. To date, a successful embedding of inflation into high-energy theories remains an open problem [60].

3.2 Simple single-field models

The simplest model of inflation includes a real scalar field minimally coupled to gravity:

$$S = \int \mathrm{d}^4 x \sqrt{-g} \left(\frac{1}{2} M_{\mathrm{pl}}^2 R - \frac{1}{2} g^{\mu\nu} \partial_\mu \phi \partial_\nu \phi - V(\phi) \right) , \qquad (3.5)$$

where we used the definition of the Planck mass $M_{\mathrm{pl}} \equiv (8\pi G_{\mathrm{N}})^{-1/2}$ in the natural units $\hbar = c = 1$. Variation of the action with an FLRW ansatz for the metric

$$\mathrm{d}s^2 = -\mathrm{d}t^2 + a(t)^2 \, \mathrm{d}\boldsymbol{x} \cdot \mathrm{d}\boldsymbol{x} , \qquad (3.6)$$

provides the two linearly independent Einstein's field equations for the unknown metric function $a(t)$ (one evolution equation and one constraint) and the generalized Klein-Gordon equation for the scalar field $\phi(t)$. Both equations can be be written in compact form with the introduction of the

Hubble parameter,

$$3M_{\mathrm{pl}}^2 H^2 = \frac{1}{2}\dot{\phi}^2 + V \,, \tag{3.7}$$

$$M_{\mathrm{pl}}^2 \dot{H} = -\frac{1}{2}\dot{\phi}^2 \,, \tag{3.8}$$

$$\ddot{\phi} + 3H\dot{\phi} + \frac{\mathrm{d}V}{\mathrm{d}\phi} = 0 \,. \tag{3.9}$$

The latter two equations form a non-linear system for the unknown functions $\phi(t)$ and $a(t)$ (or $H(t)$) which is in general unsolvable for an arbitrary potential function $V(\phi)$.

A useful measure of deviations from de Sitter expansion is the first slow-roll parameter (3.4), with $\epsilon = 0$ for de Sitter. When $\epsilon < 1$ the Hubble radius shrinks and the universe inflates. Through the Einstein's field equations we can relate the slow-roll parameter to the kinetic (K) and potential energy densities of the scalar field

$$\epsilon = \frac{3K}{K + V} \,, \tag{3.10}$$

and the condition $\epsilon < 1$ translates to $2K < V$. The quasi-de Sitter limit corresponds to $\epsilon \ll 1$, which is equivalent to $K \ll V$ and hence to potential domination. Furthermore, sustained inflation forces the derivative of ϵ with respect to the number of e-folds to be small, $\epsilon' \ll 1$. This can be achieved if the inflaton slowly descends its potential for a prolonged period of time. The heuristic picture is the following: Hubble friction causes dissipation of the excess initial kinetic energy until the inflaton reaches a "terminal" velocity. The magnitude of this velocity depends on the strength of the potential gradient. For certain models, soon after the beginning of inflation the system finds itself at a state with $\ddot{\phi} \approx 0$ which gives an approximate terminal velocity [61]

$$\dot{\phi}_{\mathrm{SR}} \approx -\frac{1}{3H}\frac{\mathrm{d}V}{\mathrm{d}\phi} \,. \tag{3.11}$$

Consistency of this solution requires the smallness of its time derivative

$$\ddot{\phi}_{\mathrm{SR}} \approx \frac{\mathrm{d}V}{\mathrm{d}\phi}\left(\frac{1}{3H^2}\frac{\mathrm{d}^2V}{\mathrm{d}\phi^2} - \frac{1}{3}\epsilon\right) \,. \tag{3.12}$$

Neglecting the kinetic energy of the inflaton the square of the Hubble parameter becomes proportional to the potential $V \approx 3M_{\mathrm{pl}}^2 H^2$; using (3.11) in the definition of ϵ the terms in the parenthesis become functions of the
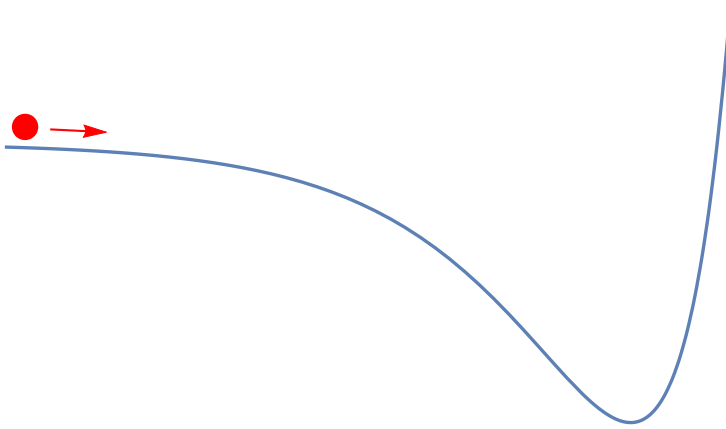
FIGURE 3.2
A potential with a sufficiently flat region that satisfies the potential slow-roll conditions
(3.14).

potential and its derivatives. This motivates us to define the *potential slow-roll parameters*

$$\epsilon_V \equiv \frac{M_{\text{pl}}^2}{2V^2} \left(\frac{\mathrm{d}V}{\mathrm{d}\phi} \right)^2 , \qquad \eta_V \equiv \frac{M_{\text{pl}}^2}{V} \frac{\mathrm{d}^2 V}{\mathrm{d}\phi^2} , \tag{3.13}$$

and demand

$$\epsilon_V , |\eta_V| \ll 1 , \tag{3.14}$$

(see Fig. 3.2 for a toy model).

To quantify the smallness of ϵ' we can define its logarithmic derivative in terms of the *e*-folding number as a new parameter

$$\eta \equiv \frac{\epsilon'}{\epsilon} . \tag{3.15}$$

A prolonged de Sitter phase requires the smallness of η as well. Whenever the potential slow-roll parameters are small they can be related to ϵ and η as

$$\epsilon \approx \epsilon_V , \qquad \eta \approx -2\eta_V + 4\epsilon . \tag{3.16}$$

When the latter conditions are satisfied the system undergoes a quasi-de Sitter expansion and one can estimate how many *e*-folds are required before the system settles down at the slow-roll solution. The estimate depends on the initial velocity or equivalently the initial value of ϵ; the lowest amount of

necessary e-folds corresponds to the de Sitter limit $\mathrm{d}V/\mathrm{d}\phi \to 0$, while the maximum amount depends on the maximum value of the potential gradient at that interval [62]. When ϵ_0 is far from kinetic domination ($\epsilon = 3$) then one finds $\dot{\phi} \approx \dot{\phi}_{\mathrm{SR}}e^{-3N}$, which explains why the slow-roll solution has been referred to as attractor in phase space [61,63]. Based on that, inflationary models achieve a notion of initial conditions independence (we will illustrate this later in Sec. 3.5 using the quadratic potential as an example). Usually, we require around 50-60 e-folds of inflation in order to solve the horizon and flatness problems [63].

3.3 Cosmological perturbations

The previous toy model is supposed to describe our universe on the largest of scales where homogeneity and isotropy are observed. On smaller scales, such as clusters of galaxies, solar systems, atoms, etc.., one can parametrize these inhomogeneities as small fluctuations on the FLRW background and solve the Einstein's field equations perturbatively.[1] The scalar field is written as a perturbative expansion

$$\varphi = \varphi^{(0)} + h\varphi^{(1)} + \cdots , \tag{3.17}$$

where h is a small parameter along with the definitions $\varphi^{(0)} \equiv \phi(t)$ and $h\varphi^{(1)} \equiv \delta\phi$. Through the Einstein's field equations an expansion over the field induces a similar expansion on the metric

$$g_{\mu\nu} = g_{\mu\nu}^{(FLRW)} + hg_{\mu\nu}^{(1)} + \cdots . \tag{3.18}$$

From this point one can either expand the action to second order or expand the equations of motion. Before doing so it is important to properly identify the physical degrees of freedom.

We will extend the FLRW metric ($\kappa = 0$) to include first order perturbations which are similarly projected along the time-like vector $\boldsymbol{\partial}_t$. Applying the scalar-vector-tensor decomposition (see App. A.2) we are able to identify the degrees of freedom that transform as scalars, vectors and tensors accordingly. The metric can be written as

$$\mathrm{d}s^2 = -(1 - 2A)\,\mathrm{d}t^2 + B_i\,\mathrm{d}t\,\mathrm{d}x^i + a^2\left[(1 + 2\psi)\,\delta_{ij} + e_{ij}\right]\,\mathrm{d}x^i\,\mathrm{d}x^j , \tag{3.19}$$

where A, ψ are scalars, B_i is a vector, e_{ij} is a symmetric traceless tensor and the previous are defined on the three-dimensional subspace. Equations

---

[1] In the effective field theory of large scale structure the expansion is performed over the wavenumber k instead (see e.g. [64]).

of motion in Fourier space decouple at linear order in this decomposition
and one can study each mode separately.

However, as explained in App. A.1, the Einstein's field equations can
not be solved unless the unphysical degrees of freedom are removed (in
cosmology this fact is known as the gauge issue of cosmological perturbation
theory). Extracting the physical content can be achieved by fixing the gauge
(similar to what is done in electromagnetism or the study of gravitational
waves) or by constructing gauge-invariant quantities [65, 66]. Under the
infinitesimal diffeomorphism

$$x^\mu \to y^\mu = x^\mu + h\xi^\mu \,, \tag{3.20}$$

any tensorial quantity C transform as [67][2]

$$C \to \tilde{C} = C - h\mathcal{L}_\xi C \,, \tag{3.22}$$

where $\mathcal{L}_\xi$ is the Lie derivative along the vector $\boldsymbol{\xi}$ that generates the diffeo-
morphism. Note that $\boldsymbol{\xi}$ should preserve the slicing of the spacetime and
the background space should not be affected by the diffeomorphism [68].
Decomposing ξ^μ in its scalar-vector part one can calculate how the differ-
ent modes transform under the previous action. For example, the lapse
function (the coefficient of $\mathrm{d}t^2$ in (3.19)) transforms to $-1 - 2A + \dot{\xi}^0$ from
which we can deduce the transformation $2A \to 2A - \dot{\xi}^0$. The tensor mode
of the three-metric does not receive contributions from the vector ξ^μ (since
it contains only scalar and vector modes) and therefore does not transform
under these diffeomorphisms. Forming linear combinations of the metric
functions and their derivatives one can construct gauge-invariant quantities.

When only scalar fields are considered, vector perturbations are not ex-
cited during inflation because they satisfy first order (constraint) equations
and thus are non-dynamical. On the contrary, scalar and tensor modes
satisfy second order equations, while perturbations of the inflaton field are
related to scalar metric perturbations via the Einstein's field equations.
An important scalar gauge-invariant quantity is the co-moving curvature
perturbation defined as

$$\mathcal{R} \equiv \psi + \frac{H}{\dot{\phi}}\delta\phi \,. \tag{3.23}$$

---

[2]The variation of C satisfies $\delta C = -\mathcal{L}_\xi C$. This can be easily seen e.g. when C is a
scalar and the Lie derivative becomes the directional derivative. Under the diffeomor-
phism (3.20) the transformation law is

$$\mathcal{L}_\xi C \equiv \lim_{h \to 0} \frac{1}{h}\left(C(y^k) - \tilde{C}(y^k)\right) = \lim_{h \to 0} \frac{1}{h}\left(C(x^k) - \tilde{C}(x^k)\right) = \xi^k C_{,k} \,, \tag{3.21}$$

and to first order we obtain $\tilde{C}(x^k) = C(x^k) - h\mathcal{L}_\xi C$.

Its evolution can be determined from the scalar part of the quadratic action [69]

$$S_{\mathcal{R}} = \frac{1}{2} \int d^4x \frac{a^3 \dot{\phi}^2}{H^2} \left(\dot{\mathcal{R}}^2 - \frac{1}{a^2} (\boldsymbol{\nabla}\mathcal{R})^2 \right). \tag{3.24}$$

Alternatively, one can use the gauge-invariant field perturbation

$$Q \equiv \delta\phi + \frac{\dot{\phi}}{H}\psi, \tag{3.25}$$

which is related to the curvature perturbation as $Q = \mathcal{R}\dot{\phi}/H$, and its second order action

$$S_Q = \frac{1}{2} \int dt \, d^3x \, a^3 \left[\dot{Q}^2 - \frac{1}{a^2}(\boldsymbol{\nabla}Q)^2 - V_{,\phi\phi}Q^2 - \frac{1}{a^3}\frac{d}{dt}\left(\frac{a^3\dot{\phi}^2}{H}\right)Q^2 \right]. \tag{3.26}$$

Although both descriptions are equivalent, the second quantity is easier to generalize to the case with more fields (see Ch. 4). Similarly, the action for the tensor modes is

$$S_{\mathrm{t}} = \frac{M_{\mathrm{pl}}^2}{8} \int d^4x \, a^3 \left(\dot{\gamma}_{ij}^2 - \frac{1}{a^2}(\boldsymbol{\nabla}\gamma_{ij})^2 \right), \tag{3.27}$$

and we observe that it is analogous to the action of a massless field in a de Sitter background.

To study solutions of the equations of motion it is more convenient to switch to conformal time $dt = a \, d\tau$ and rescale fields appropriately.[3] In this coordinate system the actions (3.24), (3.26) and (3.27) resemble the action of a free field with a time-dependent mass term. The solution of the quadratic equation of motion

$$\frac{d^2 v_k}{d\tau^2} + \omega_k(\tau)^2 v_k = 0, \tag{3.28}$$

is found in Fourier space after the transformation

$$v(\tau, \vec{x}) = \int d^3k \, v_k(\tau) e^{i\boldsymbol{k}\cdot\boldsymbol{x}}. \tag{3.29}$$

In de Sitter space the frequency term is $\omega_k^2 = k^2 - 2/\tau^2$ and the solution can be found analytically

$$v_k(\tau) = c_k e^{-ik\tau} \left(1 - \frac{i}{k\tau} \right) + d_k e^{ik\tau} \left(1 + \frac{i}{k\tau} \right). \tag{3.30}$$

---

[3]The proportionality constant of the rescaled fields differs for scalars and tensors. Tensor modes are rescaled as $h_{ij} \to v_{ij} = ah_{ij}$, while scalars as $\mathcal{R} \to v_{\mathcal{R}} = a\dot{\phi}/H\mathcal{R}$.

From these two classical plane-wave solutions we choose the positive energy modes, assuming that for $k \gg (aH) \approx -\tau^{-1}$ modes are in the Minkowski vacuum (Bunch-Davies vacuum [70]) and so $d_k = 0$. For later convenience, we will fix the other normalization constant using the Wronskian condition

$$v_k^* \frac{\mathrm{d}v_k}{\mathrm{d}\tau} - \frac{\mathrm{d}v_k^*}{\mathrm{d}\tau} v_k = -i \,, \tag{3.31}$$

which yields $c_k = 1/\sqrt{2k}$. This ensures that creation and annihilation operators satisfy the canonical commutation relations

$$[a_{\boldsymbol{k}}, a_{\boldsymbol{k}'}^{\dagger}] = \delta(\boldsymbol{k} + \boldsymbol{k}') \,. \tag{3.32}$$

The mode functions of a free field in de Sitter background with Bunch-Davies initial conditions evolve as

$$v_k(\tau) = \frac{e^{-ik\tau}}{\sqrt{2k}} \left(1 - \frac{i}{k\tau}\right) \,. \tag{3.33}$$

Note that these variables are not observables because they diverge for $\tau \to 0$. In order to properly account for the asymptotic behaviour of physical quantities we need to consider the original fields $u_k = v_k/a$ and calculate their norm

$$|u_k|^2 = \frac{H^2}{2k^3} \left[1 + (k\tau)^2\right] \,, \tag{3.34}$$

which is well defined for both $\tau \to -\infty$ and $\tau \to 0$. Having found the time-dependence of the mode functions, we can canonically quantize them and make the connection to observations. This is the topic of the next section.

3.4 Power spectra

Promoting fields to operators, $u \to \hat{u}$, where $u = \mathcal{R}, Q, \cdots$, we define the power spectrum $P_u(\tau, \boldsymbol{k})$ from the two-point correlation function as

$$\langle \hat{u}(\tau, \boldsymbol{k})^{\dagger} \hat{u}(\tau, \boldsymbol{k}') \rangle = (2\pi)^3 P_u(\tau, \boldsymbol{k}) \delta(\boldsymbol{k} + \boldsymbol{k}') \,, \tag{3.35}$$

and the normalized power spectrum

$$\mathcal{P}_u(\tau, \boldsymbol{k})^2 \equiv \frac{k^3}{2\pi^2} P_u(\tau, \boldsymbol{k}) \,. \tag{3.36}$$

In de Sitter space the power spectrum of a massless scalar field is found to be

$$\mathcal{P}_{\delta\phi}^2 = \left(\frac{H}{2\pi}\right)^2 (1 + (k\tau)^2) \,. \tag{3.37}$$

The scale dependence of the power spectrum is determined from its logarithmic derivatives with respect to $\ln k$. It can be shown that for modes outside the horizon, $|k\tau| \ll 1$, the power spectra of curvature and tensor perturbation freeze as $|\tau_{\text{end}}| < 1$ [71]. More precisely, for a given mode k_* there is insignificant change after horizon crossing and to a good approximation the power spectrum at the end of inflation will be given by its value close to horizon crossing $k_* \tau_* = -1$. Then, Taylor expanding around that wavenumber $\ln k_*$ yields

$$\ln \mathcal{P}_u^2 = \ln \mathcal{P}_u^2\big|_{k=k_*} + \frac{\partial \mathcal{P}_u^2}{\partial \ln k}\Big|_{k=k_*} \Delta \ln k + \cdots . \tag{3.38}$$

The first-order derivative is called the spectral index

$$n_u - 1 \equiv \frac{\partial \mathcal{P}_u^2}{\partial \ln k} , \tag{3.39}$$

and measures deviation from scale invariance. The CMB data [22, 23, 72] are consistent with an almost scale invariant power spectrum and therefore we will keep only the first two terms in the expansion on superhorizon scales

$$\mathcal{P}_u^2 \approx \mathcal{P}_u^2\big|_{k=k_*} \ln \left(\frac{k}{k_*} \right)^{n_u - 1} . \tag{3.40}$$

For slow-roll single-field inflation ($\epsilon, |\eta| \ll 1$) the power spectra of scalar and tensor modes are given by [73] (see also the lectures notes of A. Riotto [69] and the TASI lectures of D. Baumann [74] for more details)

$$\mathcal{P}_{\mathcal{R}}^2 = \frac{2}{M_{\text{pl}}^2 \epsilon_*} \left(\frac{H_*}{2\pi} \right)^2 , \qquad \mathcal{P}_t^2 = \frac{8}{M_{\text{pl}}^2} \left(\frac{H_*}{2\pi} \right)^2 , \tag{3.41}$$

where t stands for tensor and every quantity is defined when a given scale crosses the Hubble horizon.[4] From these two expressions we arrive at the two observable quantities used in inflationary model buildings, namely the spectral index

$$n_s - 1 \equiv \frac{\partial \mathcal{P}_s^2}{\partial \ln k} \approx -2\epsilon_* - \eta_* \approx -6\epsilon_{V*} + 2\eta_{V*} , \tag{3.42}$$

---

[4]Comparing (3.41) with (3.37) may create some confusion on how to obtain the de Sitter limit $\epsilon \to 0$ for the curvature perturbation $\mathcal{P}_{\mathcal{R}}^2$. Even though the power spectrum can be defined for different gauge-invariant quantities, not all of them are equally appropriate to describe a given problem. For instance, to properly take the de Sitter limit we should have examined $\lim_{\epsilon \to 0} \mathcal{P}_Q^2$, instead of $\mathcal{R}$, as the former is properly defined for $\epsilon \to 0$. The reason why we use $\mathcal{R}$ in inflationary models is because it is conserved on superhorizon scales and can thus be related with physical observables, whereas Q is not.

and the tensor-to-scalar ratio

$$r \equiv \frac{\mathcal{P}_t^2}{\mathcal{P}_s^2} \approx 16\epsilon_* \,. \tag{3.43}$$

These fluctuations, once crossed the horizon, become indistinguishable from classical random variables and seed structure formation. Therefore, inflation provides a mechanism for generation of small inhomogeneities from an otherwise homogeneous and isotropic background by stretching the initial quantum fluctuations to large scales. This is considered to be an example of a quantum-to-classical transition in nature (see for instance [75–77]).

Finally, the bispectrum is defined from

$$\langle \mathcal{R}(\boldsymbol{k}_1)\mathcal{R}(\boldsymbol{k}_2)\mathcal{R}(\boldsymbol{k}_3)\rangle = (2\pi)^3 B(\boldsymbol{k}_1, \boldsymbol{k}_2, \boldsymbol{k}_3)\delta(\boldsymbol{k}_1 + \boldsymbol{k}_2 + \boldsymbol{k}_3)\,, \tag{3.44}$$

where the function B is usually given by the shape function S, that provides information about the various configurations of the three momenta (which must add up to zero), and the non-linear parameter f_{NL}

$$B(\boldsymbol{k}_1, \boldsymbol{k}_2, \boldsymbol{k}_3) = \frac{18}{5}f_{\mathrm{NL}}S(\boldsymbol{k}_1, \boldsymbol{k}_2, \boldsymbol{k}_3)\,. \tag{3.45}$$

It is worth mentioning that the squeezed limit of the bispectrum, namely the limit where one momentum becomes much smaller than the other two, is determined by the spectral index [78]

$$\lim_{\boldsymbol{k}_1 \to 0}\langle \mathcal{R}(\boldsymbol{k}_1)\mathcal{R}(\boldsymbol{k}_2)\mathcal{R}(\boldsymbol{k}_3)\rangle = -(n_s - 1)P_v(\boldsymbol{k}_2)P_v(\boldsymbol{k}_3)(2\pi)^3\delta(\boldsymbol{k}_1 + \boldsymbol{k}_2 + \boldsymbol{k}_3)\,. \tag{3.46}$$

This result relies only on the assumption of a single field that drives inflation and shows that the squeezed bispectrum will be suppressed by $n_s - 1$ for any single-field model [79, 80]. A future detection of large non-Gaussianity can rule out this class of inflationary models.

The best current estimated values for the previous set of observables were reported in the latest *Planck* 2018 results [72]: $n_{\mathrm{s}} = 0.963$, $r < 0.1$ and $f_{\mathrm{NL}}^{\mathrm{local}} = -0.9 \pm 5.1$ (see Fig. 3.3 for constraints of various models based on the *Planck* collaboration analysis). These bounds may get tighter with future observations such as LSS surveys [81] and 21 cm tomography [82].

3.5   Case example: the quadratic potential

We close this chapter by examining the simplest inflationary model consisting of a quadratic self-interacting field $V = 1/2m^2\phi^2$. The Klein-Gordon equation is

$$\ddot{\phi} + 3H\dot{\phi} + m^2\phi = 0\,, \tag{3.47}$$
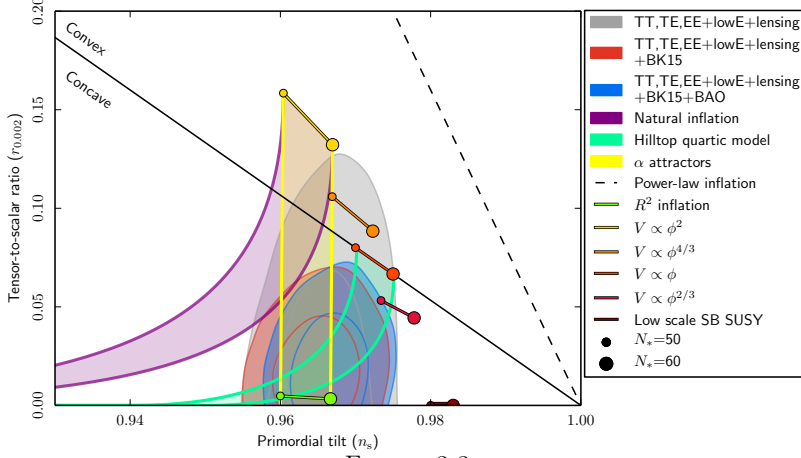
FIGURE 3.3

Constraints on the tensor-to-scalar ratio and spectral index and the viability of a variety of single-field models (from the Planck collaboration).

admitting a slow-roll solution

$$\dot{\phi} \approx -\text{sgn}(\phi)\sqrt{\frac{2}{3}}m\,, \tag{3.48}$$

the validity of which is depicted at Fig. 3.4. The potential slow-roll parameters are

$$\epsilon_V = \eta_V = \frac{2}{\phi^2}\,. \tag{3.49}$$

It is instructive to express these quantities in terms of the number of *e*-folds in the spirit of [83, 84]; for this model

$$N = -\frac{1}{4}\left(\phi^2 - \phi_{\text{end}}^2\right)\,, \tag{3.50}$$

where the endpoint can be estimated by

$$\epsilon_V = 1 \Rightarrow \phi_{\text{end}} \approx \sqrt{2}\,, \tag{3.51}$$

and so

$$\epsilon_V = \eta_V = \frac{1}{1-2N}\,. \tag{3.52}$$

The spectral index (3.42) reads

$$n_{\text{s}} - 1 = -4\epsilon_{V*} \approx \frac{2}{N_*}\,, \tag{3.53}$$
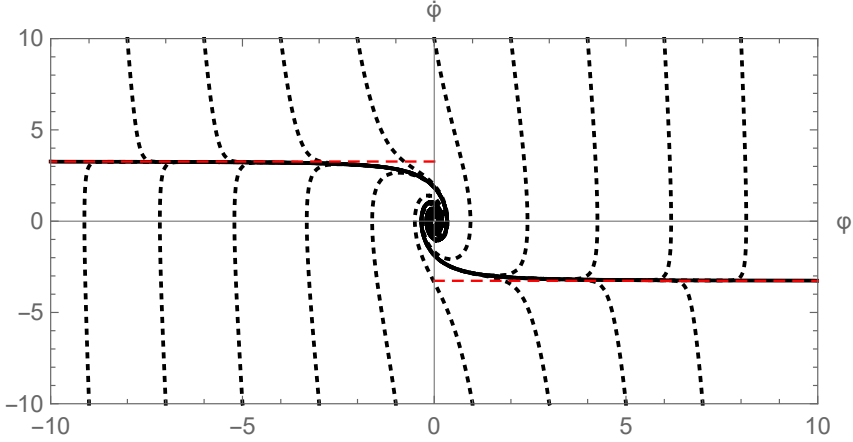
FIGURE 3.4

The numerical solution of the parametric relation $\dot{\phi}(\phi)$ for the quadratic potential.
Dotted lines represent solutions for different initial conditions and the red lines are the
slow-roll expression (3.48). The system always approaches the two solid black lines
before settling at its minimum.

with $N_* = -55$, and the tensor-to-scalar ratio is

$$r_{\mathrm{t}} = -\frac{8}{N_*} \, .$$ (3.54)

We should note that this simple model has already been excluded as obser-
vationally viable from the joint analysis of BICEP2/*Keck Array* and *Planck*
data [85].

4
Multi-field models

We motivate multi-field inflation and explore in detail the dynamics of two-field models in the adiabatic/entropic decomposition and the superhorizon behaviour of perturbations. Following the literature, we derive observables for models admitting the gradient-flow approximation.

4.1   Motivation for multiple fields

Single-field models have been proven very useful in providing a dynamical mechanism to explain structure formation and correlated features in the power spectrum of the CMB. Despite its phenomenological successes, embedding inflation into known high-energy theories remains challenging (see e.g. [60]). In the effective field theory (EFT) approach of inflation, sensitivity of the inflaton to higher-order corrections [1] and, in particular, to dimension-six operators of the form

$$\frac{\mathcal{O}_6}{M_{\text{pl}}^2} = \frac{\mathcal{O}_4}{M_{\text{pl}}^2}\phi^2\,, \tag{4.2}$$

can lead to the so-called η-problem [86]. These higher order terms may acquire vacuum expectation values comparable to the potential energy, $\langle\mathcal{O}_4\rangle \sim V$, and overall increase the energy scale at which inflation is allowed because larger field displacements are required in order for the slow-roll parameter to remain small; alternatively this leads to violation of the slow-roll condition for η at a given energy scale. This increase, especially for models where inflation takes place at super-planckian field displacements, leads to further sensitivity to higher-order terms and the theory may lose perturbative control. One way to redeem the problem is to assume a shift-symmetry that will protect the inflaton from quantum corrections.

Another challenge is the presence of extra fields from models that are preferred from string theory and its lower-energy limit supergravity. These theories generally predict more than one, and typically many, light fields during inflation, where by light we refer to them being dynamical. The usual way to reduce the multi-field problem to single-field dynamics is to consider steep gradients that would stabilize the excess fields at their respective minima. This, however, does not always work for the following reason: in multi-field models considering a bottom-up approach would yield generic

---

[1]In the EFT approach one writes down an expansion over all operators (divided by a mass scale) and consistent with the symmetries of the problem. The cut-off scale is assumed to be a few orders of magnitude lower than the Planck mass and one can assume derivative or non-derivative operators, for instance:

$$\sum \frac{c_n \phi^n}{\Lambda^{n-4}}\,, \qquad \sum \frac{d_n (\partial_\mu \phi \partial^\mu \phi)^n}{\Lambda^{4n-4}}\,. \tag{4.1}$$

In what follows, we will focus on non-derivative operators with $n = 6$. Note that this operator is important for inflationary models with both subplanckian (small-field) or superplanckian (large-field) displacements. In contrast, operators of dimension greater than six are important only for the latter models [74].

derivative couplings between the fields in the Lagrangian [87] which manifest themselves as generalized centrifugal forces in the equations of motion. Thus, even if the gradients are steep enough, centrifugal forces can drive fields away from their minima resulting into pure multi-field dynamics (we will explore this in detail in Ch. 7). This has profound consequences on observables and can leave imprints on the CMB (see e.g. [88–90]).

Multi-field models display rich dynamics and phenomenology, and have been extensively studied in the last 20 years. They introduce several new features: the (possible) generation of isocurvature (or entropic) perturbations and subsequently the superhorizon evolution of the curvature perturbation; the possibility for the power spectrum's enhancement that can lead to large non-Gaussianities [91–95] and primordial black holes formation [96, 97]; and the evasion of swampland conjectures [98–103], to list a few. Before exploring these endless possibilities one has to understand the underlying dynamics and the unique features of multi-field inflation. To this end, the rest of this chapter serves as an introduction on the developments of multi-field theory, focusing on background dynamics for generic models and the derivation of observables for certain models following the gradient-flow approximation.

4.2   The orthonormal basis

For $\mathcal{N}$ fields with minimal derivative couplings the general form of the scalar-field action is

$$S = \int \mathrm{d}^4 x \sqrt{-g} \left(-\frac{1}{2} G_{ij}(\phi^k) \partial_\mu \phi^i \partial^\mu \phi^j - V(\phi^k) \right) , \qquad (4.3)$$

where the couplings G_{ij} have been introduced to make the kinetic term manifestly invariant under reparameterizations of the fields $\phi^i \to \tilde{\phi}^i$. In this way, G_{ij} can be interpreted as a metric on the field space. The Klein-Gordon equations become

$$\mathrm{D}_t \dot{\phi}^i + 3H \dot{\phi}^i + V^{,i} = 0, \qquad (4.4)$$

where D_t is the covariant total derivative operator with respect to the parameter t and associated with the field metric $\boldsymbol{G}$

$$\mathrm{D}_t A^i \equiv \dot{A}^i + \Gamma^i_{jk} A^j \dot{\phi}^k . \qquad (4.5)$$

Likewise, the Hamiltonian constraint is

$$3H^2 = \frac{1}{2} G_{ij} \dot{\phi}^i \dot{\phi}^j + V . \qquad (4.6)$$

In terms of the *e*-folding number, equations of motion read

$$\mathrm{D}_N v^i + (3 - \epsilon)\left(v^i + (\ln V)^{,i}\right) = 0\,, \tag{4.7}$$

where $v^i \equiv (\phi^i)'$ and the slow-roll parameter takes the simple form

$$\epsilon = \frac{1}{2}G_{ij}v^i v^j\,. \tag{4.8}$$

Contracting Eq. (4.7) with v_i yields the evolution equation for the slow-roll parameter ϵ

$$\epsilon' + (3 - \epsilon)\left(2\epsilon + (\ln V)_{,i}v^i\right) = 0\,, \tag{4.9}$$

from which we observe that the logarithmic gradient terms are the relevant quantities that determine the evolution of ϵ.

Working in the field space it is often useful to switch from the coordinate basis $\{\phi^i\}$ (with basis vectors $\boldsymbol{e}_i = \partial_i$) to a local orthonormal basis. In general, basis vectors are not orthogonal to each other

$$\boldsymbol{G}(\boldsymbol{e}_i, \boldsymbol{e}_j) = G_{ij} \neq 0\,, \quad \text{for } i \neq j\,. \tag{4.10}$$

With a suitable redefinition of the basis vectors, e.g. $\hat{\boldsymbol{e}}_i = E_i^j \boldsymbol{e}_j$, the coefficients E_i^j can be chosen such that

$$\boldsymbol{G}(\hat{\boldsymbol{e}}_i, \hat{\boldsymbol{e}}_j) = \delta_{ij}\,. \tag{4.11}$$

To avoid confusion between indices referring to different bases we will use lower case letters for components in the coordinate basis and capital letters for the orthonormal basis. Hence, the orthonormal basis vectors will be denoted as

$$\hat{\boldsymbol{e}}_A = E_A^j \boldsymbol{e}_j\,, \qquad \text{and} \qquad \boldsymbol{e}_i = E_i^A \hat{\boldsymbol{e}}_A\,, \tag{4.12}$$

with E_i^A is the inverse matrix defined from $E_A^j E_i^A = \delta_i^j$. Eq. (4.11) implies that the coefficients E_A^i satisfy

$$G_{ij}E_A^i E_B^j = \delta_{AB}\,. \tag{4.13}$$

Inversion of the latter yields

$$G_{ij} = \delta_{AB}E_i^A E_j^B\,, \tag{4.14}$$

known as the orthogonal decomposition of the metric.

A particularly useful orthonormal basis is the Frenet system.[2] Working in 2D for simplicity, the unit tangent vector and the normal (or curvature) vector provide an orthonormal basis. The unit tangent vector is

$$t^i \equiv \frac{\dot\phi^i}{|\dot\phi^i|} = \frac{\dot\phi^i}{\sqrt{\mathcal{G}_{ij}\dot\phi^i\dot\phi^j}} = \frac{\mathrm{d}\phi^i}{\mathrm{d}\sigma}\,, \tag{4.15}$$

where in the last we defined the length of the curve (σ) in the field space from $\dot\sigma \equiv \sqrt{\mathcal{G}_{ij}\dot\phi^i\dot\phi^j}$. Since the previous vector has unit length, its derivative with respect to some parameter (e.g. σ) should vanish

$$\frac{\mathrm{d}}{\mathrm{d}\sigma}t^i t_i = 2t_i\,\mathrm{D}_\sigma t^i = 0 \Rightarrow \mathrm{D}_\sigma t^i \perp t^i\,. \tag{4.16}$$

This relation provides a way to define the orthogonal (to the unit) vector. The normal vector will be proportional to the covariant total derivative of the tangent vector $n^i \propto \mathrm{D}_\sigma t^i$. Dividing with its norm we define the normal vector as

$$n^i \equiv \frac{\mathrm{D}_\sigma t^i}{|\mathrm{D}_\sigma t^i|}\,. \tag{4.17}$$

For these two vectors the E coefficients are found to be

$$E^1_i = t_i\,, \qquad E^2_i = n_i\,, \tag{4.18}$$

and Eq. (4.14) yields the following decomposition of the metric

$$\mathcal{G}_{ij} = t_i t_j + n_i n_j\,, \tag{4.19}$$

valid for two fields.

When the cosmic time is considered the proportionality constant in the covariant derivative of the tangent vector is called the turn rate

$$\mathrm{D}_t t^i = \omega n^i\,. \tag{4.20}$$

This proportionality constant (called curvature of the line in differential geometry [104]) measures deviation from geodesic motion. Indeed, when it vanishes we have

$$\mathrm{D}_t\dot\phi^i = \frac{\ddot\sigma}{\dot\sigma}\dot\phi^i\,, \tag{4.21}$$

---

[2]In 3D this is known as the tnb system, where the initials stand for tangent, normal and binormal accordingly (see Fig. 4.1).
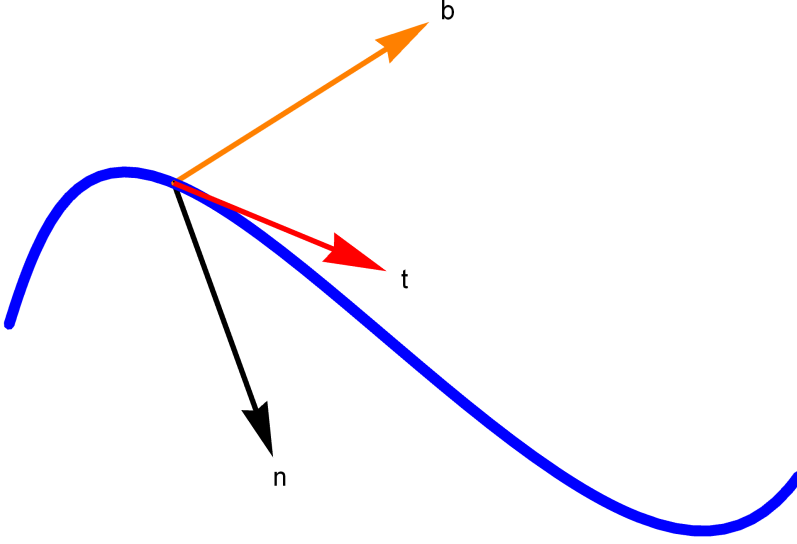
FIGURE 4.1
Illustration of the local orthonormal basis for a curve in three dimensions.

which is known as the pre-geodesic equation, i.e. geodesic equation up to a non-affine reparameterization. Switching to the σ parameterization we obtain

$$\dot{\sigma}\, \mathrm{D}_t \left(\frac{\mathrm{d}\phi^i}{\mathrm{d}\sigma} \right) + \ddot{\sigma}\frac{\mathrm{d}\phi^i}{\mathrm{d}\sigma} = \frac{\ddot{\sigma}}{\dot{\sigma}}\dot{\phi}^i \Rightarrow \mathrm{D}_\sigma \left(\frac{\mathrm{d}\phi^i}{\mathrm{d}\sigma} \right) = 0\,, \qquad (4.22)$$

that is the geodesic equation.

This base can be utilized to extract some useful information about the dynamics of the model. Projecting the equations of motion along the tangent direction gives the evolution equation of σ[3]

$$t_i\, \mathrm{D}_t \dot{\phi}^i + 3Ht_i\dot{\phi}^i + V^{,i}t_i \Rightarrow \ddot{\sigma} + 3H\dot{\sigma} + \frac{\mathrm{d}V}{\mathrm{d}\sigma} = 0\,. \qquad (4.25)$$

---

[3]With boldface subscript we denote the derivative of a scalar function in the direction of a vector $\boldsymbol{a}$

$$V_{,\boldsymbol{a}} \equiv \frac{\partial V}{\partial \boldsymbol{a}} \equiv \lim_{h \to 0} \frac{V(\boldsymbol{\phi}_0 + h\boldsymbol{a}) - V(\boldsymbol{\phi}_0)}{h} = \mathbf{d}V(\boldsymbol{a}) = a^i V_{,i}\,. \qquad (4.23)$$

When $a^i = \mathrm{d}\phi^i/\mathrm{d}\sigma$ then the directional derivative becomes a total derivative with respect to the parameter σ

$$V_{,\boldsymbol{a}} = \frac{\mathrm{d}V}{\mathrm{d}\sigma} \equiv \mathrm{d}_\sigma V\,. \qquad (4.24)$$

In a loose sense, σ can be thought of as a canonically normalized field subject to the gradient $V_{,\boldsymbol{t}}$. Similarly, projecting the gradient vector along n^i gives an expression proportional to the turn rate

$$\omega = -\frac{n^i V_{,i}}{\dot{\sigma}} . \tag{4.26}$$

Using Eq. (4.25) we can express the normal vector in terms of $\mathrm{d}_\sigma V$

$$\mathrm{D}_t t^i = \frac{\mathrm{D}_t \dot{\phi}^i}{\dot{\sigma}} - \frac{\ddot{\sigma}}{\dot{\sigma}} t^i = -\frac{V^{,i} - t^i V_{,\boldsymbol{t}}}{\dot{\sigma}} , \tag{4.27}$$

and further obtain an expression for the turn rate

$$\omega^2 = \frac{V^{,i} V_{,i} - V_{,\boldsymbol{t}}^2}{\dot{\sigma}^2} . \tag{4.28}$$

Alternatively, ω can be expressed in terms of ϵ and η using Eq. (6.3) as

$$\omega^2 = H^2 (3 - \epsilon)^2 \left[\frac{\epsilon_V}{\epsilon} - \left(\frac{\eta}{2(3 - \epsilon)} + 1 \right)^2 \right] . \tag{4.29}$$

When the slow-roll conditions are satisfied we find two limiting cases: in the slow-turn limit (i.e. $\eta, (\omega/H) \ll 1$) the potential and Hubble slow-roll parameters coincide $\epsilon \approx \epsilon_V$, whereas in the large turn-rate limit ($\eta \ll 1$ and $\omega/H \gg 1$) the slow-roll parameter satisfies $\epsilon \ll \epsilon_V$. In the latter case, Eq. (4.29) reduces to the expression first given in [105]. Thus, in multi-field inflation with $\epsilon' \ll 1$ we have $\epsilon \leq \epsilon_V$.

All we did in this section was to express the equations of motion in the local orthonormal basis. The advantage of this basis will become clear when studying slow-roll inflation for multiple fields; this is the topic of the next section.

4.3 Multi-field slow-roll conditions

At the background level, the single-field slow-roll conditions (3.13) classify potentials according to their ability to sustain slow-roll behaviour. The classification of various models with standard kinetic terms is based completely on two properties of the potential, namely the relative magnitudes of $V_{,\phi}$ and $V_{,\phi\phi}$ with V.

For multiple fields the situation is more complicated because one has to take into account geometric contributions originating from the field metric.

A slow-roll approximation becomes more obscure because even if second-order time derivatives are neglected, one is still left with an algebraic system for the velocities which in general is second order (through the Christoffel terms) and not covariant. Therefore, it is not entirely clear which time-derivative terms should be omitted.

As a first step, we will consider the most trivial requirement for slow-roll inflation, $\epsilon' \ll 1$, since otherwise ϵ will grow fast enough and inflation will not last for a sufficient number of e-folds. Eq. (4.7) implies that the condition

$$\epsilon' \ll 1 \,, \tag{4.30}$$

is equivalent to

$$2\epsilon \approx -p_i v^i = -\frac{V_{,i}\dot{\phi}^i}{VH} \Rightarrow \sqrt{2\epsilon} \approx -\frac{V_{,t}}{V} \,. \tag{4.31}$$

Comparing the latter with Eq. (4.25) implies that the adiabatic field follows its potential gradient:

$$\epsilon \approx \frac{1}{2}\left(\frac{V_{,t}}{V}\right)^2 \equiv \epsilon_{\mathrm{ad}} \,. \tag{4.32}$$

In addition, the derivative with respect to the e-folding number of Eq. (4.32) should be small as well

$$
\begin{aligned}
\epsilon' &= \frac{V_{,t}}{V}\left(\frac{V_{;ij}t^i v^j}{V} + \frac{V_{,i}\,\mathrm{D}_N t^i}{V} - \frac{V_{,t}}{V}\frac{V_{,i}v^i}{V}\right)\\
&= \sqrt{2\epsilon}\frac{V_{,t}}{V}\left(\frac{V_{;ij}t^i t^j}{V} + \frac{\omega V_{,i}n^i}{VH\sqrt{2\epsilon}} - \left(\frac{V_{,t}}{V}\right)^2\right) \,,
\end{aligned}
\tag{4.33}
$$

or

$$\frac{1}{2}\eta \approx -\frac{V_{;ij}t^i t^j - \omega^2}{V} + 2\epsilon \,. \tag{4.34}$$

This motivates us to define a slow-roll parameter in the adiabatic direction as the second order directional derivative in the direction of the tangent vector [4] [106, 107]

$$\eta_{\sigma\sigma} \equiv \frac{1}{V}\frac{\mathrm{d}^2 V}{\mathrm{d}\sigma^2} = \frac{V_{;tt}}{V} = \frac{V_{;ij}t^i t^j - \omega^2}{V} \,. \tag{4.36}$$

---

[4]Note that the second order directional derivative is not in general equal to the projection of the Hessian along the vectors

$$\frac{\partial^2 V}{\partial t^2} \neq V_{;ij}t^i t^j \,. \tag{4.35}$$

The additional contribution exists whenever the tangent vector varies in space which is the case for a curved field space.

The slow-roll conditions $\epsilon, |\eta| \ll 1$ become equivalent to $\epsilon_{\mathrm{ad}}, |\eta_{\sigma\sigma}| \ll 1$, which, however, are not very useful in this form as they require knowledge of the background solutions $\dot{\phi}^i$. On the contrary, for a given model it is desirable to derive conditions on the derivatives of the potential, similar to the slow-roll conditions (3.14). We will devote the next section as well as Ch. 7 on methods to derive solutions in terms of the covariant derivatives of the potential and the metric.

4.4 The gradient flow approximation

The simplest way to satisfy the condition (4.30) is the case of vanishingly small components of the accelerating vector $\mathrm{D}_N v^i \ll 1$. This defines the *potential gradient flow*

$$v^i \approx -\frac{V^{,i}}{V} \,, \tag{4.37}$$

because motion is (almost) aligned with the flow of the potential gradient resulting to negligible turn rate. Substituting this into the slow-roll parameter $\eta_{\sigma\sigma}$ gives two conditions that restrict the norm of the gradient vector and the projection of the Hessian $V_{;i}{}^{j}$ along the gradient vector [108, 109]

$$\frac{G^{ij}V_{,i}V_{,j}}{2V^2} = \epsilon_V \approx \epsilon \ll 1 \,, \qquad \left|\frac{V_{;ij}V^{,i}V^{,j}}{VV^{,k}V_{,k}}\right| \ll 1 \,. \tag{4.38}$$

Both expressions reduce to their single-field counterparts for $\mathcal{N} = 1$. For gradient flow we can calculate the turn rate to first order in the slow-roll parameters. First, we will cast Eq. (4.29) into a more convenient form:

$$\Omega^2 = \frac{1}{2\epsilon}\,\mathrm{D}_N v^i\,\mathrm{D}_N v_i - \frac{\eta^2}{4} \,, \tag{4.39}$$

which gives us the expression for the turn rate

$$\Omega^2 \approx \left(G^{mn}\frac{V_{;im}}{V}\frac{V_{;jn}}{V} - \frac{V^{,m}V^{,n}}{V^{,k}V_{,k}}\frac{V_{;mn}}{V}\frac{V_{;ij}}{V}\right)\frac{V^{,i}V^{,j}}{V^{,k}V_{,k}} \,. \tag{4.40}$$

Using the relation $\omega = -n^i V_i/\dot{\sigma}$, which we rewrite as $\Omega = -(3 - \epsilon)n^i p_i$, we see that substituting the gradient flow solution $p_i \approx -v_i$ gives $\Omega \approx 0$. To get a better estimate we parametrize the error of the gradient-flow approximation as

$$E_i = v^i + p^i \,, \tag{4.41}$$

which obeys the differential equation

$$\mathrm{D}_N E_i = -(3 - \epsilon)E^i + \mathrm{D}_N p^i \,. \tag{4.42}$$

The error is supposed to satisfy $|E_i| \ll |v^i|, |p^i|$ and similarly $|\mathrm{D}_N E_i| \ll |\mathrm{D}_N v^i|, |\mathrm{D}_N p^i|$. Since $\mathrm{D}_N p^i$ is assumed to be small, it is reasonable to expect that the differential equation (4.42) admits a slow-roll solution for E^i and we get an estimate for the magnitude of the error

$$E^i \approx \frac{\mathrm{D}_N p^i}{(3 - \epsilon)} \,. \tag{4.43}$$

Using the latter we can estimate the difference of ϵ to ϵ_V as

$$\epsilon \approx \epsilon_V - p_i E^i \Rightarrow \epsilon - \epsilon_V \approx -p_i \frac{\mathrm{D}_N p^i}{(3 - \epsilon)} \approx -\frac{\epsilon \eta}{(3 - \epsilon)} \,, \tag{4.44}$$

and substituting back in Eq. (4.29) we observe that the term linear in η vanishes. Therefore, the turn rate in Eq. (4.39) is $\Omega^2 \sim \mathcal{O}\left(\epsilon \eta, \eta^2\right)$. We will examine this type of approximation in detail later in Sec. 4.8. Having thoroughly examined the background motion we turn our attention to linear perturbations.

4.5 Adiabatic and entropic perturbations

Similar to the one-field case (3.25), we define gauge-invariant perturbations

$$Q^i \equiv \delta \phi^i + \frac{\psi}{H} \dot{\phi}^i \,, \tag{4.45}$$

which obey the following equations [110]

$$\mathrm{D}_t^2 Q^i + 3H \mathrm{D}_t Q^i + \left(\frac{k^2}{a^2}\delta_j^i + M^i{}_j\right)Q^j = 0 \,. \tag{4.46}$$

In the latter expression M, often called 'mass matrix', is given by

$$M^i{}_j = G^{ik}V_{;kj} - R^i{}_{kmj}\dot{\phi}^k\dot{\phi}^m - \frac{1}{a^3}\mathrm{D}_t\left(\frac{a^3\dot{\phi}^i\dot{\phi}_j}{H}\right) = 0 \,. \tag{4.47}$$

Eq. (4.46) can be obtained from the second order part of the scalar-field action

$$S_2 = \frac{1}{2}\int \mathrm{d}t\,\mathrm{d}^3 x a^3 \left(\mathrm{D}_t Q^i\,\mathrm{D}_t Q_i - \frac{1}{a^2}\nabla Q_i \nabla Q^i - M_{ij}Q^iQ^j\right) \,. \tag{4.48}$$

Following the covariant formalism of Ref. [111], in the case of $\mathcal{N} = 2$ fields the metric can be decomposed into the direct sum of two orthogonal spaces $G = V_1 \oplus V_2$. In this decomposition, field-space vectors can be expressed as

$$Q^i = Q_\sigma t^i + Q_s n^i \,, \tag{4.49}$$

using the standard definitions for the two fields [5]

$$Q_\sigma \equiv Q^i t_i \,, \qquad Q_s \equiv Q^i n_i \,. \tag{4.50}$$

The orthonormal basis defined in the previous section has significant advantages in the calculation of observables. Perturbations along the motion correspond to adiabatic perturbations, whereas those along the orthogonal directions correspond to isocurvature (entropic) perturbations [112, 113]. After some algebra and the definition of the *effective mass of isocurvature perturbations on subhorizon scales* [6]

$$m_{\rm s}^2 \equiv V_{;ij} n^i n^j + \epsilon R H^2 - \omega^2 \,, \tag{4.51}$$

the quadratic part of the action in the adiabatic/entropic decomposition reads

$$S_2 = \frac{1}{2} \int \mathrm{d}t\, \mathrm{d}^3 x a^3 \Big[\dot{Q}_s^2 - \frac{1}{a^2} (\nabla Q_s)^2 - m_{\rm s}^2 Q_s^2 + 4\omega \left(\frac{\ddot{\sigma}}{\dot{\sigma}} + \frac{\dot{\sigma}^2}{2H} \right) Q_s Q_\sigma + \dot{Q}_\sigma^2$$
$$- \frac{1}{a^2} (\nabla Q_\sigma)^2 - \left((3 - \epsilon) H^2 (\eta_{\sigma\sigma} + 2\epsilon) + \frac{2\dot{\sigma} V_\sigma}{H} \right) Q_\sigma^2 - 4 \dot{Q}_\sigma \omega Q_s \Big] \,. \tag{4.52}$$

The equations of motion for the two gauge-invariant perturbations are

$$\ddot{Q}_\sigma + 3H\dot{Q}_\sigma - \frac{1}{a^2}\nabla^2 Q_\sigma + \left((3 - \epsilon) H^2 (\eta_{\sigma\sigma} + 2\epsilon) + \frac{2\dot{\sigma} V_\sigma}{H} \right) Q_\sigma =$$
$$2\,\mathrm{d}_t(\omega Q_s) - 2\omega \left(\frac{V_{,\sigma}}{\dot{\sigma}} - \frac{\dot{\sigma}^2}{2H} \right) Q_s \,, \tag{4.53}$$

$$\ddot{Q}_s + 3H\dot{Q}_s - \frac{1}{a^2}\nabla^2 Q_s + m_{\rm s}^2 Q_s = -2\omega\dot{Q}_\sigma + 2\omega \left(\frac{\ddot{\sigma}}{\dot{\sigma}} + \frac{\dot{\sigma}^2}{2H} \right) Q_\sigma \,, \tag{4.54}$$

where all expressions are exact.

---

[5] Recall that the components of Q in the orthonormal basis are raised and lowered using the Euclidean metric and so $Q^A = Q_A$.

[6] This term is called a mass because for geodesic motion ($\omega = 0$) Q_s decouples from Q_σ and its sign determines the growth or decay of isocurvature perturbations.

Similar to the one-field case, we define the curvature and entropic perturbations as

$$\mathcal{R} \equiv \frac{H}{\dot{\sigma}} Q_\sigma \,, \qquad \mathcal{S} \equiv \frac{H}{\dot{\sigma}} Q_s \,. \tag{4.55}$$

The derivative of the curvature perturbation can be expressed as

$$\mathcal{R}' = \frac{1}{\epsilon} \left(\frac{k}{aH} \right)^2 \Psi + 2\Omega\mathcal{S} \,. \tag{4.56}$$

The presence of isocurvature perturbations is responsible for the evolution of the curvature perturbation on superhorizon scales. Using the previous relation we can cast Eq. (4.54) into the more convenient form

$$\ddot{Q}_s + 3H\dot{Q}_s + \left(\frac{k}{a} \right)^2 Q_s + \left(m_{\mathrm{s}}^2 + 4\omega^2 \right) Q_s = 4M_{\mathrm{pl}}^2 \frac{\omega}{\dot{\sigma}} \left(\frac{k}{a} \right)^2 \Psi \,. \tag{4.57}$$

At large scales the equation of motion becomes

$$\ddot{Q}_s + 3H\dot{Q}_s + \mu_{\mathrm{s}}^2 Q_s \approx 0 \,, \tag{4.58}$$

where we defined the *effective mass of isocurvature perturbations on superhorizon scales*

$$\mu_{\mathrm{s}}^2 \equiv m_{\mathrm{s}}^2 + 4\omega^2 \,, \tag{4.59}$$

valid for two fields.

In order for the curvature perturbation to freeze at some point on superhorizon scales, orthogonal perturbations must decay and, hence, in general we demand this effective mass to be positive. Note that Eq. (4.58) is analogous to the background equation of motion for a quadratic field with a time-dependent mass. Therefore, if $\mu_s^2 > 0$ then $Q_s \rightarrow 0$ and it is reasonable to expect that the second derivatives will be subdominant.

Similarly, the evolution equation of the entropic perturbation $\mathcal{S}$ is found to be

$$\mathcal{S}'' + (3 - \epsilon + \eta)\mathcal{S}' + \left(\frac{3}{2}\eta + \frac{\mu_{\mathrm{s}}^2}{H^2} - \frac{3}{2}\eta\epsilon + \frac{1}{2}\frac{\epsilon''}{\epsilon} - \frac{1}{4}\eta^2 \right) \mathcal{S} = 0 \,. \tag{4.60}$$

When the slow-roll conditions hold, i.e. $\epsilon, |\eta| \ll 1$, and the term that multiplies $\mathcal{S}$ is positive, then to lowest order $\mathcal{S}$ obeys the following slow-roll equation

$$\mathcal{S}' \approx - \left(\frac{1}{2}\eta + \frac{\mu_{\mathrm{s}}^2}{3H^2} \right) \mathcal{S} \approx - \left(2\epsilon - \eta_{\sigma\sigma} + \frac{\mu_{\mathrm{s}}^2}{3H^2} \right) \mathcal{S} \,, \tag{4.61}$$

given that the term in parenthesis, denoted by β, is positive. Integrating Eq. (4.61) we obtain

$$\mathcal{S}(N) = \mathcal{S}_* e^{\int_{N_*}^N \mathrm{d}N' \beta} \,, \tag{4.62}$$

and the curvature perturbation on superhorizon scales becomes

$$\mathcal{R}(N) \approx \mathcal{R}_* + \mathcal{S}_* \int_{N_*}^N \mathrm{d}N' 2\Omega e^{\int_{N_*}^{N'} \mathrm{d}N'' \beta} \,, \tag{4.63}$$

where N_* is the reference number of e-folds. Note that at superhorizon scales there is no transfer from $\mathcal{R}$ to $\mathcal{S}$. The N-dependent terms of the above two equations are known as the transfer functions [114, 115]

$$T_{\mathcal{SS}} \equiv e^{\int_{N_*}^N \mathrm{d}N' \beta} \,, \qquad T_{\mathcal{RS}} \equiv \int_{N_*}^N \mathrm{d}N' 2\Omega T_{\mathcal{SS}} \,, \tag{4.64}$$

because they evolve the perturbations from a reference time (N_*) to the end of inflation ($N = 0$)

$$\mathcal{S}(N) = T_{\mathcal{SS}} \mathcal{S}_* \,, \qquad \mathcal{R}(N) \approx \mathcal{R}_* + T_{\mathcal{RS}} \mathcal{S}_* \,. \tag{4.65}$$

The power spectra are calculated from the correlation functions of these variables

$$\mathcal{P}_{\mathcal{R}}^2 \propto \langle \mathcal{RR} \rangle = \langle \mathcal{R}_* \mathcal{R}_* \rangle + T_{\mathcal{RS}}^2 \langle \mathcal{S}_* \mathcal{S}_* \rangle + 2 T_{\mathcal{RS}} \langle \mathcal{R}_* \mathcal{S}_* \rangle \,, \tag{4.66}$$

$$\mathcal{P}_{\mathcal{S}}^2 \propto \langle \mathcal{SS} \rangle = T_{\mathcal{SS}}^2 \langle \mathcal{S}_* \mathcal{S}_* \rangle \,, \tag{4.67}$$

$$\mathcal{C}_{\mathcal{RS}}^2 \propto \langle \mathcal{RS} \rangle = T_{\mathcal{SS}} \langle \mathcal{R}_* \mathcal{S}_* \rangle + T_{\mathcal{RS}} T_{\mathcal{SS}} \langle \mathcal{S}_* \mathcal{S}_* \rangle \,, \tag{4.68}$$

where we omitted the delta functions to suppress notation.

The superhorizon evolution calculated above will hold for all models with $\epsilon, |\eta| \ll 1$ and independently of the field-space geometry. To proceed we need an expression for the amplitude of perturbations at the reference time. It is useful to rewrite the action in terms of conformal time $\mathrm{d}t = a \, \mathrm{d}\tau$

$$
\begin{aligned}
S_2 = \frac{1}{2} \int \mathrm{d}\tau \, \mathrm{d}^3 x \Big[& \left(a \frac{\mathrm{d}Q_\sigma}{\mathrm{d}\tau} \right)^2 - (a\nabla Q_\sigma)^2 - (a\nabla Q_s)^2 - m_{\mathrm{s}}^2 \left(a^2 Q_s \right)^2 \\
& - \left((3-\epsilon) H^2 (\eta_{\sigma\sigma} + 2\epsilon) + \frac{2\dot{\sigma} V_\sigma}{H} \right) \left(a^2 Q_\sigma \right)^2 + \left(a \frac{\mathrm{d}Q_s}{\mathrm{d}\tau} \right)^2 \\
& - 4a^2 \frac{\mathrm{d}Q_\sigma}{\mathrm{d}\tau} \omega a Q_s + 4\omega \left(\frac{\ddot{\sigma}}{\dot{\sigma}} + \frac{\dot{\sigma}^2}{2H} \right) a^4 Q_s Q_\sigma \Big] \,.
\end{aligned}
\tag{4.69}
$$

Then, we define the Mukhanov-Sasaki variables $u^I \equiv aQ^I$ and using the following definitions

$$\frac{1}{a}\frac{\mathrm{d}^2 a}{\mathrm{d}\tau^2} = 2a^2 H^2 - a^2 \frac{1}{2}\dot\sigma^2 \,, \tag{4.70a}$$

$$\frac{1}{z}\frac{\mathrm{d}z}{\mathrm{d}\tau} = a\frac{\ddot\sigma}{\dot\sigma} + a\frac{\dot\sigma^2}{2H} + aH \,, \tag{4.70b}$$

$$\frac{1}{z}\frac{\mathrm{d}^2 z}{\mathrm{d}\tau^2} = -a^2\left(m_{\mathrm{s}}^2 + (3-\epsilon)\dot\sigma^2 + \frac{2\dot\sigma V_\sigma}{H}\right) + 2a^2 H^2 - a^2 \frac{1}{2}\dot\sigma^2 \,, \tag{4.70c}$$

the action takes the simpler form

$$S_2 = \frac{1}{2}\int \mathrm{d}\tau\,\mathrm{d}^3 x\Big[\left(\frac{\mathrm{d}u_\sigma}{\mathrm{d}\tau}\right)^2 - (\nabla u_\sigma)^2 + \frac{1}{z}\frac{\mathrm{d}^2 z}{\mathrm{d}\tau^2}u_\sigma^2 + \left(\frac{\mathrm{d}u_s}{\mathrm{d}\tau}\right)^2 - (\nabla u_s)^2$$
$$+ \left[\frac{1}{a}\frac{\mathrm{d}^2 a}{\mathrm{d}\tau^2} - a^2 m_{\mathrm{s}}^2\right]u_s^2 - 4a\frac{\mathrm{d}u_\sigma}{\mathrm{d}\tau}\omega u_s + 4\omega\frac{1}{z}\frac{\mathrm{d}z}{\mathrm{d}\tau}au_s u_\sigma\Big] \,. \tag{4.71}$$

The equations of motion are

$$u_\sigma'' - \nabla^2 u_\sigma - \frac{1}{z}\frac{\mathrm{d}^2 z}{\mathrm{d}\tau^2}u_\sigma - 2(a\omega u_s)' - 2\omega\frac{1}{z}\frac{\mathrm{d}z}{\mathrm{d}\tau}au_s = 0 \,, \tag{4.72}$$

$$u_s'' - \nabla^2 u_s - \left[\frac{1}{a}\frac{\mathrm{d}^2 a}{\mathrm{d}\tau^2} - a^2 m_{\mathrm{s}}^2\right]u_\sigma + 2a\omega u_\sigma' - 2\omega\frac{1}{z}\frac{\mathrm{d}z}{\mathrm{d}\tau}au_\sigma = 0 \,, \tag{4.73}$$

and describe a system of coupled oscillators with friction. It should be noted that solving the previous equations is a highly non-trivial task. In the following section we will show how to derive observables in the simplest scenario of gradient flow.

4.6   Power spectra for trivial field geometry

For models with standard kinetic terms covariant time derivatives become ordinary derivatives and the perturbations' equations simplify to

$$\ddot Q^i + 3H\dot Q^i + \left[\frac{k^2}{a^2}\delta^i_j + \delta^i_j V_{,kj} - \frac{1}{a^3}\,\mathrm{D}_t\left(\frac{a^3\dot\phi^i\dot\phi_j}{H}\right)\right]Q^j = 0 \,. \tag{4.74}$$

This has an important implication: perturbations are coupled only via $A^i_j Q^j$ terms and not through time derivatives of the fields. If we denote the term in the parenthesis as A^i_j, the equations in matrix form can be written as

$$\ddot{\boldsymbol{Q}} + 3H\dot{\boldsymbol{Q}} + \boldsymbol{A}\cdot\boldsymbol{Q} = 0 \,, \tag{4.75}$$

where Q and A are 2×1 and 2×2 matrices respectively. Deep inside the horizon, the k-dependent part of A dominates and equations of motion describe two uncoupled oscillators; perturbations Q^i are in the Bunch-Davies vacuum. However, perturbations are coupled at horizon crossing due to the off-diagonal components of A. To find an expression for the amplitude of these perturbations close to $k_* \approx a_* H_*$ we will consider the k-dependent part constant, and then perform an orthogonal rotation of Q that diagonalizes A [116]. The two equations can be decoupled:

$$\ddot{U} + 3H\dot{U} + D \cdot U = 0 \,, \tag{4.76}$$

where D is a diagonal matrix and $U = LQ$. If the slow-roll parameters are slowly varying then we can treat the elements of the matrix D as constant and find solutions in terms of the Hankel's functions.

With Q^i known, $\mathcal{R}$ and $\mathcal{S}$ can be calculated using the linear relations between them (Eqs. (4.62) and (4.63)), which amounts to an extra rotation in field space. For slow-turn models a close look at Eq. (4.72) shows that the two perturbations are also (almost) uncorrelated at horizon crossing. Therefore, the lowest order part will be given by the usual single-field amplitude

$$|\mathcal{R}_*| \sim |\mathcal{S}_*| \sim \sqrt{\frac{2}{\epsilon}} \frac{H_*}{2\pi} \,, \tag{4.77}$$

while the cross-correlations are negligible. The power spectra (at the end of inflation) are given by

$$\mathcal{P}_\mathcal{R}^2 = \frac{H_*^2}{2\pi^2 \epsilon_*} \left(1 + T_{\mathcal{RS}}^2 \right) \,, \qquad \mathcal{P}_t^2 = \frac{8}{M_{\text{pl}}^2} \left(\frac{H_*}{2\pi} \right)^2 \,, \tag{4.78}$$

from which we can calculate the spectral index and the tensor-to-scalar ratio

$$n_s = n_s(N_*) + \frac{\partial T_{\mathcal{RS}}}{\partial N_*} \frac{2T_{\mathcal{RS}}}{1 + T_{\mathcal{RS}}^2} \,, \qquad r = \frac{16\epsilon_*}{1 + T_{\mathcal{RS}}^2} \,. \tag{4.79}$$

Note that for most models the transfer functions have to be computed numerically.

On the contrary, non-Gaussian signatures are much harder to compute analytically and the computation becomes problem dependent. One has to resort to the δN formalism [117] but even in this case the method is limited to specific potentials (sum- or product-separable) in addition to the gradient-flow approximation [118, 119]. Nevertheless, certain conclusions can be derived in a model-independent way by studying the EFT of fluctuations. Regarding multi-field effects, the different possibilities for

predictions depend on the magnitude of the effective mass on superhorizon scales, leading to the following three regimes:

- the light regime, $\mu_s \ll H$, is realized by the gradient-flow models studied in this section. They usually produce local-type non-Gaussianity [120, 121].

- the heavy-field regime, $\mu_s \gg H$, along with a few other requirments, allows the derivation of an effective description by integrating out the heavy field and results in a single-field problem with reduced speed of sound. These models can have either small [88–90] or large turn rate [122] and can produce large equilateral non-Gaussianity [123].

- the intermediate regime, $\mu_s \approx H$, was extensively studied in the cosmological collider paradigm [124]. The squeezed limit of the bispectrum offers rich phenomenology and opportunities to test for new physics, while its non-Gaussianity interpolates from local-type to equilateral (see also [125] for a recent study in this direction).

4.7   Challenges of multi-field model building

Arguably, the most serious problem one faces when considering more than one fields is the initial conditions dependence during the inflationary phase. This becomes apparent for models following the gradient flow approximation, which fixes only the velocities through the relations

$$v^i \propto (\ln V)^{,i} . \tag{4.80}$$

This system of $\mathcal{N}$ equations can be solved in terms of a reference field $\phi^{(k)}$

$$\frac{\mathrm{d}\phi^i}{\mathrm{d}\phi^{(k)}} = \frac{V^{,i}}{V^{,(k)}} , \tag{4.81}$$

which provides $\mathcal{N} - 1$ parametric relations $\phi^i = \phi^i(\phi^{(k)}, \phi_0^j)$. For sum- or product-separable potentials analytical expressions for these relations are guaranteed (see e.g. [126]). The crucial difference with single-field models is the dependence on extra parameters which results to different background quantities, all compatible with the slow-roll conditions (4.38). Different background quantities lead to different predictions and multi-field inflation becomes non-predictive (we will study initial conditions dependence in more detail in Ch. 8).

The only way to overcome this issue is to consider models that utilize an attractor mechanism that stabilizes all fields but one and sufficiently

fast during the evolution. In general, these models require a hierarchy between the parameters of the model, such as the fields' masses (more precisely the gradients), coupling parameters in non-minimally coupled scenarios (e.g. [111, 127–130]), or lengths associate with derivatives of the field metric. In the next chapter we will explicitly demonstrate how a hierarchy in the strength of the field metric leads to quick stabilization of the extra field which, nevertheless, leaves significant imprints on observables.

4.8 Case example: the quadratic potential revisited

We conclude this chapter with an explicit demonstration of a number of novelties that one encounters when going from one to multiple fields during inflation. We will first illustrate this behaviour in the very simplest multi-field model consisting of $\mathcal{N}$ fields with a quadratic potential and a flat field-space background

$$V = \frac{1}{2} \sum m_i^2 \phi_i^2 \,. \tag{4.82}$$

The model admits approximate solutions following the gradient flow (with negligible acceleration)

$$\dot{\phi}_i = -\frac{m_i^2}{\sqrt{3V}} \phi_i \,, \tag{4.83}$$

and so one can find the parametric relations between the fields using Eqs. (4.81)

$$\phi_i = \phi_{i,0} \left(\frac{\phi_1}{\phi_{1,0}} \right)^{m_i^2/m_1^2} \,, \tag{4.84}$$

in terms of e.g. the reference field ϕ_1. Using these relations, the number of e-folds can be calculated as a function of the fields; in fact, for this particular problem it is simpler to switch to polar coordinates and invert the radial velocity to solve for N

$$\Delta N = \int \mathrm{d}r \frac{\mathrm{d}N}{\mathrm{d}r} = -\int \mathrm{d}r \frac{V}{V^{,r}} = -\frac{1}{4} \sum \left(r^2 - r_{\mathrm{end}}^2 \right) \,, \tag{4.85}$$

where N runs from negative values to zero at the end of inflation and $r^2 = \sum \phi_i^2$. Note that contrary to the single-field case, the time of generation of fluctuations (which we consider to be at $N = -55$) is not uniquely defined, but rather it is represented by the $\mathcal{N} - 1$ hypersphere $r^2 = 4 \cdot 55$ (where again the contribution from the endpoints is negligible to first order in
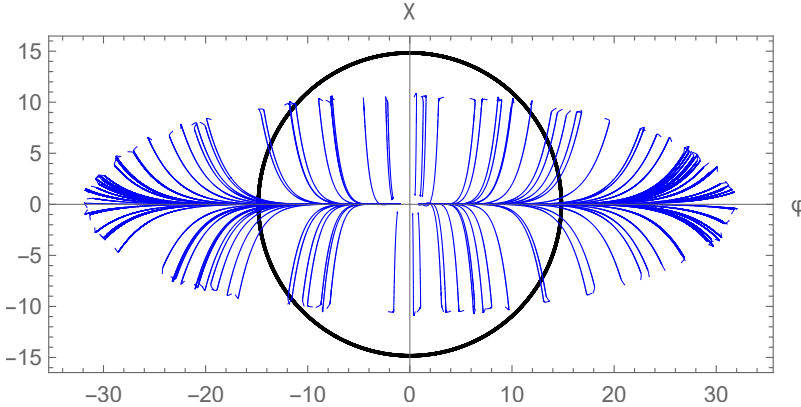
FIGURE 4.2

Numerical trajectories projected in the (ϕ_1, ϕ_2) plane with $m_\chi = 3m_\phi$ for 120 realizations with random initial conditions satisfying $\epsilon_0 = 0.9$ and $V_0 = 500$. The black line corresponds to the field values at 55 e-folds before the end of inflation.

the slow-roll parameters). Every trajectory crossing this hypersphere will provide 55 *e*-folds and so the notion of initial conditions independence of single-field models is lost when more fields are considered. We have plotted several trajectories for two fields in Fig. 4.2.

This initial conditions dependence of the background is inherited to observables as well. To derive the latter we will make use of the horizon-crossing approximation [110], which is an alternative method to calculate the curvature perturbation. This method is restricted to models following the gradient flow and it also assumes that an adiabatic limit has been reached before inflation ends [131]; at the level of perturbations this means that isocurvature perturbations have decayed a few *e*-folds before the end of inflation. In the horizon-crossing approximation the power spectra are given in terms of field derivatives of the *e*-folding number as

$$\mathcal{P}_\mathcal{R}^2 = \left(\frac{H}{2\pi}\right)^2 N^{,i} N_{,i}\Big|_{N=N_*} = -\left(\frac{H_*}{2\pi}\right)^2 N_* \,, \tag{4.86}$$

$$\mathcal{P}_t^2 = \frac{8}{N^{,i} N_{,i}}\Big|_{N=N_*} = -\frac{8}{N_*} \,. \tag{4.87}$$

Remarkably, the tensor-to-scalar ratio is uniquely determined (to lowest order), even though the background evolution is not, and independently of the number of fields. For two fields, in particular, the scalar spectral index

becomes a function of the angle [132]:

$$n_s|_{2f} = 1 + \frac{1}{N_*}\left(1 + \frac{\cos^2\theta_* + R_m^2\sin^2\theta_*}{(\cos^2\theta_* + R_m\sin^2\theta_*)^2}\right),\qquad(4.88)$$

where we have defined the ratio between the two masses as $R_m \equiv m_2^2/m_1^2$. Two values are worth highlighting, in view of the multi-field discussion that will follow: the first is the diagonal value at $\theta = \pi/4$; here the spectral index takes the value

$$n_s|_{2f-\text{diag}} = 1 + \frac{1}{N_*}\left[2 + \left(\frac{R_m - 1}{R_m + 1}\right)^2\right],\qquad(4.89)$$

where we have separated off the single-field result (coinciding with $m_1 = m_2$, where one has an $SO(2)$ symmetric potential and hence radial motion). The second value is $\theta_* = \text{arccot}(m_2/m_1)$ where the spectral index takes the smallest, most redshifted, value:

$$n_s|_{2f-\text{equip}} = 1 + \frac{1}{N_*}\left(2 + \frac{(R_m - 1)^2}{4R_m}\right).\qquad(4.90)$$

This corresponds to an energy equipartition between both fields, i.e. $m_1^2\phi_1^2 = m_2^2\phi_2^2$. Note that we have strictly $n_s|_{\text{equip}} < n_s|_{\text{diag}} < n_s|_{\text{single}}$ for all $m_1 \neq m_2$, turning into equalities in the case of equal masses.

The above calculations for the spectral index have a natural generalization to $\mathcal{N}$ fields, with CMB horizon crossing being an $(\mathcal{N}-1)$-dimensional hypersphere. The explicit parametrization of the spectral index in terms of the different angles becomes somewhat cumbersome; however, for the two specific cases that we highlighted one finds significant simplifications. To this end, we write the spectral index as

$$n_s|_{\text{multi}} - 1 = \frac{1}{N_*} - \frac{4\sum m_i^4\phi_i^2}{(\sum m_i^2\phi_i^2)^2} = \frac{1}{N_*}\left(1 + \frac{\sum m_i^4\tilde{\phi}_i^2}{\left(\sum m_i^2\tilde{\phi}_i^2\right)^2}\right),\qquad(4.91)$$

where we have rescaled the field values at CMB horizon crossing with $\sum\phi_i^2 = 4N$ to $\tilde{\phi}_i$ with norm 1, which can therefore be interpreted as a probability distribution and the fraction in brackets is always greater or equal to one. *This shows that the multi-field result is bounded from above by the single-field result.* This was known for a long time [133] but the lower bound was missing from the literature; we will calculate it in what follows. For three masses the configuration that makes ϵ maximum (and hence n_s

minimum) corresponds to the two extrema fields (i.e. the lightest and heaviest fields) participate with equal energies. Based on this observation, for any other configuration with an arbitrary number of fields ϵ will bounded by the equipartitioned two-field result and we **strictly** have

$$n_s|_{\text{2f}-\text{equip}} < n_s|_{\text{multi}} < n_s|_{\text{single}} \,. \tag{4.92}$$

Therefore, for a given set of masses, the lowest value for the spectral index is obtained by storing equal energies in the fields with lowest and highest masses, and zero energies in all fields in between.

5
Angular inflation

In this chapter we study observational signatures from a two-field generalization of the usual α-attractor model. We consider a hyperbolic field space, written in Poincaré coordinates, and two massive quadratic fields. We explore the dynamics for a wide range of the model's parameters, namely the mass ratio of the two fields (R_m) and the curvature of the field space $(8/\alpha)$. This chapter is largely based on the publication [106] with the addition of Sec. 5.3.1.

5.1   Relevance of α-attractor models

While many models have been constructed to date, following the *Planck* 2013 release [134] a different argumentation has been put forward. This employs the non-trivial structure of multi-field kinetic terms. At the two-derivative level, these can be interpreted as a scalar geometry G_{ij}. Inflation on a curved scalar manifold displays a variety of novel signatures due to geometric effects, including imprints from heavy fields during turns in field space [89, 90], curvature fluctuations from ultra-light entropy modes [135], as well as inflationary destabilization due to curvature [87].

Remarkably, in the specific (and highly symmetric) case of a hyperbolic scalar geometry, one naturally satisfies the Planck bounds on the spectral index and tensor-to-scalar ratio. As a result of the kinetic interactions on the hyperbolic manifold, there is a significant insensitivity to the potential interactions, leading to robust predictions that take the form [136]

$$n_{\rm s} \sim 1 + \frac{2}{N_*}\,, \qquad r \sim \frac{12\alpha}{N_*^2}\,, \tag{5.1}$$

to leading order in an expansion in the inverse number of *e*-folds $1/N$, where we consider the CMB-relevant perturbations to have exited the horizon N_* *e*-folds before the end of inflation. These depend on a single parameter α that sets the hyperbolic curvature. The same predictions can be reached from different perspectives, including Starobinsky's model with $\alpha = 1$ [54] and non-minimal couplings with $\alpha = 1 + 1/(6\xi)$ [137, 138]. At some level, the unifying feature of all these approaches can be attributed to a singularity in the kinetic sector, whose leading Laurent expansion determines the inflationary predictions [139].

Importantly, the above predictions were derived under the assumption of an effectively single-field trajectory. This can be achieved by the inclusion of higher-order terms that render the orthogonal directions heavy (see e.g. Ref. [140]). However, it would be interesting to see what genuine multi-field effects can arise in a more general situation. From a theoretical perspective, our current understanding of high-energy theories suggests a multitude of scalar fields, without an a priori reason that only one of these should be light. Similarly, from an observational perspective, such multi-field effects might allow for novel signatures, as has been studied in great detail in a wide variety of models, including $\mathcal{N}$-flation [141], many-field models [142, 143] or inspired by random matrix theories [144, 145].

Recently, a study of multi-field effects in a hyperbolic manifold, as suggested by the *Planck* results, was undertaken in Ref. [146]. Remarkably,

it was found that under a set of conditions, even multi-field inflationary trajectories on a hyperbolic manifold adhere to the above universal predictions. For instance, one can consider a scalar potential with a rotationally symmetric mass term and a symmetry-breaking quartic term, both of which live on the Poincare disk (and admit a simple supergravity embedding when $\alpha = 1/3$). The background dynamics was found to be almost perfectly radial in a range of parameter values, "rolling on a ridge", despite the presence of an angular slope. Moreover, perturbations around this non-trivial background have a remarkable structure that results in predictions identical to those in Eq. (5.1) despite the presence of multi-field effects.

This chapter will build on previous work by investigating the multi-field behaviour of α-attractors in a wide range of parameter space, and by pointing out multi-field effects that go beyond the universal behaviour. As the simplest possible case, we will study quadratic potentials on the Poincaré disk and consider a range of masses and hyperbolic curvatures. In addition to the above radial dynamics with universal behaviour, we will display a second regime of inflation that proceeds along the angular direction. Instead of the radial dynamics, which corresponds to gradient flow, angular inflation only employs this approximation for the angular coordinate, while the radial coordinate to a first approximation is frozen. We will outline when this novel regime appears, why it can be thought of as an alternative attractor,[1] and how it modifies the duration and predictions of inflation.

5.2   Background evolution

5.2.1   The multi-field α-attractor model

The two fields Φ, X take values on the Poincaré disk with the field-space metric

$$G_{ij} = \frac{6\alpha}{(1 - \Phi^2 - X^2)^2} \delta_{ij} \,, \tag{5.2}$$

in which the fields are dimensionless, since we are measuring both the fields and the curvature parameter α in units of M_{pl}. We use a quadratic potential, due to its simplicity and as a first step towards a generalization

---

[1]One might think that this regime is related to that of hyperinflation [147,148], which also crucially relies on the hyperbolic manifold. However, hyperinflation is an alternative to slow-roll inflation in the case of a very steep and rotationally symmetric potential.

of extensive studies of multi-field effects in inflation [132]:

$$V = \frac{6\alpha}{2} \left(m_\phi^2 \Phi^2 + m_\chi^2 X^2 \right) , \quad R_{\rm m} \equiv \frac{m_\chi^2}{m_\phi^2} . \tag{5.3}$$

For concreteness we will always consider $R_{\rm m} > 1$. Note that the factor 6α has been inserted to give the potential the correct dimensions and to recover the usual quadratic potential in the flat limit $\alpha \to \infty$ (after the appropriate rescaling of the fields).

Due to the spherical symmetry of the field-space manifold, it will be useful to introduce polar coordinates $\Phi = r\cos\theta$ and $X = r\sin\theta$. In this parametrization of the hyperbolic geometry, the scalar field equations read

$$\ddot{r} + 3H\dot{r} + \frac{1}{6} \left(m_\phi^2 \cos^2\theta + m_\chi^2 \sin^2\theta \right) (1-r^2)^2 r + \frac{2r\dot{r}^2}{1-r^2}$$
$$- \frac{r(r^2+1)}{1-r^2}\dot{\theta}^2 = 0 , \tag{5.4}$$

$$\ddot{\theta} + \frac{2(1+r^2)}{r(1-r^2)}\dot{r}\dot{\theta} + 3H\dot{\theta} + \frac{1}{12}(m_\chi^2 - m_\phi^2)\left(1-r^2\right)^2 \sin(2\theta) = 0 . \tag{5.5}$$

In some of the following plots we will use the canonical radius $\psi = \sqrt{6\alpha}\tanh^{-1}(r)$ to visualize the different regimes of the fields' evolution, with horizontal and vertical components $\phi = \psi\cos\theta$ and $\chi = \psi\sin\theta$.

5.2.2 'Radial' slow-roll inflation

Starting with the radial equation of motion, it was shown in Ref. [146] that for initial conditions placing the two fields close to the boundary of the Poincaré disc, a period of radial inflation with $\theta(t) \simeq \theta_0$ is supported, where θ_0 is the initial value of the angle in field-space. Provided the initial velocities are sufficiently small, a phase of slow-roll inflation ensues during which the gradient term is counterbalanced by the Hubble friction. Intuitively, this can be understood as the Christoffel terms depend quadratically on the velocities whereas the accelerations can be viewed as finite differences of small quantities.

More precisely, the range of validity of the gradient flow approximation can be measured by the smallness of the multi-field generalization of the single field slow roll parameters given by Eq. (4.38). If both parameters remain small up to the last few *e*-folds, then the evolution equations can be approximated by slow roll and the end of inflation can be estimated by $\epsilon_V \approx 1$. Using the slow roll expressions for the velocities

$$\frac{\dot{r}_{\rm SR}}{\dot{\theta}_{\rm SR}} = \frac{V^{,r}}{V^{,\theta}} , \tag{5.6}$$

we can obtain the relation $r(\theta)$. Since the metric is conformally flat it drops out from the above expression and the parametric relation $r(\theta)$ has exactly the same form as in the flat case. It is straightforward to calculate the number of e-folds:[2]

$$N_{\text{radial}} = -\int_{r_{\text{end}}}^{r} \mathrm{d}\tilde{r} \frac{V}{V_{,\tilde{r}}} = -\frac{3\alpha}{2}\left(\frac{1}{1-r^2} - \frac{1}{1-r_{\text{end}}^2}\right). \tag{5.7}$$

The number of radial e-folds has the same form as in single-field α-attractors [136] and is controlled by the curvature of field-space and the proximity of the initial conditions to the boundary of the Poincaré disc. At the end of inflation, given the fact that the potential has a light direction, the system will have to relax in such a way, as to evolve along the light direction. For the parameter range considered in Ref. [146], where both the angular gradients and the field space curvature were small (this statement will be quantified shortly), this relaxation towards the light field direction only lasts for one or two e-folds (an illustration of this can be found in the left panel of Fig. 5.1). Before we proceed we must note that, although the trajectories considered in Ref. [146] are highly radial, the existence of a non-zero turn rate is important and one cannot neglect multi-field effects.

However, the validity of the slow-roll approximation breaks down earlier as one considers large hyperbolic curvatures. The first slow-roll parameter is given by

$$\epsilon_{\text{curved}} = \frac{(1-r^2)^2}{6\alpha}\frac{2(\cos^4\theta + R_{\text{m}}^2\sin^4\theta)}{r^2(\cos^2\theta + R_{\text{m}}\sin^2\theta)^2} = \frac{(1-r^2)^2}{6\alpha}\epsilon_{\text{flat}}, \tag{5.8}$$

where we define ϵ_{flat} as the potential slow-roll parameter one would get without the conformal factor of the metric

$$\epsilon_{\text{flat}} \equiv \frac{1}{2}\frac{\delta^{ij}V_{,i}V_{,j}}{V^2}. \tag{5.9}$$

The latter is greater than 1 (inside the Poincaré disc) and diverges when $r \to 0$. For small α the condition $\epsilon_{\text{curved}} < 1$ implies that the fields must inflate close to the boundary and at the end of inflation $1 - r_{\text{end}}^2 = \mathcal{O}(\sqrt{\alpha})$ should hold.[3] At the same time, the leading contribution in $\eta_{\sigma\sigma}$ contains

---

[2]Note that our model, with a product-separable potential (or sum separable when written in Cartesian coordinates) plus a conformally flat metric, is a third example of models which admits analytic calculation of the number of e-folds in the slow-roll slow-turn approximation, along with the sum- or product-separable potentials in flat space [126, 149].

[3]We say that a quantity y is of order $\mathcal{O}(x)$ if the limit $\lim_{x\to 0} y/x$ is a constant number. On the contrary, for the little-o notation $y = o(x)$ if the limit $\lim_{x\to 0} y/x = 0$.
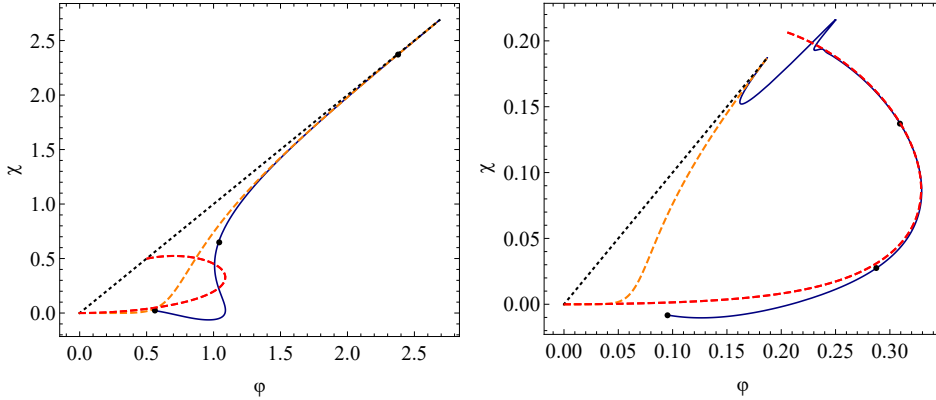
Figure 5.1

The evolution of the system in terms of the canonically normalized radius ψ using the full equations of motion (blue) and using the analytic slow-roll expression (orange-dashed) for the parameter values $R = 9$, $\theta_0 = \pi/4$, and $\alpha = 1/6$, $r_0 = 0.999$ (left panel) and $\alpha = 1/600$, $r_0 = 0.99$ (right panel). The red dashed line in the right panel is the angular inflation approximation. The black dotted line is the diagonal and the black dots correspond to 55 (CMB point), 2 and zero e-folds before the end of inflation.

terms that scale as

$$\frac{(1 - r^2)^3}{\alpha^2}, \tag{5.10}$$

implying that when this term becomes of order one, the scaling between the two variables is $1 - r^2_{\text{end}} = \mathcal{O}(\alpha^{2/3})$. By comparing the two we conclude that when α is small there will be a region before the end of inflation in which the potential gradient flow approximation fails. This is the regime that we will turn to next.

5.2.3   Angular inflation

It follows from the scalar field equations (5.4) and (5.5) that the only terms which are enhanced by the field-space curvature close to the boundary of the Poincaré disc are the Christoffel terms. However, they are velocity-suppressed during radial slow-roll inflation. Towards the end of radial inflation, the fields speed up and the increase in $\dot{r}$ boosts the Christoffel terms.

   This gives rise to two competing effects; the geodesic motion aims to push both fields to the boundary of the disk following a circular arc, whereas the gradient of the potential attracts both fields to the origin. Unlike $\dot{\theta}$, which becomes zero close to the minimum of the potential at $\theta = 0, \pi/2$, $\dot{r}$ can vanish away from the minimum because of the presence of $\Gamma^r_{\phi\phi}$. A
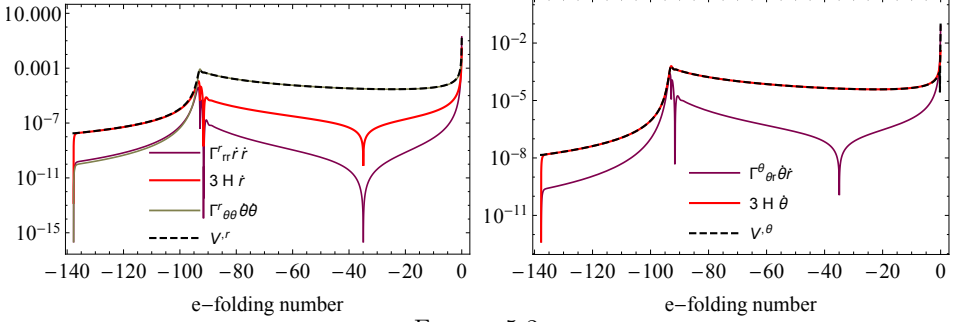
FIGURE 5.2

Numerical comparison of various terms in equations (5.4) *(left) and* (5.5) *(right) for*
$\alpha = 1/600$, $R = 9$, $\theta_0 = \pi/4$ *and* $r_0 = 0.99997$. *We have chosen these conditions to support both a period of radial as well as a angular inflation. The dominant terms in each period are indeed those corresponding to the relevant approximations.*

solution with $\dot{r} \approx 0$ can be sustained either by sufficiently reducing α (so that inflation takes place closer to the boundary of the space where the Christoffel $\Gamma^r_{\theta\theta}$ becomes important) or by increasing the mass ratio (and hence the velocity $\dot{\theta}^2$). An illustration of this can be found in the right panel of Fig. 5.1, which shows the non-monotonic behaviour of the radial coordinate. Moreover, it highlights that the trajectory proceeds for a significant portion along an angular direction, i.e. with $\dot{r}$ nearly vanishing.

This can be understood by considering the third and last term of Eq. (5.4), which do not depend on $\dot{r}$ and have opposite signs. If they almost cancel each other then the radius will be a slowly varying function and therefore fields will perform a predominately angular motion. Indeed, one can show numerically that the dominant terms of the radial and angular equations of motion are

$$\frac{(2r^3 + 2r)}{2r^2 - 2}\dot{\theta}^2 + \frac{1}{6}\left(m_\phi^2 \cos^2\theta + m_\chi^2 \sin^2\theta\right)(1 - r^2)^2 r \approx 0, \qquad (5.11)$$

$$3H\dot{\theta} + \frac{1}{12}(m_\chi^2 - m_\phi^2)\left(1 - r^2\right)^2 \sin(2\theta) \approx 0. \qquad (5.12)$$

Hence the angular motion is dominated by the usual slow-roll combination of the potential and Hubble drag terms, while the radial equation instead is dominated by the potential and the $\Gamma^r_{\theta\theta}$ Christoffel term, with all other terms being subdominant. Fig. 5.2 shows the magnitude of the various terms for a characteristic choice of parameters, supporting a prolonged period of angular motion. We see that our approximations leading to Eqs. (5.11) and (5.12) are justified.
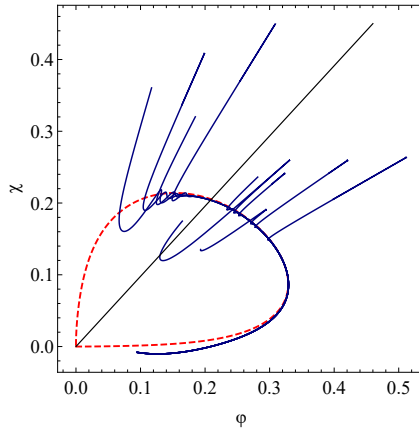
FIGURE 5.3
Plot of the angular attractor for $\alpha = 1/600$, $R = 9$ and a wide range of initial data (the black line is the diagonal). We observe that the angular solution captures very well the evolution for $\theta < \pi/4$.

The regime of angular inflation allows for a simple derivation of the trajectory through field space. One can eliminate $\dot{\theta}$ from the approximate equations (5.11) and (5.12). Under the additional assumption that the Hubble function is dominated by the potential $H^2 \simeq \frac{1}{3}V$ (the neglect of the kinetic terms can easily be justified as the angular motion is slow-rolling, while the radial motion is even slower), one obtains a parametric equation for the field trajectory during angular motion

$$
r(\theta) = \frac{1}{\sin 2\theta (R_{\mathrm{m}} - 1)} \Big[-\frac{9}{2}\alpha \left((1 - R_{\mathrm{m}})\cos 2\theta + R_{\mathrm{m}} + 1\right)^2 +
$$
$$
\sqrt{\frac{81}{4}\alpha^2((1 - R_{\mathrm{m}})\cos 2\theta + R_{\mathrm{m}} + 1)^4 + (1 - R_{\mathrm{m}})^4 \sin^4 2\theta} \Big]^{1/2} , \tag{5.13}
$$

where R_{m} is defined in Eq. (5.3). We have verified the attracting nature of this solution for a wide range of initial conditions in Fig. 5.3. The remarkable property of this solution is that it only depends on α, the mass ratio R_{m} and the initial angle θ_0, while all other initial data have dropped out. In contrast, for the slow roll approximation (or any other approximation that only fixes the velocities), one obtains a family of trajectories in the multi-dimensional field space - which is e.g. a one-parameter family for the two-field case. In a sense, the angular inflation solution is therefore closer to the notion of single-field attractor as it depends on only one initial condition.[4]

---

[4]This type of coordinate-dependent approximation, like the case of hyperinflation, is

While it captures the angular inflation regime very well and has the remarkable property of a dynamical attractor, the solution $r(\theta)$ it is somewhat complicated and difficult to use. Later on we will often use the quantity $1 - r^2$, which encodes the stretching of the field-space as one nears the boundary of the Poincaré disk. Expanding in terms of α, this can be written as

$$1 - r^2 \simeq \frac{9\alpha(\cot\theta + R_{\mathrm{m}}\tan\theta)^2}{2(R_{\mathrm{m}} - 1)^2}\,. \tag{5.14}$$

This relation breaks down close to the two axes. It is easy to see that unless the initial angle is close to the heavy field direction $\theta \approx \pi/2$, the two expressions given by Eqs. (5.13) and (5.14) match very well. There is some disagreement close to the light direction $\theta = 0$, but there we expect the slow-roll approximation to break either way, so the comparison is meaningless. From now on, we will always use the approximation of Eq. (5.14), unless otherwise noted.

We now move to computing the first slow-roll parameter ϵ. Using the above approximations, amounting to $\dot{r} \approx 0$, $H^2 \approx \frac{1}{3}V$ and $\dot{\theta} = \dot{\theta}_{\mathrm{SR}}$, one has

$$\epsilon = -\frac{\dot{H}}{H^2} \approx \frac{3}{2}\left(1 - r^2\right)\,, \tag{5.15}$$

where we expanded this relation close to the boundary $r = 1$. The minimum value of ϵ during the angular motion (in the small α approximation) occurs at and is given by

$$\theta_{\epsilon,\mathrm{min}} = \arctan\left(\frac{1}{\sqrt{R_{\mathrm{m}}}}\right)\,, \qquad \epsilon_{\mathrm{min}} = \frac{27\alpha R_{\mathrm{m}}}{(R_{\mathrm{m}} - 1)^2}\,. \tag{5.16}$$

This is significantly higher than the value of ϵ during inflation along the radial direction.

Using the expression for ϵ we can compute the angle at which angular inflation ends. The equation $\epsilon = 1$ can be solved, using Eq. (5.15), however the solution is not very insightful. At small α and large R_{m} it reads

$$\theta_{\mathrm{end}} = \frac{3\sqrt{3\alpha}}{2(R_{\mathrm{m}} - 1)}\,, \tag{5.17}$$

which is indeed close to $\theta = 0$. Since close to $\epsilon = 1$ our approximations break down, for small α and / or large mass ratio we can safely take angular inflation to end for $\theta = 0$, without introducing extra errors.[5]

more obscure in Cartesian coordinates because the Christoffel terms of the light field are not balanced by the gradient term. The attractor solution is, of course, independent of coordinate system but an approximate form would be very hard to find.

[5]In fact, computing $N(\theta = \theta_{\mathrm{end}})$ and $N(\theta = 0)$ gives agreement to within a few decimal points, so we will set $\theta = 0$ as the end-point of angular inflation.

Finally, computing the number of *e*-folds during angular motion is straightforward using the angular slow-roll approximations for H and $\dot{\theta}$

$$N = \int_{t_0}^{t_{\mathrm{end}}} H \, dt = \int_{\theta_0}^{\theta_{\mathrm{end}}} \frac{H}{\dot{\theta}} \, d\theta \,. \tag{5.18}$$

The integration is performed from the initial angle θ until the final angle which we take to be $\theta = 0$. The result is

$$N = -\frac{1}{27\alpha}(R_{\mathrm{m}} + 2) + \frac{4}{27\alpha} \frac{(1 - R_{\mathrm{m}}^2)\cos 2\theta + R_{\mathrm{m}}^2 + R_{\mathrm{m}} + 1}{((1 - R_{\mathrm{m}})\cos(2\theta) + R_{\mathrm{m}} + 1)^2}$$
$$+ \frac{9\alpha + 2}{27\alpha} \log\left[\frac{1}{2}((1 - R_{\mathrm{m}})\cos 2\theta + R_{\mathrm{m}} + 1)\right] \,. \tag{5.19}$$

This relation outlines where in the parameter space there is a significant number of *e*-folds during angular inflation. Fig. 5.4 shows the number of non-radial *e*-folds for a broad range of parameters. We see that for large R_{m}/α, the contours of N give a linear relation between $\log(R_{\mathrm{m}})$ and $\log(\alpha)$. This can also be calculated by expanding the above in $\alpha \ll 1$ and $R_{\mathrm{m}} \gg 1$:

$$N \approx -\frac{R_{\mathrm{m}}}{27\alpha} - \frac{2 - 2\csc^2\theta - (9\alpha + 2)\log\left(R_{\mathrm{m}}\sin^2\theta\right)}{27\alpha} + \cdots \,. \tag{5.20}$$

While it is non-trivial to invert the number of *e*-folds and get the function $\theta(N)$, some analytical progress can be made towards this goal. Specifically, we can neglect the logarithms in the function of $N(\theta)$ after which we obtain

$$\theta(N) \simeq \frac{1}{2}\cos^{-1}\left(\frac{R_{\mathrm{m}}^2 + R_{\mathrm{m}}(1 + 27\alpha N) - 2\sqrt{-27\alpha R_{\mathrm{m}} N + 1} + 27\alpha N}{(R_{\mathrm{m}} - 1)(R_{\mathrm{m}} + 27\alpha N + 2)}\right), \tag{5.21}$$

where we took $\theta_0 = \pi/4$. One can check that this an increasingly good approximation for larger R_{m}.

It is important to note that the number of *e*-folds quoted above also includes the final stage of inflation, which is more like single-field inflation along the horizontal axis (corresponding to the lightest field) than angular inflation along the boundary. This is illustrated in Fig. 5.5. This feature is particularly noticeable in the case where the mass ratio is large: in this situation there is a sizeable number of *e*-folds produced in this final stage of inflation. In a somewhat rough sense, the two parameters of our model trigger the two regimes: smaller values of α increase the number of *e*-folds during the angular trajectory, while a larger mass ratio does the same for
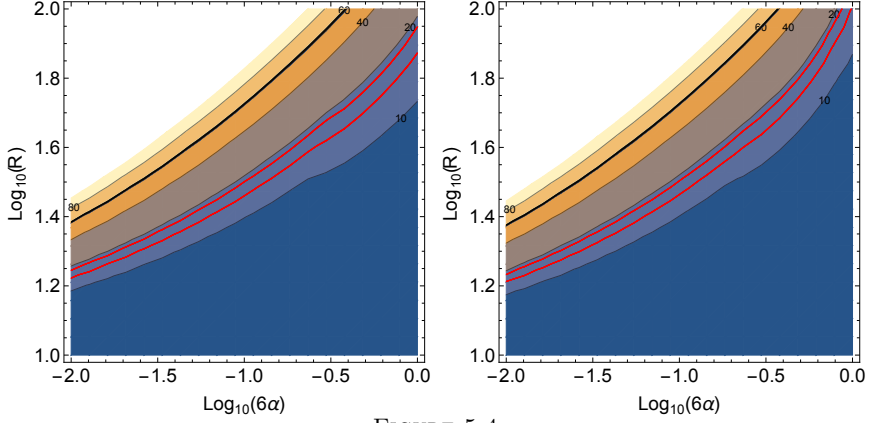
FIGURE 5.4

The number of e-folds, occurring after the initial period of radial inflation for a wide range of the field-space curvature, characterized by α and the mass ratio of the two fields $R_{\rm m}$ for initial angles $\theta_0 = \pi/4$ (left) and $\theta_0 = \pi/3$ (right). The thick black line corresponds to 60 e-folds of non-radial inflation and the red to the Planck contours to the point where the predictions of our model exit the Planck 1σ and 2σ regions, as computed in Eq. (5.39) and discussed in Section 5.3.2. The two panels are very similar since small changes in the initial angle do not alter the duration of the angular regime significantly. This can be seen in the expression for the number of e-folds of angular inflation in Eq. (5.20), where the θ-dependence is not present in the lowest order term.

the single-field regime along the light axis prior to the end of inflation. For very large mass ratios, the number of *e*-folds during this final stage exceeds that of the CMB window, and as a result the observable part of inflation will be effectively single-field (with a very heavy orthogonal direction). In this case the inflationary predictions will coincide with the single-field ones. In all other cases one needs to evolve the quantum fluctuations during the angular regime, which is the topic that we turn to next.

5.3 Perturbation analysis

5.3.1 Evolution during gradient flow

As we saw in Sec. 5.2.2, for small curvature ($\alpha \sim \mathcal{O}(1)$) both ϵ_V and $\eta_{\sigma\sigma}$ are small and hence the system follows the potential gradient flow approximately. This results into small turn rate which implies that perturbations at horizon crossing will have the same amplitude $\delta\Phi^i \sim H^2/(2\pi)$. In the following we will calculate the power spectra using both the slow-roll equations for the two perturbations (4.62)-(4.63) and the horizon-crossing formula.

FIGURE 5.5

The evolution of the system in terms of the canonically normalized field ψ with identical colour-coding and parameters as in Fig. 5.1 but with $R = 500$, $\alpha = 1/60$, $\theta_0 = \pi/4$ and $r_0 = 0.9999$. Note that this plot contains all possible different kinds of evolution and at the time of generation of fluctuations the evolution of the system can be well described by a single field.

First, we need the leading order expressions for background quantities. We write the slow roll parameter as

$$\epsilon \approx \frac{(1 - r^2)^2}{6\alpha}(4 + p^2) = \epsilon_r \left(1 + \frac{1}{4}p^2 \right) , \tag{5.22}$$

where $p \equiv V_{,\theta}/V$, and the turn rate using Eq. (4.40)

$$\Omega \approx p \frac{2(1 - r^2)}{3\alpha} . \tag{5.23}$$

The previous two quantities can be written as a $1/N$ expansion using the expression (5.7)

$$\epsilon \approx \frac{3\alpha}{16N^2}(4 + p^2), \qquad \Omega \approx \frac{p}{2N} . \tag{5.24}$$

The highest order terms in the definition of β, which controls the growth ($\beta > 0$) or decay ($\beta < 0$) of the isocurvature mode, are

$$\frac{M_{\sigma\sigma} - M_{ss}}{3H^2} \approx \frac{2}{N} , \tag{5.25}$$

and so the isocurvature mode slowly decreases as inflation proceeds

$$\mathcal{S} \approx \mathcal{S}_* \left(\frac{N}{N_*} \right)^2 . \tag{5.26}$$

The curvature mode is

$$\mathcal{R} \approx \mathcal{R}_* - \mathcal{S}_* \frac{p}{2} \,, \tag{5.27}$$

from which we read the transfer function as $T_{\mathcal{R}\mathcal{S}} = p/2$. The dimensionless power spectrum at the end of inflation is thus

$$\mathcal{P}_{\mathcal{R}}^2 = |\mathcal{R}_*^\dagger \mathcal{R}_*| + |\mathcal{S}_*^\dagger \mathcal{S}_*| \frac{p^2}{4} = \frac{H^2}{(2\pi)^2 \epsilon_*} \left(1 + \frac{1}{4} p^2 \right) = \frac{H_*^2}{(2\pi)^2 \epsilon_{r*}} \,, \tag{5.28}$$

which matches the single-field result. Here we used the fact that for slow-turn models the amplitude of curvature and entropy perturbations at horizon crossing is the same $|\mathcal{R}_*| \sim |\mathcal{S}_*|$.

The tensor power spectrum is unaffected by the presence of more scalar degrees of freedom and is given by its value at horizon crossing $\mathcal{P}_t^2 = 2H_*^2/\pi^2$. With both spectra computed the tensor-to-scalar ratio and the scalar spectral index are given by

$$r = 16\epsilon_{r*} \sim \frac{12\alpha}{N_*^2} \,, \qquad n_{\text{s}} \sim 1 + \frac{2}{N_*} \,. \tag{5.29}$$

In contrast, the horizon-crossing formula yields a cleaner expression for the power spectrum that entails two limits of interest, namely moderate curvature $\alpha \sim \mathcal{O}(1)$, $r \to 1$ and the flat case $\alpha \to \infty, r \to 0$. For generic curvature it is given as

$$\mathcal{P}_{\mathcal{R}}^2 = \left(\frac{H}{2\pi} \right)^2 N^{,i} N_{,i} = \left(\frac{H}{2\pi} \right)^2 \left(\frac{4N^2}{\alpha} - N \right) \,. \tag{5.30}$$

The tensor to scalar ratio is similarly defined from

$$r = \frac{8}{N^{,i} N_{,i}} = \frac{8\alpha}{4N^2 - \alpha N} \,. \tag{5.31}$$

Taking the time derivative of the power spectrum yields the scalar spectral index

$$n_{\text{s}} - 1 = -\frac{2\alpha}{(4N - \alpha)^2} \epsilon_{\text{flat}} + \frac{8N - \alpha}{4N^2 - N\alpha} \,, \tag{5.32}$$

where we equated the slow-roll parameter ϵ to ϵ_V, which scales as

$$\epsilon_V = \frac{\alpha}{(4N - \alpha)^2} \epsilon_{\text{flat}} \,. \tag{5.33}$$

For $\alpha \sim \mathcal{O}(1)$ the spectral index receives the dominant contribution from the $2/N$ term, r has quadratic dependence on $1/N$ and we arrive at Eq. (5.28).

We observe that these models have predictions that depend weakly on initial conditions. For moderate values of the mass gap, this dependence becomes important at second order in the $1/N$ expansion. The same will be true for arbitrary number of fields that follow the potential gradient flow. In Ch. 8 we will examine the flat case at the many-field limit, i.e. $\mathcal{N} \to \infty$.

5.3.2   Evolution during angular inflation

We will focus on the regime of small α and large R_{m}, where significant analytical progress can be made. The intuition gained from this regime will be checked numerically and extended to the region of $\alpha \sim 1$. First of all, using the fact that the motion occurs predominately along the angular direction, the tangent vector can be approximated by

$$\hat{\sigma} \approx \left(0, \sqrt{\mathcal{G}^{22}}\mathrm{sgn}(\dot{\theta})\right) = \hat{\boldsymbol{e}}_{\boldsymbol{\theta}} \,.$$

Hence the normalized turn rate vector will be along the radial direction,

$$\hat{\boldsymbol{s}} = \mathrm{sgn}(\dot{\theta})\hat{\boldsymbol{e}}_{\boldsymbol{r}} = (\mathrm{sgn}(\dot{\theta})\sqrt{\mathcal{G}^{11}}, 0) \,.$$

It is easy to show that

$$\omega^2 = \frac{G^{rr}V_r^2}{\dot{\sigma}^2} \,. \tag{5.34}$$

Normalizing the turn-rate by the Hubble scale, we arrive at the relation

$$\Omega^2 = \frac{4}{3\alpha}\epsilon \,. \tag{5.35}$$

We see that the turn rate is proportional to the curvature of the field-space manifold. It is illustrated in Fig. 5.6 that our analytic result agrees very well with the numerical evolution of the background fields. Moreover, using the expression for ϵ in the small α regime, the adiabatic second slow-roll parameter becomes

$$\eta_{\sigma\sigma} \approx \mathcal{O}\left(\frac{1 - r^2}{\alpha}\right) = \mathcal{O}(\epsilon) \,, \tag{5.36}$$

as expected. Finally, using similar approximations the effective mass becomes

$$\frac{\mu_{\mathrm{s}}^2}{H^2} = \frac{2(1 - r^2)}{\alpha} \,, \tag{5.37}$$
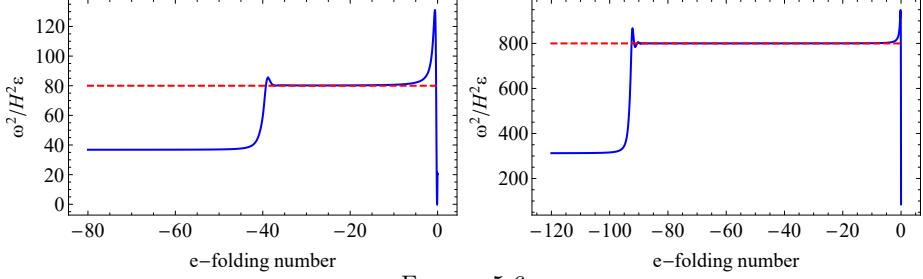
FIGURE 5.6

The normalized turn-rate $|\omega|/(H\sqrt{\epsilon})$, computed numerically in blue for $\alpha = 0.016$, $R_{\rm m} = 25$ (left) and $\alpha = 0.0016$, $R_{\rm m} = 9$ (right). The red-dashed lines correspond to $8/\alpha$, with excellent agreement in the angular regime (the last 40 and 90 e-folds respectively). Note that the same combination is constant in the radial part (before the transition occurring halfway), as was found in Ref. [146].

and the isocurvature modes do not grow on super-horizon scales during angular inflation. We now have all the components that go into the parameter β resulting in

$$\beta \approx -\frac{3(\cot\theta + R_{\rm m}\tan\theta)^2}{(R_{\rm m} - 1)^2} \,. \tag{5.38}$$

This shows that the isocurvature modes will decay exponentially during the angular part of the inflationary trajectory. As seen in Fig. 5.7, Eq. (5.38) is an excellent approximation to the numerical evaluation of β in the angular inflation regime and in fact $|\beta| = \mathcal{O}(1)$, hinting at a severe suppression of isocurvature modes on super-horizon scales. Without an amplification, or at least a moderate decay, of the isocurvature modes, even a large turn-rate is insufficient to source any super-horizon evolution of the adiabatic modes. Hence, all adiabatic perturbation modes that have crossed the horizon before the onset of the period of angular inflation will be frozen and so will their spectral index $n_{\rm s}$ and their amplitude that defines r.

   With all the ingredients in place, it is a simple exercise to compute the super-horizon evolution of the adiabatic and isocurvature modes during the non-radial part of inflation. Since, as we showed, during angular inflation, $\beta < 0$, we expect that the isocurvature modes will be quickly damped and hence the adiabatic modes will not be sourced. This is exactly what is shown in Fig. 5.8, which presents a characteristic example from a larger number of simulated inflationary trajectories. We see a mild decay of the isocurvature modes during radial inflation, which can -through the non-zero turn rate- lead to a sourcing of the adiabatic modes [146]. However, once radial inflation ends and the system transitions into the angular regime, the
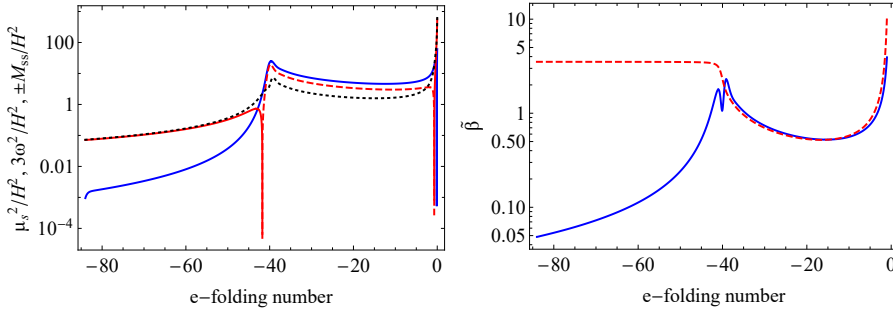
FIGURE 5.7

Left: *The effective isocurvature mass-squared μ_s^2/H^2 (black-dotted), along with the turn rate contribution $3\omega^2/H^2$ (blue) and the mass-squared M_{ss}/H^2 (red) and $-M_{ss}/H^2$ (red-dashed). All curves are computed numerically for $R_{\rm m} = 25$ and $\alpha = 0.016$, without using any approximations. We see that during angular inflation, which lasts for the final 40 e-folds, $\mu_s^2/H^2 \sim O(1) > 0$, while it is small and positive during the initial quasi-radial evolution.*

Right: *The isocurvature growth parameter $\tilde{\beta}$ for the same parameters numerically (blue-solid) and using the approximations of Eq. (5.38) (red-dashed). We see excellent agreement in the angular inflation regime.*

isocurvature modes quickly decay and the transfer of power to the adiabatic modes ceases ($T_{\mathcal{RS}} = \text{const}$). Looking at $\Delta T_{\mathcal{RS}} \equiv T_{\mathcal{RS}}(N_{\rm end}) - T_{\mathcal{RS}}$ we can see that $T_{\mathcal{RS}}$ grows during the radial part, hence adiabatic modes are continuously sourced by isocurvature ones. However, this sourcing stops immediately after the radial part has ended (hence $T_{\mathcal{RS}}$ stops increasing), signalling the fact that the curvature fluctuation has reached its adiabatic limit. By taking the fiducial scale N_* close to the end of the initial period of radial inflation, $T_{\mathcal{SS}}$ is quickly forced towards zero and so $T_{\mathcal{RS}}$ becomes constant.

In specific regimes of parameter space, the period of angular inflation can serve as a second phase of inflation that shifts the effective number of e-folds during the initial radial phase. This is in particular the case when the number of e-folds during angular inflation amounts to at most a few decades, such that the observable CMB window still takes place during the radial phase. This offset in e-folds due to the angular phase is given by $N(\theta_0)$ in Eq. (5.19), where the angle should be taken at the point where the inflationary trajectory joins the angular phase (which depends on the initial conditions). Due to the decay of the isocurvature modes and the lack of significant feeding into the adiabatic modes, the CMB predictions
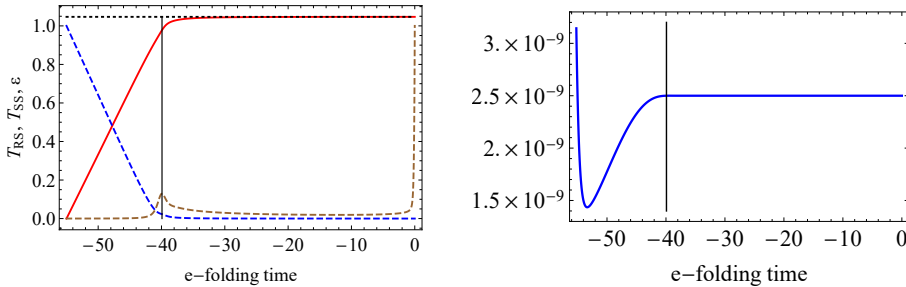
FIGURE 5.8

Left: *The transfer functions $T_{\mathcal{R}\mathcal{S}}$ (red) and $T_{\mathcal{S}\mathcal{S}}$ (dashed-blue) along with ϵ (dashed-brown) for $\alpha = 0.016$ and $R_{\mathrm{m}} = 25$. The vertical line at $N \simeq -40$ signals the onset of the angular inflation period. We see that the transfer of power from the isocurvature to the adiabatic modes is negligible during angular inflation.*
Right: *Evolution of the power spectrum for the same parameters. The mode shown leaves the horizon 55 e-folds before the end of inflation and the vertical line shows the onset of the angular inflation regime at $N \simeq -40$.*

are therefore identical to those during the radial phase modulo the offset:[6]

$$n_{\mathrm{s}} = 1 + \frac{2}{N - N(\theta_0)}, \qquad r = \frac{12\alpha}{(N - N(\theta_0))^2}, \qquad (5.39)$$

where $N \sim 55 - 60$ e-folds before the end of inflation and $N(\theta_0)$ depends on the initial angle as well as the parameters α and R_{m}. Fig. 5.9 shows the evolution of the observables on the $n_{\mathrm{s}} - r$ plane for varying field-space curvature and varying mass asymmetry between the two fields. We can see, as expected from the analysis of Section 5.2, that smaller α requires less mass asymmetry to deviate significantly from the single-field observables. Furthermore, for low values of α, the curves in the left panel of Fig. 5.9 become degenerate (green to blue curves), hence the spectral index depends only on the combination R_{m}/α, as is expected from the leading term in the series expansion of Eq. (5.20). Going back to the contour plots of Fig. 5.4, for pairs of R_{m} and α that are below the two red lines, the observables are within the 1σ and 2σ regions of *Planck* respectively. We also expect the local non-Gaussianity to be similarly affected by the angular inflation regime, retaining its form $f_{NL} \propto -N^{-1}$ given in Ref. [146], with the substitution $N \rightarrow N - N(\theta)$.

Going to larger curvatures and mass ratios will lead to a number of angular e-folds $N(\theta)$ that exceeds the observable ones, implying that the CMB horizon crossing point is not during the radial but rather during

---

[6]We have also verified numerically these relations using **m.transport** [150].
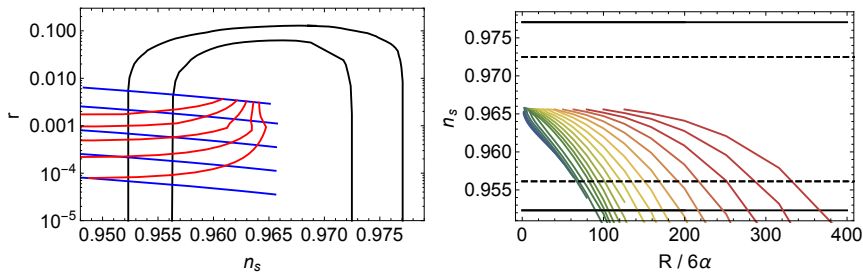
Left: *The evolution of the primordial observables on the $n_s - r$ plane. Each blue line corresponds to a fixed value of α and varying R and is of the form $r = 3\alpha(n_s - 1)^2$. The parameters are (from top to bottom) $6\alpha \simeq 0.8, 0.3, 0.1, 0.03, 0.01$. Each red line corresponds to a fixed value of R_m and varying α. The parameters are (from top to bottom) $R_m \simeq 25, 16, 10, 6, 4$.*
Right: *The scalar spectral index n_s as a function of $R/(6\alpha)$ for various values of α, ranging from $6\alpha = 0.01$ (blue) to $6\alpha \simeq 0.8$ (red) . The horizontal black-dashed and solid-black lines correspond to the Planck 1σ and 2σ intervals respectively. In both panels we took the CMB-relevant modes to have crossed the horizon 60 e-folds before the end of inflation.*

the angular phase. This corresponds to the part of parameter space that lies above the thick black line of Fig. 5.4. The calculation of inflationary observables during this phase is non-trivial, since the value of the turn-rate $\Omega = \mathcal{O}(1)$ makes the adiabatic and isocurvature perturbations coupled at sub-horizon scales [122].

5.4   Summary and comparison to non-minimally coupled models

In this chapter, we have investigated multi-field α-attractors in different regions of the parameter space. For moderate values of the field-space curvature and the mass ratio, inflation proceeds with a small turn-rate, which leads to a continuous but mild transfer of power from the isocurvature to the adiabatic mode. This regime was recently explored in Ref. [146], where it was found that the final values of the cosmological observables n_s and r do not deviate from their single-field counterparts.

The situation alters drastically when one increases the field-space curvature or potential gradients. In this case, as shown in Fig. 5.4, the system can show a large number of e-folds along a non-radial direction. This can be a combination of angular inflation, where the two fields move along the angular direction close to the boundary of the Poincaré disk, and a

period of inflation along the direction of the light field. Specifically, we have identified the attractor solution of Eq. (5.13) corresponding to angular inflation, which differs from the usual slow-roll one. This leads to the following sequence of phases:

- Starting with zero velocities the fields will accelerate towards the origin following an almost radial motion. The duration of this stage in *e*-folds is given by the usual single-field α-attractor formula of Eq. (5.7).

- After a quick transient, which is very close to geodesic motion, the system is set into angular motion close to the boundary of the Poincaré disk. There is a very accurate analytical description of the dynamics in this regime for larger values of the mass ratio and the curvature.

- If the mass ratio is very large, the system can inflate along the direction of the light field for a significant amount of *e*-folds. This regime is well described as single-field or quasi-single-field evolution.

For parameter values that lead to at most a number of decades of angular *e*-folds in the last two phases, the predictions for the CMB observables are altered in a very simple and intuitive way based on the offset with the additional angular phase (5.39). This follows from our analysis in Section 5.3.2: during the angular part of the evolution, the isocurvature modes are quickly damped on super-horizon scales, leading to the effective freeze-out of the adiabatic modes. This means that the adiabatic modes retain their amplitude since the end of the radial part of inflation.

An interesting question regards the analysis of and predictions for inflationary observables for the range of parameter space with all sixty *e*-folds of angular inflation, which will be presented separately. Similarly, given the higher-dimensional moduli spaces of string theory, it would be interesting to analyse an α-attractor model with more fields and a certain distribution of masses. Interesting questions include the duration of the angular phase as a function of the number of fields. Moreover, whether there is an emergent simplicity in the many-field limit, as has been shown for the flat geometry case [142], remains to be seen.

It is also interesting to contrast this behaviour to non-minimally coupled models, which together with α-attractors are among the most studied and well motivated inflationary models involving a non-trivial field space metric. In that case, it has been shown that for generic initial conditions and randomly chosen potential parameters (constrained to provide enough *e*-folds of inflation and the observed amplitude of density perturbations),

the cosmological observables, such as n_s and r fall within the *Planck* allowed region, on top of the predictions of the Starobinsky model and the single field predictions of α-attractors, given in Eq. (5.1). The "lumpy" potential in simple models of quartic non-minimally coupled inflation, leads to a quick transient period, in which the fields quickly relax into a potential "valley" and inflate along it, leading to largely parameter-independent predictions for the CMB observables [138, 151]. In order to go beyond this universal behaviour, one needs to fine-tune the potential parameters and also fine-tune the initial conditions [152]. Hence, in simple non-minimally coupled models, deviations from Eq. (5.1) require extreme fine-tuning, or some other mechanism, like a softly broken symmetry accompanied by an early phase of inflation ending at a waterfall transition, placing the field exponentially close to a potential "ridge".

It is quite remarkable that non-minimally coupled models and α-attractors (with moderate parameter values) both respect their single-field predictions, even for multiple inflaton fields, however they do so in completely different ways: in non-minimally coupled models the large angular gradients force the fields into a single-field trajectory, while for α attractors the "stretching" of field space along the angular directions allows for a quasi-single field trajectory with a small turn rate.

6

Scaling attractors

In this chapter we investigate scaling solutions and their stability properties emphasizing bifurcations between different solutions. We propose a classification scheme depending on the number of "frozen" solutions and then demonstrate how the hyperinflation model, that attracted a lot of attention lately, is a special case of these solutions. The analysis of this chapter is an extensive rewriting of publication [153].

6.1   Single-field scaling solutions

The dynamics of the multi-field alpha attractors studied in Ch. 5 is not a unique feature of the model. A closely related model that appeared in the literature around the same time, dubbed "sidetracked inflation", displays a similar phenomenon [154]. In both models the original gradient-flow phase is succeeded by a novel one with large turning rate, albeit by a different dynamical mechanism. These prototype examples included a sum-separable potential and a hyperbolic field metric written in a different parameterization. The similarity between the two models encourages further investigation of this behaviour.

To better understand how the system departs from gradient flow to different solutions we will first study scaling solutions instead. The reason is simple: for trivial geometry small potential gradients over short timescales are approximately constant and the potential may be approximated by exponentials [62]. The attractor behaviour of slow-roll models can be understood as being small deformations of models that possess proper mathematical attractors which can be found analytically. We will therefore start by classifying scaling solutions for non-trivial geometry and then attempt to link this novel behaviour to the existence of corresponding scaling solutions with similar properties.

Before discussing two-field scaling solutions we will recap the single-field case. The dynamics for one field can be written in terms of the number of *e*-folds as

$$\phi' = v \,, \tag{6.1}$$

$$v' + \left(3 - \frac{1}{2}v^2\right)(v + p) = 0 \,, \tag{6.2}$$

where $p = (\ln V)_{,\phi}$. When p is constant, and therefore the potential is an exponential, the second equation decouples from the first and can be studied separately. Its critical points are called scaling solutions and satisfy $\epsilon' = 0$. We can also use this argument backwards to investigate what kinds of potentials give rise to scaling solutions. In this way we can make the transition to more than one fields smoother. Eq. (6.4) can be written as a differential equation for the potential

$$\epsilon' + (3 - \epsilon)\left(2\epsilon + (\ln V)'\right) = 0 \,, \tag{6.3}$$

with solution

$$V(N) = (3 - \epsilon)e^{-2\int \epsilon \, \mathrm{d}N'} \,. \tag{6.4}$$

On the scaling solution, $\epsilon' = 0$, the potential exhibits exponential dependence on the e-folding number

$$V(N) \propto e^{-2\epsilon_{\mathrm{cr}}N} \,. \tag{6.5}$$

If only one field is present then the requirement $\epsilon(N) = \epsilon_{\mathrm{cr}}$ on the scaling solution is another trivial differential equation for the field yielding linear relation between $\Delta\phi$ and the e-folding number

$$\phi' = \sqrt{2\epsilon_{\mathrm{cr}}} \Rightarrow \phi = \phi_0 + \sqrt{2\epsilon_{\mathrm{cr}}}N \,. \tag{6.6}$$

The potential is then uniquely determined as $V = V_0 e^{\sqrt{2\epsilon_{\mathrm{cr}}}\phi}$.

Since scaling solutions are defined from the asymptotic behaviour of the dynamical system it is possible to construct more generic potentials that support this behaviour for $t \to +\infty$. This can be achieved for potentials that asymptote to an exponential for $\phi \to \pm\infty$ resulting into a vast and complex family of potentials with this property. For the purposes of this thesis, we will restrict our analysis to potentials and metrics for which the scaling solution can be defined for every t, and then form different classes compatible with these assumptions. Having thoroughly examined the single-field case we proceed to investigate scaling solutions for multiple fields.

6.2 Two-field dynamics

6.2.1 Frozen solutions

The easiest way to make this transition is to retain the exponential dependence of the potential on one of the two fields in order for the single-field solution to carry over the multi-field model. From Eqs. (6.4) and (6.3), which remain unchanged in the presence of more fields, requiring a linear relation between N and ϕ results into exponential dependence of the potential in terms of ϕ and, hence, the second field should be non-dynamical, or *frozen*, during the evolution. These two requirements result in a product-separable potential

$$V = h(\chi)e^{p\phi} \,, \tag{6.7}$$

with ϕ assumed to be the inflaton. Regarding the metric, the most general form in two dimensions is

$$\mathrm{d}s^2 = f(\chi,\phi)^2 \, \mathrm{d}\phi^2 + g(\chi,\phi)^2 \, \mathrm{d}\chi^2 \,, \tag{6.8}$$

with the following non-zero Christoffel symbols

$$\Gamma^\chi_{\chi\chi} = \frac{g_{,\chi}}{g}, \qquad \Gamma^\chi_{\phi\chi} = \frac{g_{,\phi}}{g}, \qquad \Gamma^\chi_{\phi\phi} = -\frac{gg_{,\phi}}{f^2},$$
$$\Gamma^\phi_{\phi\phi} = \frac{f_{,\phi}}{f}, \qquad \Gamma^\phi_{\chi\phi} = \frac{f_{,\chi}}{f}, \qquad \Gamma^\phi_{\chi\chi} = -\frac{ff_{,\chi}}{g^2}. \tag{6.9}$$

The solution $v =$const and $\chi' = 0$ should satisfy the system of Eqs. (4.7). It is more convenient to consider instead the normalized velocities $x = g\chi'$ and $y = f\phi'$, which represent the two parts in the definition of ϵ

$$\epsilon = \frac{1}{2} G_{ab} v^a v^b = \frac{1}{2} x^2 + \frac{1}{2} y^2, \tag{6.10}$$

for which the dynamical system becomes

$$\phi' = \frac{y}{f}, \tag{6.11a}$$

$$\chi' = \frac{x}{g}, \tag{6.11b}$$

$$y' = -(3 - \epsilon)\left(y + \frac{p_\phi}{f}\right) - \frac{f_{,\chi}}{fg}xy + \frac{g_{,\phi}}{fg}x^2, \tag{6.11c}$$

$$x' = -(3 - \epsilon)\left(x + \frac{p_\chi}{g}\right) - \frac{g_{,\phi}}{fg}xy + \frac{f_{,\chi}}{fg}y^2, \tag{6.11d}$$

where we defined $p_\chi \equiv (\ln V)_{,\chi}$ and $p_\phi \equiv (\ln V)_{,\phi}$. We will give the physical interpretation of these equations later with examples.

Next, we will look for solutions where the individual parts of ϵ vanish independently, i.e. $x' = 0$ and $y' = 0$.[1] Since both parts of ϵ should be constants, f should not depend on ϕ and the metric (6.8) is restricted to

$$\mathrm{d}s^2 = f(\chi)^2 \, \mathrm{d}\phi^2 + g(\chi, \phi)^2 \, \mathrm{d}\chi^2. \tag{6.12}$$

Plugging $x = 0$ in the $y' = 0$ equation gives the following solution for y

$$y = -\frac{p_\phi}{f}, \tag{6.13}$$

and the inflaton field follows its potential gradient. Similarly, the $x' = 0$ equation requires the following relation to be satisfied

$$\frac{1}{g}\left((3 - \epsilon)p_\chi - \frac{f_{,\chi}}{f}y^2\right) = 0. \tag{6.14}$$

---

[1]This is the usual way to derive scaling solutions in the literature (see also [155–160]).

We observe that the existence of a root requires the metric function f and the potential to share the same monotonicity in terms of χ. The previous two equations combined determine all possible values of χ.

When $p_\chi = 0$, which implies that χ is at the minimum of its potential, then (6.14) requires $f_{,\chi} = 0$ as well. In this case the slow-roll parameter becomes equal to ϵ_V describing a gradient-flow (slow-turn) solution. If p_χ is non-zero, it is possible to express the slow-roll parameter in terms of p_χ and $f_{,\chi}$ in Eq. (6.14), using $y^2 = 2\epsilon$ and obtain

$$\epsilon = \frac{3p_\chi}{2(\ln f)_{,\chi} + p_\chi}\,. \tag{6.15}$$

This formula for ϵ will prove advantageous later.

6.2.2 Kinetic domination and de Sitter solutions

Slow-roll inflation takes place at the regime of potential dominance $K \ll V$. The opposite regime, $K \gg V$, gives $\epsilon \lessgtr 3$ and it is not sustained for potentials that support a slow-roll phase of inflation. It should be stressed that kinetic domination may include infinite realizations, all of which correspond to solutions with $\epsilon = 3$. However, plugging $\epsilon = 3$ into the dynamical system (6.11) the terms involving derivatives of the metric should be set equal to zero. Therefore, not every realization with $\epsilon = 3$ is possible; for example, the frozen solution $x = 0$ requires $f_{,\chi} = 0$, while, the solution $y = 0$ requires $g_{,\phi} = 0$. Similarly, for a cosmological constant contraction with v_i in the Klein-Gordon equations provides the evolution equation of the kinetic energy

$$K = K(0)e^{-3N}\,, \tag{6.16}$$

independently of the field-space geometry, and the de Sitter solution is the final state of the system. Note that the previous two solutions may describe the future asymptotic behaviour of the system when no other frozen solution is possible.

6.3 Stability criteria for frozen solutions

The stability of background solutions is determined by the eigenvalues of the Jacobian matrix evaluated on the solution (see App. B.1 for more details). For the potential (6.7) and the metric (6.12) the stability matrix of frozen

solutions (excluding kinetic domination) becomes

$$
\begin{pmatrix}
-(3-\epsilon+D) & -\frac{6\Omega}{3-\epsilon} & \frac{3(\epsilon-1)\Omega^2 g}{3-\epsilon} + \frac{2\epsilon f_{,\chi\chi}}{fg} - \frac{(3-\epsilon)V_{,\chi\chi}}{Vg} & 0 \\
\Omega & \epsilon-3 & (3-\epsilon)\Omega g & 0 \\
\frac{1}{g} & 0 & 0 & 0 \\
0 & \frac{1}{f} & \frac{\Omega g}{f} & 0
\end{pmatrix}, \quad (6.17)
$$

where we defined

$$
D \equiv \frac{\operatorname{sgn}(y)\sqrt{2\epsilon}\,g_{,\phi}}{fg}\,, \tag{6.18}
$$

and expressed derivatives of f in terms of the turn rate according to Eq. (4.28). Since one column is zero then at least one eigenvalue is zero. This is a reflection of our requirement that the solution can be defined for every N, and subsequently for every ϕ, as the two are linearly dependent. To find the eigenvalues we will calculate the characteristic equation of the Jacobian matrix

$$
\lambda^4 + \lambda^3(6-2\epsilon+D) + \lambda^2\left[(3-\epsilon)(3-\epsilon+D) + \frac{M^2}{H^2}\right] + \lambda(3-\epsilon)\frac{M^2}{H^2} = 0\,, \tag{6.19}
$$

with the additional definition

$$
M^2 \equiv \frac{V_{,\chi\chi}}{g^2} + 3\Omega^2 H^2 - \frac{2f_{,\chi\chi}}{fg^2}\epsilon H^2\,. \tag{6.20}
$$

The non-zero eigenvalues are then

$$
\lambda_1 = 3 - \epsilon\,, \tag{6.21}
$$

$$
\lambda_{\pm} = -\frac{1}{2}\left(3-\epsilon+D \pm \sqrt{(3-\epsilon+D)^2 - 4(M/H)^2}\right)\,. \tag{6.22}
$$

A sufficient condition for the non-positivity of the eigenvalues is to demand (see also App. B.2)

$$
3 - \epsilon + D \geq 0\,, \qquad M^2 \geq 0\,. \tag{6.23}
$$

For a frozen solution that describes kinetic domination the stability matrix becomes

$$
\begin{pmatrix}
0 & 0 & \frac{1}{f} & 0 \\
0 & 0 & 0 & \frac{1}{g} \\
0 & 0 & \sqrt{6}\left(\sqrt{6}+s\frac{p}{f}\right) & 0 \\
0 & \frac{6f_{,\chi\chi}}{fg} & s\frac{\sqrt{6}p_{\chi}}{g} & -s\frac{\sqrt{6}g_{,\phi}}{fg}
\end{pmatrix}, \tag{6.24}
$$

assuming $x = 0$ which as was explained earlier forces $f_{,\chi} = 0$ as well, and defining for convenience $s \equiv \text{sgn}(y)$. The non-zero eigenvalues are

$$\lambda_1 = \sqrt{6}\left(\sqrt{6} + s\frac{p}{f}\right), \tag{6.25}$$

$$\lambda_\pm = -\sqrt{\frac{3}{2}}\frac{s g_{,\phi} \pm \sqrt{4ff_{,\chi\chi} + g_{,\phi}^2}}{fg}, \tag{6.26}$$

and the eigenvalues are non-positive when

$$\left|\frac{p}{f}\right| > \sqrt{6}, \qquad p g_{,\phi} < 0, \qquad f_{,\chi\chi} < 0. \tag{6.27}$$

To better illustrate the stability conditions of this section we will examine some familiar cases in Sec. 6.4 and provide some more physical insight in Sec. 6.7.

6.4 Examples

6.4.1 Models with one integral of motion

When the mini-superspace Lagrangian is independent of one coordinate then the corresponding canonical momentum is a constant (integral) of motion. The cyclic variable will not affect the dynamics and, hence, the inflaton can not be identified with the isometric field. Therefore, both the metric and the potential should depend only on the inflaton

$$ds^2 = d\phi^2 + g(\phi)^2 d\chi^2, \qquad V = e^{p\phi}, \tag{6.28}$$

and the dynamical system simplifies to

$$\phi' = y, \tag{6.29}$$

$$\chi' = \frac{x}{g}, \tag{6.30}$$

$$y' = -(3 - \epsilon)(y + p) - \frac{g_{,\phi}}{g}x^2, \tag{6.31}$$

$$x' = -\left(3 - \epsilon + \frac{g_{,\phi}}{g}y\right)x. \tag{6.32}$$

We discard the second equation and then study the reduced 3×3 system.

Since inflation proceeds along ϕ, a frozen solution is $(y, x) = (-p, 0)$, which exists for every metric function g and is defined for $|p| < \sqrt{6}$. The

x' equation takes the simple form $x' = -Ax$ where A is exactly the term $3 - \epsilon + D$ derived in Eq. (6.23). Its sign determines the growth or decay of linear perturbations δx around the $x = 0$ solution. With $\epsilon = \epsilon_V$ the turn rate is zero and the mass term of Eq. (6.20) is identical zero, which is understood as a consequence of the shift symmetry in χ. The turn rate for this case is zero and dynamics is essentially single-field.

Similarly, the kinetic solution exists for every p and it is stable when $|p| < \sqrt{6}$ and $pg_{,\phi} < 0$.

6.4.2   Models with a field space isometry

Excluding the existence of an integral of motion we increase the complexity of the problem by assuming a field-metric isometry and a potential depending on both fields. In contrast to the previous subsection, inflation can proceed along either the isometry or the orthogonal (to the isometry) field.

In the first case, we assume that the metric is shift symmetric in χ [2]

$$ds^2 = d\phi^2 + g(\phi)^2 d\chi^2, \qquad V = h(\chi)e^{p\phi}, \qquad (6.33)$$

the normalized Killing vector is $k^i = (0, 1/g)$, while the vector orthogonal to k^i is $b^i = (1, 0)$. The two normalized velocities represent the projections of the velocity vector along and orthogonal to the Killing vector

$$x = k^i v_i, \qquad y = b^i v_i. \qquad (6.34)$$

Eq. (6.14), which determines the possible values of the orthogonal field, requires $p_\chi = 0$ and so the isometry field should be frozen at a critical point of h. As a result $\epsilon = \epsilon_V$ and the turn rate vanishes resulting to single-field dynamics similar to the previous subsection. The condition $M^2 > 0$ gives $h_{,\chi\chi} > 0$ and the critical point should be a minimum, as expected. The other condition relates the gradient of the potential with the monotonicity of the metric function through the relation

$$3 - \epsilon + D > 0 \Rightarrow p^2 + 2p\frac{g_{,\phi}}{g} - 6 < 0. \qquad (6.35)$$

This condition is satisfied for p belonging to the interval between the two roots

$$-\sqrt{6 + \left(\frac{g_{,\phi}}{g}\right)^2} - \frac{g_{,\phi}}{g} < p < \sqrt{6 + \left(\frac{g_{,\phi}}{g}\right)^2} - \frac{g_{,\phi}}{g}. \qquad (6.36)$$

---

[2]Eq. (6.33) describes the most general form of a metric with one isometry (see App. B.3.

Moreover, the requirements for stable kinetic solutions are the same as in the previous subsection.

Turning to the second possibility, we identify the inflaton with the isometry field

$$\mathrm{d}s^2 = f(\chi)^2 \, \mathrm{d}\phi^2 + \mathrm{d}\chi^2 \,, \qquad V = h(\chi)e^{p\phi} \,. \tag{6.37}$$

Likewise, the normalized Killing vector is $K^i = (1/f, 0)$, while the vector orthogonal to it is $B^i = (0, 1)$ and the two normalized velocities are

$$x = B^i v_i \,, \qquad y = K^i v_i \,. \tag{6.38}$$

1. When $p_\chi(\chi_0) = 0$ it is also required that $f_{,\chi}(\chi_0) = 0$ and the orthogonal field is stabilized at a minimum of its potential, effectively describing a single-field model. The condition for stability is then $|p|/f(\chi_0) < \sqrt{6}$ and if violated the system departs to kinetic domination.

2. Now we will examine the case $p_\chi(\chi_0) \neq 0$. Due to the frozen condition $\chi' = 0$, the slow-roll parameter ϵ receives contribution only from ϕ and hence $\epsilon < \epsilon_V$. This implies that the turn rate will be non zero and so motion can be strongly non-geodesic. Since $g = 1$, D is zero and the first condition of (6.23) is trivially satisfied, while M, after some algebra, becomes equal to the effective mass on super-Hubble scales (defined in Eq. (4.59)). The condition for stability is again $p/f(\chi_0) < \sqrt{6}$ but with the difference that is always satisfied given that Eq. (6.14) has a solution. To show this we use Eq. (6.15) and note that the stability condition yields

$$\left| \frac{p}{f(\chi_0)} \right| < \sqrt{6} \Rightarrow \frac{p_\chi}{2(\ln f)_{,\chi} + p_\chi} < 1 \,, \tag{6.39}$$

which holds because $p_\chi f_{,\chi} > 0$ (in order for Eq. (6.15) to be solvable). Therefore, frozen solutions with non-vanishing turn rate are always stable when they exist, and subsequently, kinetic domination is always unstable. We will show later that most novel solutions that were discovered recently belong to this class.

6.5 Field spaces with enhanced isometries

In the previous sections we imposed the frozen coordinate condition in order to derive consistent solutions different than de Sitter or kinetic domination. For generic functions f and g scaling solutions with $x, y \neq 0$ are in general

inconsistent because the Christoffel terms are field dependent and vary during the evolution; however, in two special cases the dynamical system can be reduced from four to two equations because the Christoffel terms become constants.[3]

6.5.1   Euclidean space

When the metric is Euclidean the reduced dynamical system reads

$$\begin{aligned} y' &= -(3 - \epsilon)\,(y + p_\phi)\;, \\ x' &= -\,(3 - \epsilon)\,(x + p_\chi)\;. \end{aligned} \tag{6.40}$$

For a product-exponential potential both p_ϕ and p_χ are constant, and the scaling solution is $(y, x) = (-p_\phi, -p_\chi)$ which is seemingly different than the frozen solution assumed at the beginning of the Sec. 6.2.1. Under an orthogonal rotation of x and y (similar to the various transformations used in models of assisting inflation [155, 161])

$$\begin{pmatrix} z \\ w \end{pmatrix} = \begin{pmatrix} \frac{p_\phi}{p} & -\frac{p_\chi}{p} \\ \frac{p_\chi}{p} & \frac{p_\phi}{p} \end{pmatrix} \begin{pmatrix} y \\ x \end{pmatrix}\;, \tag{6.41}$$

with $p = \sqrt{p_\chi^2 + p_\phi^2}$, the dynamical system is transformed to

$$\begin{aligned} z' &= -(3 - \epsilon)\,(z + p)\;, \\ w' &= -\,(3 - \epsilon)\,w\;, \end{aligned} \tag{6.42}$$

which supports a scaling solution $(z, w) = (-p, 0)$. By performing an isometry transformation we achieved to map the original solution into a frozen type one.

6.5.2   Hyperbolic space

For the hyperbolic space in the parameterization $g = e^{\phi/L}$ the ratio $g_{,\phi}/g$ is constant. For a single-field exponential potential the dynamical system becomes

$$\begin{aligned} y' &= -(3 - \epsilon)\,(y + p) + \frac{1}{L}x^2\;, \\ x' &= -\left(3 - \epsilon + \frac{1}{L}y\right)x\;, \end{aligned} \tag{6.43}$$

admitting three solutions:

---

[3]Even though we can not exclude other combinations of potentials and metrics that yield solutions with $x, y \neq 0$, the two examples in this section were the only results of our extensive investigation.

1. The gradient solution,

$$(y, x)_{\mathrm{gr}} = (-\lambda, 0) \, , \qquad (6.44)$$

where motion is aligned with the potential gradient flow. It is stable provided

$$-\sqrt{6 + \frac{1}{L^2}} - \frac{1}{L} < p < \sqrt{6 + \frac{1}{L^2}} - \frac{1}{L} \, , \qquad |p| < \sqrt{6} \, . \qquad (6.45)$$

2. The kinetic solution, given as

$$(y, x)_{\mathrm{kin}} = \left(\pm\sqrt{6}, 0\right) \, , \qquad (6.46)$$

and which is stable for $|p| > \sqrt{6}$ and $p/L < 0$.

3. The hyperbolic solution has $y, x \neq 0$

$$(y, x)_{\mathrm{hyper}} = \left(-\frac{6}{\frac{2}{L} + p}, \pm\frac{\sqrt{6}\sqrt{p^2 + \frac{2}{L}p - 6}}{\frac{2}{L} + p}\right) \, , \qquad (6.47)$$

and exists provided one of the following two relations is satisfied

$$p > p_{\mathrm{crit},1} = -\frac{1}{L} + \sqrt{6 + \frac{1}{L^2}} \, , \qquad (6.48)$$

$$p < p_{\mathrm{crit},2} = -\frac{1}{L} - \sqrt{6 + \frac{1}{L^2}} \, , \qquad (6.49)$$

(and so it requires $pL > 0$). Interestingly, the region of stability coincides with the domain of definition for this solution. To show this we can calculate the eigenvalues as usual but since they lead to complicate expressions we will instead use the Hurwitz-Routh stability criterion (see App. B.2) to draw conclusions about their real part. The characteristic polynomial for this problem is

$$\lambda^2 + \frac{6}{2 + Lp}\lambda + 6\frac{p^2 + 2p/L - 6}{2 + Lp} = 0 \, , \qquad (6.50)$$

and so in order for this to be positive definite we require every coefficient to be positive. The values of p and L for which both eigenvalues have non-positive real part coincides with the domain of definition of the solution (6.47) as well as the values for which the gradient and kinetic solutions are both unstable.
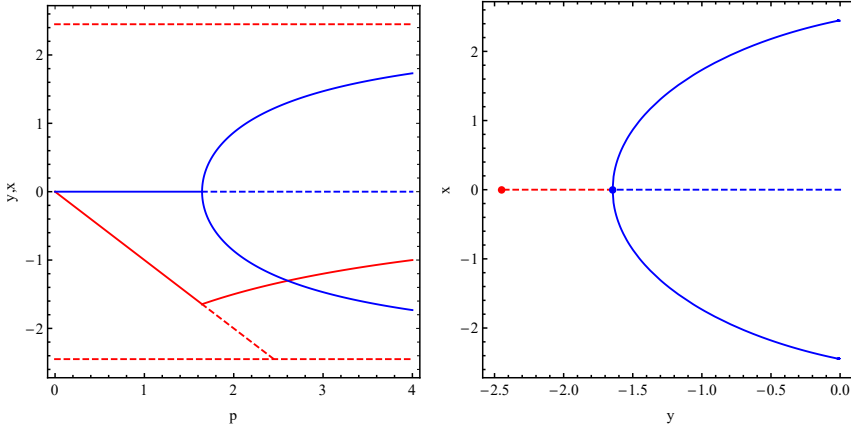
FIGURE 6.1

Left: *The bifurcation diagram for the system of Eqs.* (6.43) *on a hyperbolic space*
$f = Le^{\rho/L}$ *for a shift-symmetric potential with* $p_\phi = 0$. *The red and blue curves*
correspond to the values of x *and* y *respectively, as a function of* p_ρ, *at the various*
critical points. Solid (dashed) lines correspond to stable (unstable) solutions. We see
that for large values of the potential steepness p_ρ *the only stable solution is Eq.* (6.47).
Right: *The same bifurcation diagram given as a curve on the* (x, y) *plane.*

At the critical value $p_{\text{crit},1}$ or $p_{\text{crit},2}$ there is a transition between the gradient flow and the hyperbolic solution. This is depicted at the left panel of Fig. 6.1. The curve $x(p)$ has the typical form of a pitchfork bifurcation, with bifurcation parameter the gradient p. When the gradient exceeds the critical value p_{crit}, the orthogonal velocity x will settle at one of the two roots, depending on the sign of initial velocity χ'.

Remarkably, ϵ for the hyperbolic solution is given by

$$\epsilon = \frac{3pL}{2 + pL}\,, \tag{6.51}$$

which has the same form as the expression for the slow-roll parameter of frozen solutions given by Eq. (6.15). Prompted by this fact and our earlier investigation in flat space we will attempt to perform a transformation related to the isometries of the hyperbolic space and bring this model into a form that supports a frozen-type solution.

6.5.3   Relation between hyperbolic and frozen solutions

Our guiding principle will be the possible reparametrisations of the hyperbolic space, which can be found for example in Refs. [140, 162]. We start

with

$$\mathrm{d}s^2 = L^2 \frac{\mathrm{d}\tau \, \mathrm{d}\bar{\tau}}{(\mathrm{Im}\,\tau)^2}\,, \tag{6.52}$$

where $L = \sqrt{3\alpha/2}$, and then choose $\tau = \tilde{\phi} + iLe^{-\tilde{\chi}L}$ in order to describe the axion-dilaton system. This leads to the field-space line element

$$\mathrm{d}s^2 = \mathrm{d}\tilde{\chi}^2 + e^{2\tilde{\chi}/L} \, \mathrm{d}\tilde{\phi}^2\,. \tag{6.53}$$

By choosing an alternative coordinate basis $\tau = e^Z = e^X(\cos Y + i \sin Y)$ we can easily rewrite the metric as

$$\mathrm{d}s^2 = \frac{L^2}{\sin^2 Y}\left(\mathrm{d}X^2 + \mathrm{d}Y^2\right). \tag{6.54}$$

We now canonically normalize one of the two variables, by choosing

$$\chi = L \ln\left[\tan\left(\frac{Y}{2}\right)\right]\,, \qquad \phi = LX\,, \tag{6.55}$$

leading to

$$\mathrm{d}s^2 = \mathrm{d}\chi^2 + \cosh^2\left(\frac{\chi}{L}\right)\mathrm{d}\phi^2\,, \tag{6.56}$$

which manifests the isometry explicitly. Note that although both diagonal metrics define a hyperbolic space with the same Ricci curvature scalar, the manifest isometry direction (Killing vector) is different for the two parameterization. Equating the two expressions for τ provides the transformation rule between the coordinate systems

$$\tilde{\phi} = -\tanh\left(\frac{\chi}{L}\right)e^{\phi/L}\,, \qquad e^{\tilde{\chi}/L} = Le^{-\phi/L}\cosh\left(\frac{\chi}{L}\right). \tag{6.57}$$

Following the same transformation, we re-write the potential in the new basis $\{\chi, \phi\}$ as

$$V(\chi, \phi) = V_0 \left[\cosh\left(\frac{\chi}{L}\right)\right]^{pL} e^{-p\phi}\,. \tag{6.58}$$

This potential has the form of Eq. (6.7) and, thus, allows for a frozen solution. It is straightforward to check that the time evolution of the various coordinates based on the hyperbolic and frozen solutions respectively are related to each other by the above described coordinate transformations.

In this coordinate system, Eq. (6.14) determines the value at which χ stabilizes

$$p\left[\cosh\left(\frac{\chi}{L}\right)\right]^{-2}\tanh\left(\frac{\chi}{L}\right)\left[p^2 + 2\frac{p}{L} - 6\cosh^2\left(\frac{\chi}{L}\right)\right] = 0\,. \tag{6.59}$$

The slow-turn solution takes place at $\chi = 0$, the minimum of V in the χ direction, and hence $\epsilon = \epsilon_V$. For $\chi \neq 0$ an extra pair of roots exist provided

$$\cosh^2\left(\frac{\chi}{L}\right) = \frac{p^2 + 2\frac{p}{L}}{6} > 1\,, \tag{6.60}$$

recovering the condition (6.35).

6.6 Bifurcations in scaling solutions

When a dynamical system depends continuously on some parameters then stability of its critical points may depend on the values of those parameters. More specifically, variation of the parameters may alter the stability properties of certain critical points or it can lead to the creation (annihilation) of critical points with different stability properties.

Specializing to one dimension

$$\dot{x} = f(x, a)\,, \tag{6.61}$$

a necessary (but not sufficient) condition for the existence of a bifurcation at a critical point located at $x = 0$ and for the bifurcation parameter $a_{\mathrm{cr}} = 0$ is [163, 164]

$$f(0,0) = 0, \qquad \frac{\partial f}{\partial x}(0,0) = 0\,. \tag{6.62}$$

The next-to-leading terms in the Taylor expansion near the critical point will determine the type of bifurcation:[4]

- if $\partial_{xx}f(0,0) \neq 0$ and $\partial_{xa}f(0,0) \neq 0$ then a *transcritical bifurcation* occurs for $a = 0$. The normal form of equations around the critical point is

$$\dot{x} = c_1 a x + c_2 x^2\,. \tag{6.63}$$

- if $\partial_{xx}f(0,0) = 0$ instead, but $\partial_{xa}f(0,0) \neq 0$ and $\partial_{xxx}f(0,0) \neq 0$, then a *pitchfork bifurcation* occurs for $a = 0$. Similarly, the normal form is

$$\dot{x} = c_1 a x + c_2 x^3\,. \tag{6.64}$$

  There are two types of pitchfork bifurcations depending on the sign of c_2. In the *supercritical* case, $c_2 < 0$, a stable critical point becomes unstable and two new stable points are created. The *subcritical* case, $c_2 > 0$, two unstable critical points are annihilated and a stable critical point becomes unstable.

---

[4]With a redefinition of x the constant c_2 can be set to ± 1, while c_1 can be absorbed in the definition of the bifurcation parameter.

An example of the first kind is the exchange of stability between the solution $v = -p$ and the kinetic solution for one field when $p = \sqrt{6}$. Translating the critical point at the origin by defining $z \equiv v + p$ and changing the bifurcation parameter to $k \equiv p - \sqrt{6}$ Eq. (6.4) becomes

$$z' = \sqrt{6}kz + \sqrt{6}z^2 + \left(\frac{1}{2}k^2z + kz^2\right) . \tag{6.65}$$

Three remarks are in order: there are no first order terms in either k or z; the second order terms are exactly those mentioned above; the terms in parenthesis are higher order. Therefore, a transcritical bifurcation happens at $p = \sqrt{6}$.

An example of the second kind is the bifurcation of the normalized velocity x in the hyperbolic problem (6.43). After a similar coordinate translation the reduced two-dimensional system can be transformed to

$$z' = \frac{x^2}{L} - \frac{1}{L}\left(\sqrt{\frac{1}{L^2}+6} - \frac{1}{L}\right)z + \left(\sqrt{\frac{1}{L^2}+6} - \frac{1}{L}\right)kz \tag{6.66}$$

$$+ \frac{1}{2}\left(k^2 + x^2\right)z - \left(\sqrt{\frac{1}{L^2}+6} - \frac{1}{L} + k\right)z^2 + \frac{z^3}{2} ,$$

$$x' = x\sqrt{\frac{1}{L^2}+6}\,(k-z) + \frac{k^2x}{2} - kxz - \frac{x^3}{2} , \tag{6.67}$$

$$k' = 0 , \tag{6.68}$$

where the last equation increases the dimension of the system in order to study the bifurcation with centre manifold techniques. Parametrizing the stable direction in terms of the centre manifold variables $z = z(x,k)$ the chain rule yields

$$z' = x'\frac{\partial z}{\partial x} , \tag{6.69}$$

with $\frac{\partial z}{\partial x}(0,0) = \frac{\partial z}{\partial k}(0,0) = 0$. Thus, the lowest order terms in the Taylor expansion of z are quadratic

$$z = c_{11}x^2 + c_{12}xk + c_{22}k^2 + \cdots . \tag{6.70}$$

Since z is at least second order in terms of x,[5] centre manifold dynamics to lowest order is governed by

$$x' = xk\sqrt{\frac{1}{L^2}+6} - \frac{x^3}{2} + O(x^4) , \tag{6.71}$$

---

[5] Close to the critical point $x \sim \sqrt{k}$, so k is of order x^2.

and a pitchfork bifurcation happens at $(x, k) = (0, 0)$.

For frozen solutions with an isometry, a bifurcation is possible if $f_{,\chi}$ and p_χ share a common root which without loss of generality we consider to be at $\chi = 0$. Diagonalizing the system the zero eigenvalue occurs for the variable

$$z = \chi + \frac{x}{3 - \epsilon_c} \,, \tag{6.72}$$

while the other two variables are $x/(3 - \epsilon_c)$ and $w = y - p_\phi/f(0)$. The equation of motion for z is given by

$$z' = x \left(1 - \frac{3 - \epsilon}{3 - \epsilon_c}\right) - V_{\text{eff}}^{,\chi} \,, \tag{6.73}$$

where $V_{\text{eff}}^{,\chi}$ is the effective gradient introduced in [123] and will be extensively studied later in Ch. 7. As usual we consider x and w to be quadratic functions of z and the bifurcation parameters and the first term of Eq (6.73) is at least 4th order. Therefore, close to the critical point $V_{\text{eff}}^{,\chi}$ determines the dynamics of the centre manifold. Expanding around $z = 0$ we obtain to lowest order

$$
\begin{aligned}
z' = &-\frac{k + \sqrt{2\epsilon_c}(p^{(1)} - R)\big|_{\chi=0} \, w}{3 - \epsilon_c} z + \\
&\frac{1}{3 - \epsilon_c} \left(-\frac{R^2 \epsilon_c}{4} - \frac{1}{6}(3 - \epsilon_c)p^{(3)} + \frac{1}{3}\frac{f^{(4)}}{f}\epsilon_c\right)\bigg|_{\chi=0} z^3 \,,
\end{aligned}
\tag{6.74}
$$

$$w' = -(3 - \epsilon_c)\left(w + \frac{\sqrt{2\epsilon_c}}{4}R\right) z^2 \,, \tag{6.75}$$

where we omitted the equation for x as it does not affect the equation of the centre manifold. Since z' is at least 3rd order in z the quadratic coefficient of $w(z)$ should cancel the second term of Eq. (6.75) and so $w(z) = -\frac{1}{4}\sqrt{2\epsilon_c}R$. Substituting back to Eq. (6.74) we finally obtain the equation of the centre manifold

$$(3 - \epsilon_c)z' = -kz + \left(\frac{2p^{(1)} - 3R^2\epsilon_c}{4} - \frac{1}{6}(3 - \epsilon_c)p^{(3)} + \frac{1}{3}\frac{f^{(4)}}{f}\epsilon_c\right)\bigg|_{\chi=0} z^3 \,, \tag{6.76}$$

and a supercritical pitchfork bifurcation occurs for $k = 0$. This equation is exactly the same as the expansion of $V_{\text{eff}}^{,\chi}$ around $\chi = 0$ up to 3rd order when we have expressed every variable in terms of χ.

6.7 Comparison of different stability criteria

In Sec. 6.3 we investigated the stability of frozen solutions and derived the conditions (6.23) that determine when a solution will be stable. We observe that the effective mass of the orthogonal perturbation on super-Hubble scales, given in Eq. (4.59), is not always present in the stability criteria. Positivity of the effective mass has been considered the standard criterion of background stability for most recent novel models in non-trivial field manifolds with an isometry (see the extensive list in the next section), as well as in works which claim geometry-independent conclusions, e.g. [92,100]. As we saw in Sec. 6.4.2, for problems with an isometry in the inflationary direction the condition $\mu_s^2 > 0$ becomes necessary and sufficient for background stability. We can thus trace the potential disagreement in all other cases to the fact that the orthogonal perturbation is not canonically normalized. Notice that in the derivation of the stability criteria we calculated how 'bare' orthogonal perturbations $\delta\chi$ and $\delta(g\chi')$ evolve, whereas the adiabatic/entropic decomposition uses the 'normalized' perturbations $Q_s = g\delta\chi$, $Q_s' = (g\delta\chi)'$. In order to understand which method gives the correct result it is useful to review the notion of stability on a multi-dimensional curved scalar manifold.

To check the stability of a particular solution (e.g. ϕ_{sol}^i) one has to study the eigenvalues of the Jacobian matrix (or the local Lyapunov exponents) evaluated on that solution

$$(\delta x^i)' = J_k^i \delta x^k \,. \tag{6.77}$$

If every exponent is negative then the system converges to ϕ_{sol}^i. The case of zero eigenvalues is more intricate because stability will be determined by higher order terms. On the contrary, a positive exponent indicates an unstable direction and an overall unstable solution (with possibly chaotic behaviour). An important note is that linearised stability gives information only at a given point where the Jacobian matrix is evaluated. Thus, a small perturbation will not evolve according to the linearised equation (6.77); the Jacobian encodes information only for an infinitesimally small deformation, not defined a priori. The previous consideration implies that an unstable solution can also manifest an almost oscillating behaviour because higher order terms can attract the system back to the critical point, in contrast to the leading order terms.

In order to solve the linearised Eq. (6.77) we diagonalize the stability matrix by considering $\boldsymbol{J} = \boldsymbol{O}^{-1}\boldsymbol{\lambda}\boldsymbol{O}$ and define $\boldsymbol{z} \equiv \boldsymbol{O}\boldsymbol{\delta x}$. We then obtain

a set of decoupled equations

$$\boldsymbol{z}' = \boldsymbol{\lambda z} \Rightarrow \boldsymbol{z} = e^{\boldsymbol{\lambda} N}\boldsymbol{z}(0) \,, \tag{6.78}$$

and the solution to the original equations is given by

$$\boldsymbol{\delta x} = \boldsymbol{O}^{-1}e^{\boldsymbol{\lambda} N}\boldsymbol{O}\boldsymbol{\delta x}(0) \,. \tag{6.79}$$

If all eigenvalues are negative then the initial perturbations $\delta x^i(0)$ will decay; more precisely, this means that for the particular solution under consideration ϕ^i_{sol} there will be convergence (for instance in the L^2 sense) of the coordinates (and their derivatives) towards the assumed values: $\{\phi^i, (\phi^i)'\} \rightarrow \{\phi^i_{\text{sol}}, (\phi^i)'_{\text{sol}}\}$. The rate of convergence is given by the magnitude of the corresponding eigenvalues. Therefore, every other function of the phase space variables will converge as well, e.g. slow-roll parameters ϵ and η.

Now let's consider instead some linear combinations of the perturbations $y^I \equiv f^i_k \delta x^k$ for which the system reads

$$(y^i)' = \tilde{J}^i{}_k y^k \,, \tag{6.80}$$

where $\tilde{J}$ is the new stability matrix. The solution is similarly found by diagonalization of the new 'stability' matrix

$$\boldsymbol{y} = \tilde{\boldsymbol{O}}^{-1}e^{\tilde{\boldsymbol{\lambda}} N}\tilde{\boldsymbol{O}}\boldsymbol{y}(0) \,. \tag{6.81}$$

Knowledge of the eigenvalues of $\tilde{J}$ provides no information about the eigenvalues of the original matrix as the two are not related via a similarity transformation. As an example, we assume that y's are chosen such that $A = (y^1)^2 + (y^2)^2 = G_{ij}\delta x^i \delta x^j$. If A is decreasing, due to negative eigenvalues, then we showed that the norm of the perturbations vanishes. This is what one might expect as the definition of stability for a dynamical system involving vector quantities on a manifold. Nevertheless, this type of stability does not guarantee that other phase space functions converge as well, which is why studying perturbations in the adiabatic/entropic does not always give the correct conclusion about the homogeneous equations.

A coincidentally correct application of the effective mass criterion for background stability happens for the hyperbolic problem. Even though the 'orthogonal' field of the gradient-flow solution is not canonically normalized, the sign of μ_s^2 is sufficient to prove stability because $3 - \epsilon + D \propto \mu_s^2$. Note that this is expected because in Sec. 6.5.3 we proved that it is possible to bring the hyperbolic solution into a frozen-type one for which $M = \mu_s$,

and we expect stability conclusions to be independent of the particular coordinate system in use. For any other choice of the field-metric function g of (6.28) the quantity $3 - \epsilon + D$ is not related to the effective mass.

Because of the previous considerations, it is possible to find stable solutions with $\mu_s^2 < 0$ or unstable solutions with $\mu_s^2 > 0$. We can verify this using the 'minimal' field-space metric that was considered in the original geometrical destabilization scenario [87] but with an exponential potential

$$\mathrm{d}s^2 = \mathrm{d}\phi^2 + \left(1 + 2\frac{\phi^2}{L^2}\right)\mathrm{d}\chi^2\,, \qquad V = e^{p\phi}\,. \tag{6.82}$$

The stability criterion (6.23) determines which values of p give rise to stable solutions

$$0 < p < \sqrt{6 + \left(\frac{2\phi}{1 + 2\phi^2}\right)^2} - \frac{2\phi}{1 + 2\phi^2}\,. \tag{6.83}$$

Note that for negative values of ϕ the r.h.s. is greater than $\sqrt{6}$ and hence the gradient flow solution becomes stable for any value of $p < \sqrt{6}$ (see left panel of Fig. 6.2). For the same values of p, the effective mass is equal to

$$\frac{\mu_s^2}{H^2} = p\frac{2\left(6 - p^2\right)\phi^3 - L^2\left(2p - \left(6 - p^2\right)\phi\right)}{\left(L^2 + 2\phi^2\right)^2}\,, \tag{6.84}$$

which is positive for $0 < \phi_+ < \phi$ and negative for $\phi < \phi_- < 0$, and the two values $\phi_\pm$ depend on p, L. Considering $p = L = 1$ the effective mass becomes negative for $\phi < 0$, while motion is stable (see left panel of Fig. 6.2).

Finally, it is worth wondering what is the fate of the system when the frozen solution is unstable. If a stable kinetic solution exists then the system will depart to kinetic domination. All other cases require examination of the behaviour of the system at the boundary of the field space. For example, a de Sitter state ($x = y = 0$) can be supported as a limiting case on the boundary of the field space even though the same solution may be incompatible in the bulk of space, as it requires $p_\chi = p_\phi = 0$. When neither of the previous is possible the system is doomed to follow a never-ending oscillatory, possibly chaotic, motion. This is depicted at the right panel of Fig. 6.2 for a toy model with

$$V = (1 + 0.05\chi^2)e^{p\phi}\,, \qquad \mathrm{d}s^2 = \mathrm{d}\phi^2 + e^{-\phi^2/8}\,\mathrm{d}\chi^2\,. \tag{6.85}$$

The solution is clearly unstable while its effective mass is positive. A complete description of asymptotic states for scaling solutions lies beyond the scope of this thesis.
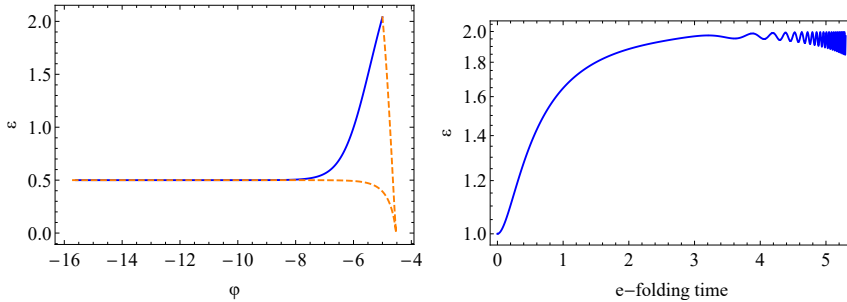
FIGURE 6.2

Left: *Evolution of ϵ for the model* (6.82) *for negative (blue line) or positive (dashed orange line) initial ϕ'.*
Right: *Evolution of ϵ for the model* (6.85). *The system quickly becomes stiff due to rapid oscillations.*

6.8   Relation to inflationary models

Now, we are able to link scaling solutions to the novel behaviour found in recent studies. An example that is close to the scaling solutions presented in Secs. 6.4.1 and 6.5.2 has been coined "hyperinflation" [147] and was studied in e.g. [99, 148]. The field-space has constant negative curvature, and is written in global coordinates as

$$\mathrm{d}s^2 = \mathrm{d}\rho^2 + L^2 \sinh^2\left(\frac{\rho}{L}\right) \mathrm{d}\phi^2 \,, \qquad (6.86)$$

where ρ, ϕ are radial and angular-like variables respectively. Note that the metric function f asymptotically behaves as an exponential for $\rho \gg L$. The late-time solution of equation (6.47) for this choice of metric can be written as

$$\dot{\rho} \approx -\frac{3HL}{\coth\left(\frac{\rho}{L}\right) + \frac{1}{2}p_\rho L} \,. \qquad (6.87)$$

For large field-space curvature $L \ll 1$ at $\rho \gg L$ the second term in the denominator is subdominant and, thus, the 'radial' velocity becomes $\dot{\rho} \approx -3HL$ which is the expression given for this model in Refs. [147, 148]. Moreover, the steepness condition for the potential $p_\rho > 3L$ corresponds to the small L limit of Eq. (6.48).

The stability of the hyperbolic solution with both positive and negative L was studied in the "ultra-light axion" scenario of [165] based on the effective mass criterion $\mu_{\mathrm{s}}^2 > 0$. Although this method gives the correct result for this particular problem (for reasons explained in Sec. 6.7) it provides inconclusive arguments when e.g. the metric $f = A_- e^{-\phi/L} + A_+ e^{\phi/L}$

is considered. In this case, it was found numerically that the background solution converges to a geodesic, while the effective mass is strictly negative. This was an example of a scaling solution displaying the "geometrical instability of ultra-light fields" that was pointed out in [166] and can be explained when the correct stability criteria are taken into account.

Models that are close to frozen solutions described in Sec. 6.4.2 include angular [106], sidetracked [154], hyperinflation [147] (after the coordinate transformation), orbital [167, 168] and the helix model [101]. Regarding background evolution these models can be cast in different classes depending on the number of late-time frozen solutions of Eq. (6.14) and most of them will asymptote to one frozen solution. Sidetracked-like scaling models exhibit pitchfork bifurcations when certain parameter values exceed a critical value. We will discuss bifurcations in more detail in Ch. 7.

To complete the discussion, we mention the case of an isometry and infinite solutions of (6.14). This set-up was investigated in Refs. [169, 170] with emphasis on the case of massless isocurvature fluctuations, $\mu_\mathrm{s}^2 = 0$. It turns out that there is a shift symmetry in the corresponding EFT of fluctuations and thus this was coined as "shift-symmetric orbital inflation". By using a product-separable potential with exponential dependence on the angle $V(\phi, \rho) = h(\rho)e^{p_\phi \phi}$ and demanding that scaling solutions exist for all values of the radius ρ and any form of the metric function $f(\rho)$, Eq. (6.14) can be integrated to give

$$h(\rho) = 1 - \frac{p_\phi^2}{6f^2(\rho)} \, . \tag{6.88}$$

Hence, by choosing the above specific relation between the metric and the potential, a scaling solution exists for any value of ρ. Trajectories [6] are related by a shift symmetry $\rho \to \rho + c$ and by using this form of the potential, the mass M in Eq. (6.20) is zero. This was derived in Ref. [169] using the different perspective of the Hamilton-Jacobi formulation with an angle-dependent Hubble function. The trajectories arising in this context can thus be seen as frozen solutions with the special property of having massless isocurvature fluctuations (in the superhorizon limit). Note that unlike other cases with a zero eigenvalue this system leads to a non-diagonalizable Jacobian matrix and, thus, stability conclusions cannot be drawn since the usual theorems do not apply.

---

[6]The exact construction of the potential relies on a multi-valued function of the angle, resulting in a "corkscrew" structure.

7

The effective potential of multi-field models

In this chapter we continue our investigation on the attractor behaviour of various models in the literature. We construct a manifestly covariant expression that describes the late-time solution of every recent proposal. Next, we demonstrate the role of an effective potential whose critical points determine the number of different late-time solutions with particular emphasis on bifurcations between different solutions. This chapter largely follows the publication [171] with the section 7.1.2 rewritten.

7.1   Single-degree evolution

7.1.1   Late-time dynamics

The 'typical' evolution of many multi-field inflationary models that achieve a notion of initial conditions independence consists of an early period of multi-field behaviour and a late period of single-clock inflation. More precisely, we can distinguish between three different phases of evolution:

1. Starting with random initial conditions the accelerations quickly dampen and the system approximately evolves on a reduced hypersurface of $\mathcal{N}$ dimensions.

2. Fields evolve on that hypersurface towards their minima, but not at the same rate; in particular, 'heavier' fields decay faster.

3. A single degree drives evolution.

An intuitive way to understand the different stages is to make the analogy with parachute fall. During the fall an observer is subject to acceleration/deceleration until his/her velocity reaches a critical value, due to the tug of war between the gravitational force and the air resistance. In the ideal case of a constant gravitational field and a friction force proportional to the velocity, the terminal velocity is constant and proportional to the mass of the falling observer. Therefore, more massive observers acquire larger velocities.

Depending on the duration of each phase, the relevant part of the evolution (i.e. the last $50 - 60$ *e*-folds) is described by an $\mathcal{M}$-dimensional hypersurface, where $\mathcal{M}$ is the number of evolving degrees of freedom, or a single trajectory if all other "orthogonal" fields have relaxed to their minima. The first stage cannot be treated analytically, as it requires knowledge of the full solution. For an initial kinetic energy that is not exponentially larger than the potential energy this phase usually lasts a few *e*-folds. The second phase can be treated analytically only for models following the gradient flow because the coupled system of equations becomes (approximately) linear in the velocities. For these models, this intermediate phase may account for a significant part of the evolution and has been extensively studied in the literature.

In the rest of this chapter we mainly focus on the last phase which can be treated analytically for generic models not necessarily following the gradient flow. To this end, we decompose the scalar fields $\Phi^k = (\phi, \chi^i)$, where ϕ is defined as the (light) inflationary direction and χ^i are the orthogonal fields that are (approximately) constant during inflation. This split is

manifested in an appropriate coordinate system where $(\chi^i)' \approx 0$ will hold as an (approximate) solution. Specializing to $\mathcal{N} = 2$ (though this argument also holds for an arbitrary number of fields), under an appropriate coordinate transformation the components of the velocity vector $\{(\psi^1_{\text{sol}})', (\psi^2_{\text{sol}})'\}$ (which can be non-zero in general) can be mapped to $\{(\phi^1_{\text{sol}})', 0\}$.[1] Since the existence of an attractor solution is assumed, velocities are given as functions of the fields, and the partial differential equation for the unknown function ϕ^2

$$\frac{\partial \phi^2}{\partial \psi^1}(\psi^1_{\text{sol}})' + \frac{\partial \phi^2}{\partial \psi^2}(\psi^2_{\text{sol}})' = 0 \,, \tag{7.1}$$

has the form of the advection equation with variable coefficients. This can always be solved (for instance with the method of characteristics) and this proves the existence of our coordinate construction.

This coordinate choice leads to [2]

$$v^k \approx (v, 0, \dots) \,, \qquad (v^k)' \approx \left(\frac{\mathrm{d}v}{\mathrm{d}N} + \Gamma^\phi_{\phi\phi} v^2, \Gamma^i_{\phi\phi} v^2 \right) \,, \tag{7.2}$$

evaluated on that particular inflationary solution.[3] We observe a particularly striking separation of the consequences of prolonged inflation ($\epsilon' \ll 1$). Along the inflationary direction $G_{\phi\phi} v \, \mathrm{D}_N v \ll 1$, which through the equations of motion (4.4) yields $v \approx -(\ln V)^{,\phi}$. This implies that the inflationary direction is subject to the usual slow-roll condition, where Hubble friction is balanced by the potential gradient. For generic potentials consistency of this solution requires the smallness of first and second slow-roll parameters in the inflationary direction (presented in Sec. 4.3). In our coordinate system the two conditions read:

$$\frac{1}{2} G^{\phi\phi} \left(\frac{V_{,\phi}}{V} \right)^2 \ll 1 \,, \qquad G^{\phi\phi} \frac{V_{,\phi\phi}}{V} \ll 1 \,. \tag{7.3}$$

The situation is radically different for the orthogonal field directions. By adapting our coordinates, we have defined these as stationary that can have a non-vanishing covariant acceleration only when deviating away from a geodesic. This introduces a (generalized) centrifugal force that is balanced

---

[1]Recall that the components of the velocity transform as $(\phi^i_{\text{sol}})' = \frac{\partial \phi^i}{\partial \psi^k}(\psi^k_{\text{sol}})'$.

[2]Note that the present construction differs from the adiabatic/entropic decomposition discussed in Sec. 4.2 since the latter does not introduce a new coordinate system. Instead, the adiabatic direction is related to our inflationary direction as $\dot{\sigma}^2 = G_{\phi\phi}\dot{\phi}^2$.

[3]While field-space manifolds with isometries provide natural choices for this parametrization (e.g. [169]), we will later show that the presence of an isometry is not necessary.

by a potential gradient: for the stationary directions equations of motion reduce to

$$V_{\text{eff}}^{,i} \equiv V^{,i} + \Gamma_{\phi\phi}^{i} v^2 H^2 \approx 0 \,. \tag{7.4}$$

We call this the *effective gradient* along the i'th direction in field space, generalizing the two-field construction of Ref. [123]. Note that contrary to the inflationary direction, consistency of these conditions imposes no restrictions on $V^{,i}$ (apart from having different signs with respect to $\Gamma_{\phi\phi}^{i}$). As we will see later the magnitude of $V^{,i}$ is related to the turn-rate ω.

Eqs. (7.4) should be seen as algebraic relations for the stationary fields χ^i in terms of the inflaton field ϕ and its velocity v. The stationary fields will adapt their values to balance the centrifugal and potential forces acting on them, as in the gelaton model [123]. Therefore, at a given moment during inflation, i.e. for a particular value of ϕ, one can view Eq. (7.4) as the gradient of an effective potential, whose extrema fix the values of these fields, akin to moduli stabilisation in string theory. When both terms in the right hand side of Eq. (7.4) vanish separately, one has potential gradient flow, which is by no means necessary in the multi-field case. For instance, negative curvature tends to induce non-geodesic motion.

There is an attractive interpretation of the above condition when formulated in phase space. The effective potential (7.4) coincides with the total energy (and the Hubble parameter) as a function of the orthogonal field values χ^i, for a given value of the inflaton ϕ and its conjugate momentum $\pi_\phi = G_{\phi\phi}\dot{\phi}$. In other words, the space-time metric and the inflaton field are assumed as a fixed time-dependent background, and the orthogonal fields are subject to the energy extremization condition

$$\partial_i \left(\frac{1}{2} G^{\phi\phi}(\phi, \chi^i) \pi_\phi^2 + V(\phi, \chi^i) \right) = 0 \,. \tag{7.5}$$

The orthogonal field dependence of the first term comes in via $G^{\phi\phi}$ which for negative curvature manifolds decreases as one moves away from the geodesic solution with $\partial_i G_{\phi\phi} = 0$. This allows for a competition between an increase in potential and a decrease in kinetic energies, providing an intuitive interpretation of geometric destabilization [87, 166, 172, 173] as a simple competition of energy contributions.

7.1.2   A coordinate invariant form of the attractor solution

We now derive a coordinate independent expression for the attractor solution in the case of two fields consisting of covariant derivatives of the potential. We find it easier to work in the kinematic basis, so first we need

to express the components of the gradient and Hessian in that basis. They are given up to η and η' terms as follows (the reason why we omit these terms will become clear in the following)

$$\frac{V_A}{V} = -\sqrt{2\epsilon}\begin{pmatrix} 1 \\ \frac{\Omega}{3-\epsilon} \end{pmatrix}, \qquad \frac{V_{AB}}{V} = \begin{pmatrix} \frac{\Omega^2}{3-\epsilon} + \epsilon & -\Omega + \frac{2\epsilon\Omega}{3-\epsilon} \\ -\Omega + \frac{2\epsilon\Omega}{3-\epsilon} & w_{nn} \end{pmatrix}, \qquad (7.6)$$

where we used the notation $V_A \equiv V_{,i}E_A^i$, $V_{AB} \equiv V_{;ij}E_A^i E_B^j$ and $w_{nn} \equiv V_{nn}/V$ (recall that E_A^i is the Jacobian matrix of the transformation from the coordinate to the orthonormal basis). Next, we calculate three curvature invariants that enable us to express the components of the Hessian in terms of them:

1. The norm of the potential gradient is

$$\frac{G^{ij}V_{,i}V_{,j}}{V^2} \equiv 2\epsilon_V \approx \epsilon\left(1 + \frac{\Omega^2}{(3-\epsilon)^2}\right), \qquad (7.7)$$

   where the latter expression is (4.29) with $\eta \approx 0$. As a side-note, the Swampland conjectures constrain the norm of the potential gradient and thus the above equation shows how one can have slow roll inflation with $\epsilon \ll 1$ on a steep potential with $\epsilon_V \geq \mathcal{O}(1)$.

2. The second curvature invariant is given by

$$c_1 \equiv \frac{V^{,i}V_{;ij}V^{,j}}{V^3} = 2\epsilon\left(2\epsilon + \frac{w_{nn} - 3 + 5\epsilon}{(3-\epsilon)^2}\right). \qquad (7.8)$$

3. The third curvature invariant is given by

$$c_2 \equiv \frac{V^{,i}V_{;ij}G^{jk}V_{;kl}V^{,l}}{V^4}$$
$$\approx 2\epsilon\left(4\epsilon^2 + \Omega^2\frac{(w_{nn}-3)^2 + 6(w_{nn}-\epsilon)\epsilon + 17\epsilon^2}{(3-\epsilon)^2} + \frac{4\epsilon^2\Omega^4}{(3-\epsilon)^4}\right). \qquad (7.9)$$

Using the previous three quantities we find the following expression for ϵ

$$\epsilon \approx \frac{2c_2\epsilon_V - c_1^2}{2(c_2 - 4c_1\epsilon_V + 8\epsilon_V^3)}. \qquad (7.10)$$

In case the denominator is zero we need to construct an alternative curvature invariant. Our fourth and final curvature invariant is the trace of the Hessian

$$d \equiv \frac{G^{ij}V_{;ij}}{V} \approx w_{nn} + 2\epsilon + \frac{\Omega^2}{3-\epsilon}. \qquad (7.11)$$

Using the condition $c_2 - 4c_1\epsilon_V + 8\epsilon_V^3 = 0$ in combination with the trace of the Hessian we find two solutions for ϵ:

$$\epsilon \approx \epsilon_V \,, \qquad \epsilon \approx \frac{3\epsilon_V}{d - \epsilon_V} \,, \tag{7.12}$$

and we obtain either gradient flow or a solution of a different type.

Note, though, that our task to find an expression for the attractor solution is not yet complete because the solution is given as a function of the two fields, ϕ and χ. As we explained in the previous section, the true attractor solution should consist of only one dynamical field, while the second one should be given as a function of the inflaton. In order to obtain the parametric relation $\chi(\phi)$ we should construct a different expression for ϵ and then equate the two. The only exception is the class of models with a cyclic variable and in this case one expression for ϵ should suffice. Using d and c_1 in combination with Eq. (7.7) gives the following quadratic equation for ϵ

$$(d - \epsilon_V)\epsilon^2 - \frac{1}{2}\left(2\epsilon_V(3 + d + \epsilon_V) - c_1\right)\epsilon + 3\epsilon_V^2 \approx 0 \,, \tag{7.13}$$

with solutions

$$\epsilon \approx \frac{2\epsilon_V(3 + d + \epsilon_V) - c_1 \pm \sqrt{[2\epsilon_V(3 + d + \epsilon_V) - c_1]^2 - 48\epsilon_V(d - \epsilon_V)}}{4(d - \epsilon_V)} \,. \tag{7.14}$$

From these two roots we find that in most cases the negative root (and hence the smallest value) accounts for the correct expression when the turn rate is large (though we do not have a proof for this observation). Equating the two expressions for ϵ provides the parametric relation $\chi(\phi)$.

It is worth mentioning the two sets of assumptions we made to derive the previous formula. Firstly, we neglected logarithmic prime derivatives of various quantities (e.g. ϵ and Ω), as it allows us to neglect second order time derivatives and subsequently make analytical approximations possible. The latter was assumed in the early works, such as Ref. [88], as a definition of slow-roll, as well as in the derivation of the rapid-turn solution in Ref. [100]. A discussion of the validity of this assumption was presented earlier in Sec. 6.8, where various two-field models have been shown to be approximated by scaling solutions with adiabatically changing parameters, for which logarithmic prime derivatives are identical zero. Secondly, we assumed that the magnitude of the tangential and orthogonal directions of the potential ($V_{\sigma\sigma}/V$, or equivalently Ω^2, and w_{nn}) are free parameters, but non-negligible compared to η and $(\ln \Omega)'$. If this is not true one obtains the slow-roll slow-turn approximation. Note that in the different steps to derive

the solution every operation will be accurate up to corrections $\mathcal{O}(\eta, (\ln \Omega)')$. The solution reduces to the slow-turn limit when the curvature invariants c_1, c_2 become of order $\mathcal{O}(\epsilon, \eta)$. Here we need to make an important observation: the condition on the trace of the Hessian $d = \mathcal{O}(\epsilon, \eta)$ is not mandatory for the validity of the gradient-flow approximation and therefore, the slow-turn limit might be different from gradient-flow (we will illustrate this point later with an example).

We should point out that the turn rate calculated from the previous solution is identical to the expression first given in Ref. [100]. To make the comparison we will simplify the expressions (7.10)-(7.14) by considering $\epsilon \ll 1$ (that was assumed in that work) and obtain

$$\epsilon \approx \epsilon_V - \frac{c_1^2}{2c_2} \,, \tag{7.15}$$

$$\epsilon \approx \frac{2\epsilon_V(3+d) - c_1 \pm \sqrt{[2\epsilon_V(3+d) - c_1]^2 - 48\epsilon_V(d - \epsilon_V)}}{4d} \,. \tag{7.16}$$

The turn rate was expressed in a basis defined from the normalized gradient vector $u^i \equiv V^{,i}/\sqrt{V^{,k}V_{,k}}$ and the vector orthogonal to it denoted by w^i. This local orthonormal basis yields the following decomposition for the metric

$$G_{ij} = u_i u_j + w_i w_j \,. \tag{7.17}$$

With these definitions we can relate the curvature invariants with projections of the Hessian matrix along these vectors as

$$d = \frac{V_{uu}}{V} + \frac{V_{ww}}{V} \,, \qquad c_1 = \frac{V_{uu}}{V} \,, \tag{7.18}$$

with $V_{uu} \equiv V_{;ij}u^i u^j$ and $V_{ww} \equiv V_{;ij}w^i w^j$. The next step is to exchange ϵ with the turn rate in Eq. (7.13) and obtain

$$\frac{V_{ww}}{V} - \frac{9}{\Omega^2}\frac{V_{uu}}{V} = 3 + \frac{1}{3}\Omega^2 \,. \tag{7.19}$$

which is Eq. (12) of [100].

Now we will use three examples from the literature to demonstrate the generality of our approach:

- Our first example is the multi-field alpha-attractor model of Ch. 5. There are effectively three quantities in this model: the distance from the boundary of the Poincaré disc, parameterized by $1 - r^2$, the field-space curvature controlled by α and the mass ratio $R_{\rm m}$, or

equivalently the potential steepness along the angular direction $V_{,\theta}/V$. Defining

$$f \equiv \cos^2 \theta + R_{\mathrm{m}} \sin^2 \theta \,, \qquad p \equiv \frac{f_{,\theta}}{f} \,, \qquad x \equiv \frac{1 - r^2}{\alpha} \,, \qquad (7.20)$$

then expanding Eqs. (7.10) and (7.14) around small α we obtain the following two expressions for ϵ

$$\epsilon \approx \frac{1}{12} \alpha p^2 x^2 \qquad \text{and} \qquad \epsilon \approx \frac{3\alpha x^2 (1 + p^2)}{36 + 8x} \,. \qquad (7.21)$$

Equating both expressions yields

$$x = \frac{18}{p^2} \,, \qquad (7.22)$$

which is identical to the parametric relation (5.14) derived in Sec. 5.2.3. When p is small then using the first expression we obtain $\epsilon \ll \epsilon_V$ which results to moderate turn rate, while large angular gradient yields $\epsilon \approx \epsilon_V$ and hence small Ω. Specifically for the latter, motion does not proceed along the potential flow, i.e. $(\phi^I)' \sim V^{,I}$ which would result into boomerang-like curves (depicted earlier in Fig. 4.2), but along the angular direction instead.[4] Therefore, this slow-turn solution is qualitatively different than gradient flow.

- Our second example is sidetracked inflation [154], originally formulated on a negatively curved space and a sum separable potential

$$\mathrm{d}s^2 = \left(1 + \frac{\chi^2}{L^2}\right) \mathrm{d}\phi^2 + \mathrm{d}\chi^2 \,, \qquad V = U(\phi) + \frac{1}{2} M^2 \chi^2 \,, \qquad (7.23)$$

where U is a single field potential corresponding to a variety of small-field inflationary models, including Starobinsky's model and natural inflation. The sidetracked phase succeeds the traditional slow-roll solution, after geometrical destabilization occurs. Setting $x = \chi/L$ and expanding around small L (which is equivalent to considering large curvature) we obtain the following two expressions for the slow-roll parameter

$$\epsilon \approx \frac{p^2}{2(1 + 2x^2)} \qquad \text{and} \qquad \epsilon \approx \frac{3M^2 L^2 (1 + 2x^2)}{4V} \,. \qquad (7.24)$$

---

[4]This can be deduced as follows: the requirement of one frozen field and one field in slow roll combined with the solution $\epsilon \approx \epsilon_\theta$ (where the latter denotes the θ part in the definition of ϵ_V), gives $\theta' \approx \theta'_{\mathrm{SR}}$ and $r' \approx 0$. Thus, this particular slow-turn solution belongs to the angular inflation regime.

Under the additional assumption that the potential energy of the two-field system is dominated by the energy of the inflaton, i.e. $V \approx U$, then equating the two previous expressions yields

$$1 + 2x^2 = \sqrt{\frac{2}{3}} \frac{|U_{,\phi}|}{ML\sqrt{U}}\,, \qquad (7.25)$$

which is the parametric relation given in Ref. [154].

- Our final example is hyperinflation [147], formulated on global hyperbolic coordinates (6.86) and a "spherically symmetric" potential $V = V(\rho)$. The Lagrangian of this model is shift-symmetric in θ and hence we need only one expression for ϵ. Even though the numerator of Eq. (7.10) is identically zero, ignoring the denominator does not yield a consistent solution for $\rho \gg L$, because it becomes zero to first order in the expansion parameters. Therefore, we have to use Eq (7.12) to find ϵ (or the more complicated expressions (7.14)). We obtain

$$\epsilon \approx \frac{1}{2}p^2 \qquad \text{or} \qquad \epsilon \approx \frac{3}{2}pL\,, \qquad (7.26)$$

where in the second equation we expanded around small L, recovering Eq. (6.51).

7.2 Stability and bifurcations

The stability conditions for a general background solution are determined by the eigenvalues of the full stability matrix spanned by the fields and their velocities. In the cases of interest in this chapter, with $\epsilon' \ll 1$ and $\chi^i \simeq$ constant, the stability criteria are given by the expansion of the effective potential at quadratic order, i.e. $\partial_\chi V_{\text{eff}}^{,\chi}$, and an algebraic restriction on ϵ (recall the analysis of Sec. 6.3). Since we substitute an approximate solution the conditions listed below will be accurate to first order in the slow-roll parameters.

To retain some analytical control we consider a more restricted version of the two-field metric (6.12)

$$\mathrm{d}s^2 = G_{\phi\phi}(\chi)\,\mathrm{d}\phi^2 + G_{\chi\chi}(\phi)\,\mathrm{d}\chi^2\,. \qquad (7.27)$$

The expression for the Ricci scalar of this manifold splits in two parts, $R = R^{(\phi)} + R^{(\chi)}$, parametrizing the derivative dependence on the two fields (there are no mixed derivatives $\partial_\phi \partial_\chi$). Motion along the ϕ direction is stable, as long as

$$3 - \epsilon + \left(\log\sqrt{G}\right)' > 0\,, \qquad (7.28)$$

where $G \equiv \det(G_{IJ})$. We will provide the physical interpretation later using hyperinflation as an example. In addition, the effective mass (defined as the linearization of $V_{\text{eff}}^{,\chi}$) reads

$$M_{\text{eff}}^2 = V_{,\chi}{}^{\chi} + \epsilon H^2 R^{(\chi)} + 3\frac{V_{,\chi} V^{,\chi}}{2\epsilon H^2}. \tag{7.29}$$

Since multi-field trajectories can deviate from the gradient flow it is important to calculate the turn rate which for our choice of coordinates is given as $\omega^2 = V_{,\chi} V^{,\chi}/(2\epsilon H^2)$.

An example with a single stable attractor is provided by the two-field α-attractor model we studied earlier (and the closely related model of Ref. [174]). It is straightforward to check that the effective gradient $V_{\text{eff}}^{,r}$ stabilizes the radius near the boundary of the Poincaré disc, leading to a late-time attractor with non-vanishing turn rate, proceeding along a non-geodesic direction in field space.

Turning to a second example, it was recently pointed out [135, 169] that neutral stability can be achieved using the Hamilton-Jacobi formalism, where the scalar potential is given in terms of the Hubble parameter by

$$V = 3H^2 - 2H_{,i} H^{,i}. \tag{7.30}$$

This formalism has an exact first-order solution for the scalar velocities [61] [5]

$$v^i = -2H^{,i}/H. \tag{7.31}$$

Upon adapting coordinates such that $H = H(\phi)$, one has a natural distinction between the inflationary and the stationary directions. Such trajectories may be (strongly) turning, however, as the Hubble gradient may differ from the potential gradient. The latter will be non-vanishing if the metric along the inflationary direction $G_{\phi\phi}$ depends on the stationary directions, resulting in

$$V^{,i} = -2\partial^i G_{\phi\phi} (H^{,\phi})^2, \tag{7.32}$$

which is equivalent to the vanishing of the effective gradient of Eq. (7.4). The latter is therefore identically satisfied, leading to neutrally stable stationary points and hence flat directions in the effective potential and Hubble parameter, which are directly related to the choice $H = H(\phi)$. This implies that the field space is spanned by adjacent trajectories. One thus has a convergence of the $2n$-dimensional phase space of initial conditions to

---

[5] This can be seen as the cosmological analogue of the first-order equation that governs AdS critical points and BPS domain walls [175, 176].
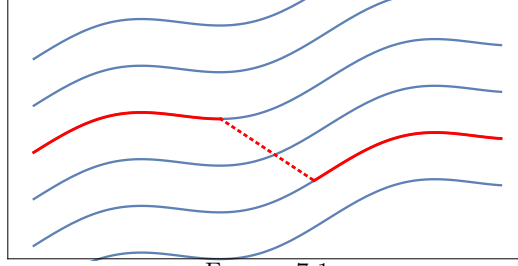
FIGURE 7.1
Various possible trajectories of the system evolving along ϕ at fixed values of χ^i. Dynamical bifurcations during inflation correspond to transitions between different trajectories.

the n-dimensional hypersurface that fixes the fields' velocity but not their positions.

For more general scalar potentials, the orthogonal directions will settle at (one or more) extrema of V_{eff} (see Fig. 7.1). The number and stability properties of these extrema can change during inflation leading to bifurcations (presented in detail in Sec. 6.6). These bifurcations are elegantly captured by V_{eff}. We will illustrate this using two characteristic examples from the recent literature.

7.3 Case examples

7.3.1 Sidetracked inflation

Arguably the simplest setting that displays the bifurcation phenomenon is sidetracked inflation (7.23). In the original set up there is a transition from the gradient flow solution to a non-geodesic solution. Using a model with quadratic potentials and 'minimal geometry':

$$V = \tfrac{1}{2}m^2\phi^2 + \tfrac{1}{2}M^2\chi^2\,,\tag{7.33}$$

we will display the opposite phenomenon, i.e. transition from non-geodesic to geodesic motion. As we will see, inflation takes place along ϕ and is thus perfectly suited to the effective potential framework.

Let us first investigate the stability of the geodesic trajectory with $\chi = 0$. Particularly for quadratic potentials, both contributions to the isocurvature mass are approximately constant and read

$$\mu^2 = M^2 - \frac{2m^2}{3L^2}\,.\tag{7.34}$$

Therefore, the curvature destabilizes the geodesic solution for

$$L < \frac{\sqrt{2}m}{\sqrt{3}M} \,. \tag{7.35}$$

However, for $\sqrt{3}ML \lesssim \sqrt{2}m$, subleading corrections to the isocurvature mass, consisting of the kinetic term for ϕ in the Hubble parameter, become important and lead to bifurcations. In particular $\mu_s^2|_{\chi=0} < 0$ at large ϕ and it slowly increases as inflation proceeds along the geodesic, becoming positive at

$$\phi_{\mathrm{cr}}^2 = \frac{4m^2}{3(2m^2 - 3L^2M^2)} \,, \tag{7.36}$$

where we have assumed $\phi > 1$.

The subleading terms also determine the fate of the background trajectory when the geodesic solution is unstable. In addition to a local maximum, the subleading terms induce two minima in the effective potential at

$$\frac{\chi_\pm^2}{L^2} = \left(\frac{\sqrt{2}m}{\sqrt{3}ML} - 1 \right) \,, \tag{7.37}$$

for $\phi \gg \phi_{\mathrm{cr}}$, which is Eq. (7.25). The background trajectory will smoothly transit from the early non-geodesic trajectory at $\chi_\pm$ to the subsequent geodesic phase at $\chi = 0$. Fig. 7.2 shows the evolution of the effective gradient $V_{\mathrm{eff}}^{;\chi}$ and its zeroes as ϕ evolves, resulting in a pitchfork bifurcation. Moreover, it is clear from the figure that the numerical trajectories converge to the geodesic solution somewhat later; this can be understood as inertia in the moduli system, and indeed the different trajectories only become geodesic when $\mu_s^2 \simeq H^2$ rather than 0.

7.3.2   Hyperinflation

A second example displaying a similar phenomenon is hyperinflation. For the simple example with the metric (6.86) and a quadratic potential

$$V = \tfrac{1}{2}m^2\rho^2 \,, \tag{7.38}$$

the trajectory undergoes such a transition at $\rho = 2/(3L)$. Remarkably, one can bring both the slow-turn and the non-geodesic solutions to proceed
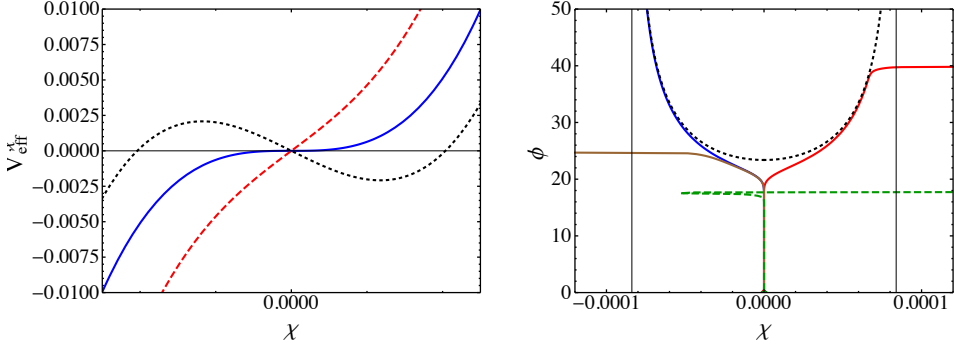
FIGURE 7.2
Left: *The effective gradient of sidetracked inflation with $L = 0.0034$, $m = 1$ and $M = 240$ along the stationary direction χ for different values of ϕ, signalling the existence of one or three points of $V_{\text{eff}}^{,\chi} = 0$. The stability of each is determined by the slope of the curve.*
Right: *The corresponding bifurcation diagram. The black-dotted curve are the non-geodesic solutions to Eq. (7.4), while the coloured curves correspond to numerical solutions of the background system.*

along a single direction via the field redefinition

$$
\begin{aligned}
\cosh\left(\frac{\rho}{L}\right) &= \cosh\left(\frac{\chi}{L}\right)\cosh\left(\frac{\phi}{L}\right), \\
\cot\theta &= \coth\left(\frac{\chi}{L}\right)\sinh\left(\frac{\phi}{L}\right),
\end{aligned}
\tag{7.39}
$$

leading to

$$
\mathrm{d}s^2 = \cosh^2\left(\frac{\chi}{L}\right)\mathrm{d}\phi^2 + \mathrm{d}\chi^2. \tag{7.40}
$$

This maps any spherically symmetric potential $V(\rho)$ onto a particular $V(\phi, \chi)$, providing all the necessary ingredients for realizing sidetracked inflation along ϕ.[6]

Close to the geodesic solution ($\chi = 0$), the scalar potential reads (assuming $\phi > L$)

$$
V = \tfrac{1}{2}m^2\phi^2 + \tfrac{1}{2}m^2\frac{\phi}{L}\chi^2. \tag{7.41}
$$

---

[6]By "sidetracked" we refer to models that admit one geodesic solution along the minimum of the "heavy" field potential and two non-geodesic ones, generalizing the specific models of Ref. [154].
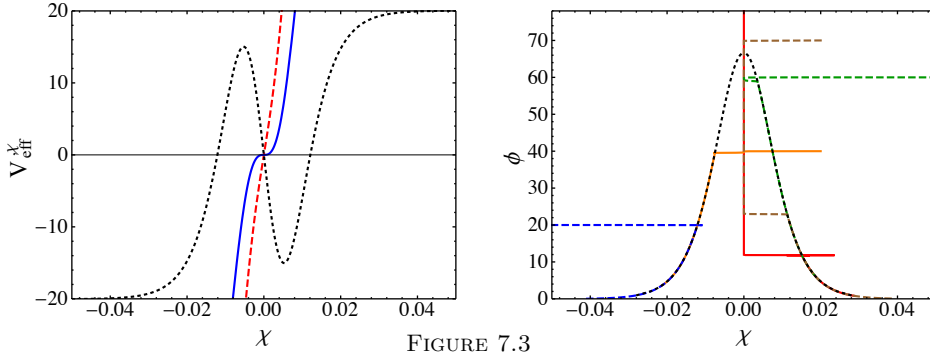
FIGURE 7.3

Left: *The effective gradient for hyperinflation in the coordinates of Eq. (7.40) at different ϕ-values with $m = 1$ and $L = 0.01$.*

Right: *The corresponding bifurcation diagram. The black-dotted curves are the non-geodesic solutions to Eq. (7.4), while the coloured curves correspond to numerical solutions of the background system.*

The effective mass for motion along $\chi = 0$ reads $M_{\text{eff}}^2 = \frac{m^2}{L}(\phi - \frac{2}{3L})$, becoming negative for $\phi < \phi_{\text{crit}} = 2/3L$. At larger field values the geodesic solution is stable as the orthogonal field is strongly stabilised, while it becomes unstable at smaller field values. At this point, two new stable non-geodesic solutions come into existence, thus making up a pitchfork bifurcation [163] (see Fig. 7.3).

7.4   Comparison with literature

In Ref. [100] a unification scheme was considered for the non-geodesic phase, based on the large turn rate of studied models. Stability of the solution was shown using the perturbations' equations in the adiabatic/entropic decomposition and requiring $\mu_s^2 > 0$ (recall that μ_s^2 is the isocurvature effective mass defined in Eq. (4.59)). However, as has been pointed out in the previous chapter and in Ref. [166], it is possible to have both a stable homogeneous solution and unstable orthogonal perturbations, leading to an apparent paradox. The resolution of this apparent paradox becomes clear if we compare μ_s with the stability criteria we presented earlier, in particular M_{eff}

$$\mu_s^2 = M_{\text{eff}}^2 - G^{\chi\chi}\Gamma_{\chi\chi}^{\phi}V_{,\phi} + \epsilon H^2 R^{(\phi)}\,. \tag{7.42}$$

Using $\chi' \approx 0$, $D = \left(\log \sqrt{G} \right)'$ and

$$D' \approx \frac{1}{2} \frac{G_{\chi\chi,\phi\phi}}{G_{\chi\chi}} v^2 - \frac{1}{2} \left(\frac{G_{\chi\chi,\phi}}{G_{\chi\chi}} \right)^2 v^2 \, , \qquad (7.43)$$

$$\epsilon R^{(\phi)} = -\frac{1}{2} \frac{G_{\chi\chi,\phi\phi}}{G_{\chi\chi}} v^2 + \frac{1}{4} \left(\frac{G_{\chi\chi,\phi}}{G_{\chi\chi} v} \right)^2 v^2 \, . \qquad (7.44)$$

we can rewrite the previous in a more geometrical way as [7] :

$$\frac{\mu_s^2}{H^2} \approx \frac{M_{\text{eff}}^2}{H^2} - (3 - \epsilon + D)\, D - D' \, . \qquad (7.45)$$

The two masses are equal when the metric has an isometry in the inflationary direction, which is the case for the examples in [100]. Otherwise, μ_s^2 and M_{eff}^2 can differ and even have opposite signs. While this might sound surprising, the situation is similar to the familiar case of a spherically symmetric quadratic potential in flat target space. In polar coordinates $G_{\chi\chi} = \phi^2$ and $V = \frac{1}{2} m^2 \phi^2$, inducing a difference between both mass notions in (7.45). The effective mass vanishes, indicating a range of neutrally stable trajectories on the attracting surface, while the isocurvature mass is positive, corresponding to a decrease of the proper distance between these trajectories, and a corresponding suppression of isocurvature fluctuations, as one approaches the minimum at $\phi = 0$.

The Hamilton-Jacobi formalism provides a clear illustration between the two (effective and isocurvature) mass notions in the absence of an isometry. The discussion around Eq. (7.32) holds for any metric of the form of Eq. (7.27) and thus generates an infinite set of adjacent, non-isolated critical points for the orthogonal fields. One can check that $M_{\text{eff}}^2 = 0$ for such constructions, highlighting the flat directions, while the isocurvature mass is proportional to the additional terms in (7.45). For example, by choosing

$$\mathrm{d}s^2 = \rho^2 \, \mathrm{d}\theta^2 + G_{\rho\rho}(\theta) \, \mathrm{d}\rho^2 \, , \ V = \frac{m^2}{2} \left(\theta^2 - \frac{2}{3\rho^2} \right) \, , \qquad (7.46)$$

the background trajectories of Ref. [169]

$$\rho = \rho_0 \, , \qquad \dot{\theta} = \pm \sqrt{2/3}\, m / \rho_0^2 \, , \qquad (7.47)$$

---

[7]An interesting parallel exists between Eq. (7.45) and Eq. (5) of [177] if one makes the substitution $D = -2h_i/H$. While both relations describe the mass of isocurvature modes, they were each derived in a different context.

carry over, while the isometry along θ is broken. One can check this by examining the background equations of motion

$$\ddot{\theta} + 3H\dot{\theta} + \frac{2}{\rho}\dot{\rho}\dot{\theta} - \frac{1}{2}\frac{\partial_\theta G_{\rho\rho}(\theta)}{\rho^2}\dot{\rho}^2 + \frac{1}{\rho^2}V_{,\theta} = 0 \,, \tag{7.48}$$

$$\ddot{\rho} + 3H\dot{\rho} + \frac{\partial_\theta G_{\rho\rho}(\theta)}{G_{\rho\rho}(\theta)}\dot{\rho}\dot{\theta} - \frac{\rho}{G_{\rho\rho}(\theta)}\dot{\theta}^2 + \frac{1}{G_{\rho\rho}(\theta)}V_{,\rho} = 0 \,. \tag{7.49}$$

We can see that Eq. (7.47) satisfies the equations of motion, since on the attractor $\dot{\rho} = 0$ the term $G_{\rho\rho}$ cancels out. The same holds for the slow-roll parameter and the Hubble parameter, while the turn rate is affected by the presence of $G_{\rho\rho}$

$$\theta' = -\frac{2}{\theta\rho_0^2} \,, \qquad \epsilon = \frac{2}{\theta^2\rho_0^2} \,, \qquad H = \frac{m\theta}{\sqrt{6}} \,, \qquad \omega^2 = \frac{2}{3}\frac{m^2}{\rho_0^2}G^{\rho\rho} \,. \tag{7.50}$$

While $M_{\mathrm{eff}}^2 = 0$, signaling the existence of background trajectories for any constant value ρ_0, as long as Eq. (7.28) is satisfied, the isocurvature mass μ_s^2 can be either stabilizing or tachyonic. In the special case of $\mu_s^2 = 0$, isocurvature modes grow on super-horizon scales at a constant rate. Combined with a constant turn rate, they continuously seed the adiabatic modes outside the horizon, leading to predictions that mimic those of single-field models [169]. To move beyond the case with an isometry, we choose a negatively curved manifold with

$$G_{\rho\rho} \sim e^{\theta/L} \,, \quad R = -\frac{1}{2L^2\rho^2} \,. \tag{7.51}$$

Even though the curvature of this manifold (given in Eq. (7.51)) is singular in the origin $\rho = 0$, we can still view it as holding for $\rho > 0$. For this model, the potential given in of Eq. (7.46) is also singular at $\rho = 0$, so the manifold must be smooth in the region of validity of the potential. The isocurvature modes in this model exhibit richer phenomenology compared to the flat metric case [169], where $\mu_s = 0$. In particular, along the (neutral) attractor at $\rho = \rho_0 = \mathrm{const.}$ the isocurvature mass is

$$\frac{\mu_s^2}{H^2} = \frac{1}{L^2\theta^2\rho_0^4}\left(3L\theta\rho_0^2 - 1\right) \,. \tag{7.52}$$

We see that $\mu_s^2 > 0$ for $\theta > 1/L\rho_0^2$ and is negative otherwise. This means that the behaviour of the isocurvature modes depends on the field-space curvature and the initial conditions, since different ρ_0 corresponds to different value of μ_s^2. Furthermore, the character of the isocurvature modes
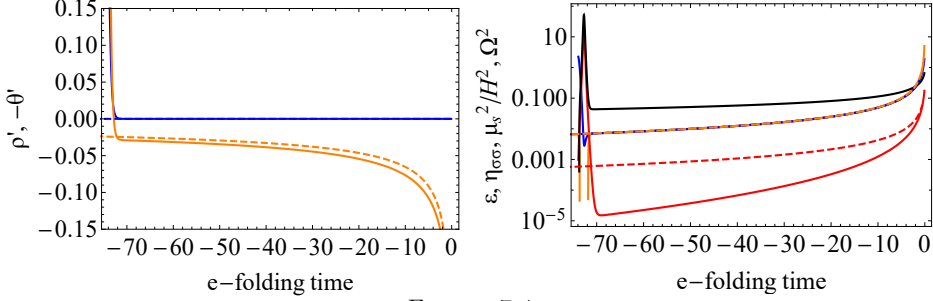
FIGURE 7.4

Various dynamical quantities for the two models (7.46) with $G_{\rho\rho} = e^{\theta}$ (solid lines), $G_{\rho\rho} = 1$ (dashed lines) and initial conditions given as $\{\rho, \theta, \sqrt{G_{\rho\rho}}\rho', \sqrt{G_{\theta\theta}}\theta'\}_{\text{init}} = \{4, 4, 1.5, 1.5\}$. Left: The velocities ρ' (blue) and θ' (orange). Right: The slow-roll parameters ϵ (blue), $\eta_{\sigma\sigma}$ (orange), turn rate Ω (red) and the isocurvature mass-squared μ_s^2 (black). The effective mass for the second model reached the precision accuracy and was omited.

can change during inflation, since θ is a monotonically decreasing function. The different behaviour is shown in Fig. 7.4. Notice that for this model

$$\eta_{\sigma\sigma} = \frac{6}{3\theta^2\rho^2 - 3}, \tag{7.53}$$

and, hence, $\eta_{\sigma\sigma} \approx \epsilon$ for $\theta^2\rho^2 \gg 1$. It is worth relating μ_s^2 to Eq. (7.28), which is a criterion for the existence of a stable solution with $\dot{\rho} = 0$. This can be written as

$$3 - \epsilon + \frac{d}{dN}\log\left(\sqrt{G}\right) = \frac{1}{L\theta\rho_0^2}\frac{\mu_s^2}{H^2} - \frac{2}{\theta^2\rho_0^2} > 0, \tag{7.54}$$

hence no stable background trajectory exists for $\mu_s^2 < 0$.

7.5 A note on perturbations

Background trajectories with a non-zero turn rate can also affect the behaviour of fluctuations. If $\mu_s^2 > 0$, then $Q_s \to 0$, allowing the co-moving curvature perturbation $\mathcal{R}$ to freeze at some point after horizon crossing. The moment of freeze-out is mostly determined by the magnitude of μ_s^2/H^2. If after horizon crossing orthogonal fields are still evolving, then the non-uniqueness of the background trajectory is inherited by observables as well.
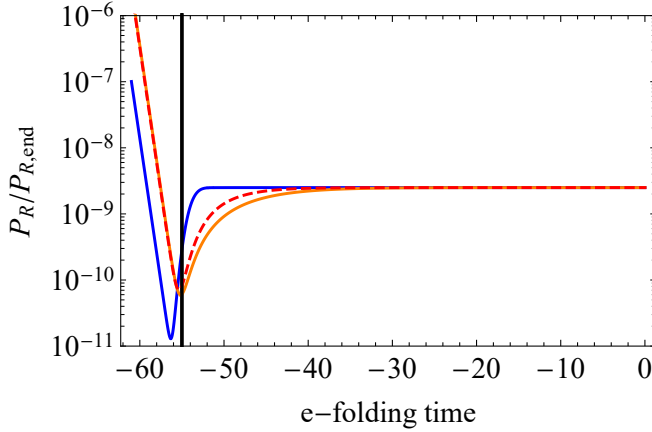
FIGURE 7.5

Power spectrum of curvature perturbation for angular inflation with $\alpha = 1/600$ and mass ratio $(m_2/m_1)^2$ equal to 9 (blue), 100 (red) and 225 (orange).

One then finds a range of possible values for $\{n_s, r, ...\}$.[8] Analytical estimates can be constructed in the following way: on sub-Hubble scales one can identify uncoupled perturbations by an appropriate time-dependent rotation [122]; close and prior to horizon crossing, if the mass of isocurvature perturbations on sub-Hubble scales m_s^2 is large enough then $\mathcal{S}$ will be stabilized at a zero of its 'effective gradient' given by [89,123]

$$\left(\frac{k^2}{a^2} + m_s^2\right)\mathcal{S} + 2\omega\dot{\mathcal{R}} = 0\,. \tag{7.55}$$

Substituting this solution into the equation for $\mathcal{R}$ provides an equation similar to the one-field case but with a k-dependent sound speed. Note that in general solving these equations is a model-dependent problem. For example, in angular inflation with $\alpha \ll 1$ when the ratio of the heavy to light field is $(m_2/m_1)^2 \lesssim \mathcal{O}(10)$, the curvature perturbation freezes shortly after horizon-crossing; when the masses of the two fields differ significantly then $|\beta| \ll 1$ and there can be substantial super-horizon evolution. Note that in both cases the background trajectory is unique, given by minimizing V_{eff}, but perturbations behave differently, as shown in Fig. 7.5.

---

[8]Multi-field α-attractors are exceptions to this rule, because the leading order contribution is independent of the specific initial state during gradient flow (see [146] and Ch. 5.

7.6   Concluding remarks

Multi-field models often display a strong attracting behaviour; orthogonal fields are stabilised by their effective potential, consisting of potential energy and generalized centrifugal forces due to non-geodesic motion. This can be interpreted as the (partial) minimisation of the total energy density given by the Hubble parameter as a function of the orthogonal fields and is the analogue of moduli stabilization, albeit on a time-dependent background. Moreover, as inflation proceeds, the stabilisation pattern can undergo pitchfork bifurcations, with a stable minimum becoming unstable with the simultaneous appearance of two new stable trajectories or vice versa. The total number of stable minus unstable solutions remains constant, characteristic of pitchfork bifurcations. This structure is reminiscent of the waterfall transition in hybrid inflation [178].

We presented a unifying perspective on different scenarios of multi-field inflation in curved geometries, based on the dynamical properties of the inflationary evolution after the decay of the initial transient regime. While angular inflation has a unique minimum of V_{eff}, both sidetracked and hyperinflation exhibit dynamical pitchfork bifurcations. This instability is therefore intrinsically of the same nature; analysing hyperinflation after the coordinate transformation of Eq. (7.39) makes it a special case of sidetracked inflation. This connects two models that were so far thought to be distinct, thus underlining the unifying nature of our approach. Moreover, it demonstrates that the conservation of angular momentum is not essential to the bifurcation in hyperinflation.

Finally, we showed that the existence of an isometry along the inflationary direction is not a necessary condition for the existence and stability of inflationary attractors with a non-zero turn-rate. By providing a simple generalization of shift-symmetric orbital inflation [169], we constructed a model in which the effective mass M_{eff} is identically zero for all members of a continuous family of trajectories with a constant radius, thus extending the notion of a neutrally stable attractor. However, the isocurvature mass on any of these trajectories is not zero but rather positive and depends on the field-space curvature. Furthermore μ_s^2 evolves in time, allowing for the generation of features in the scalar power spectrum. We leave an extensive analysis of the intruiging phenomenology of inflationary models with broken isometries for future work.

8

Observables at the many-field limit

In this chapter we examine observables at the many-field limit, i.e for infinite number of fields. We revisit claims of universality of predictions and find that, although computations greatly simplify as the number of fields increases, the result depends on the initial configuration. Therefore, the previously found universality is prior dependent. This chapter is largely based on publication [179].

8.1 From multi- to many-field $\mathcal{N}$-flation

Following our discussion in Sec. 4.8 we will consider the many-field limit, i.e. when the number of fields becomes infinite. Moreover, we will use multi- to refer to $\mathcal{N} \approx \mathcal{O}(1)$ number of fields, while many- indicates $\mathcal{N} > \mathcal{O}(10)$. As explained the gradient-flow does not lead to a unique dynamics for the background; the slow-roll equations yield an $\mathcal{N}$-dimensional hypersurface in the $2\mathcal{N}$-dimensional phase space and therefore there is an $(\mathcal{N} - 1)$-dimensional hypersurface that represents CMB horizon crossing. This results in an intrinsic dependence of the observables on the initial conditions, even in the slow-roll limit. Every configuration on this hypersurface will give exactly 55-60 e-folds of inflation and since there is no agreed measure on the space of initial conditions one can consider all of them to be equally probable. Nevertheless, this is not the only possibility: other configurations that provide a larger number of e-folds will in general favour certain points of the CMB hypersurface more than others. The choice of the initial $(\mathcal{N} - 1)$-dimensional hypersurface that gives sufficient inflation will be called the *prior*.

Turning to perturbations, analytical expressions for an arbitrary number of fields exist in the horizon-crossing approximation [110, 119, 126, 180].[1] This method takes into account the superhorizon evolution of the curvature perturbation but ignores contributions from the fields' position at the end of inflation. Moreover, it assumes the gradient-flow approximation and requires an analytic expression of N in terms of the fields, and thus its applicability is more limited. On the contrary, the standard numerical approach is by means of the transport method [145, 150, 181–184] which solves the perturbations' equations of motion equivalent to tree level in the in-in formalism, and requires no slow-roll or horizon-crossing approximations.

A simple and well-studied multi-field model is $\mathcal{N}$-flation, consisting of a sum of quadratic potentials [133, 141]. This model has received interest in the axion landscape community, see e.g. [185–187], because it can approximate inflation towards a cosine minimum. Early investigations relied on the horizon-crossing approximation which allows for simple calculation of the spectral index, tensor to scalar ratio, running and non-Gaussianity. More specifically, r and the non-Gaussianities are found independent of initial conditions and the number of fields [180, 188], whereas the spectral index and its running inherits the dependence on initial conditions [144, 189].

In the many-field limit ($\mathcal{N} \to \infty$), however, predictions for quadratic

---

[1]Despite its name it does not evaluate the power spectra at horizon crossing but rather expresses observables at the end of inflation using their horizon-crossing values [132].

fields have been shown to become sharp and universal [142], while similar predictivity has been found in recent many-field numerical investigations in other contexts [143, 145, 184, 190].[2] This universality stems from the central limit theorem and in Ref. [142] it was shown that different priors have weak, and negligible, dependence on observables. It is the goal of this chapter to investigate to what extend the results found in earlier literature are prior independent.

8.2 Observables for many-field $\mathcal{N}$-flation

Using the horizon-crossing approximation, the spectral index and other observable quantities can be expressed in terms of the fields' values at horizon crossing. However in order to study these observables' prior dependence, we need to express them in terms of the initial field configuration using the equations of motion. For any sum-separable potential, the slow-roll equations of motion (4.83) can be solved exactly, e.g. in terms of a reference field as we did in Eq. (4.84). For the quadratic potential in particular [3]

$$V = \sum_i \frac{1}{2} m_i^2 \Phi_i^2 \,, \tag{8.1}$$

we can derive the solution in terms of a different time variable τ

$$\Phi_{i,*} = \Phi_{i,0} e^{-m_i^2 \tau_*} \,,$$

where $\Phi_{i,0}$ and $\Phi_{i,*}$ are the initial and horizon-crossing field displacements respectively. The time τ is defined by $\mathrm{d}N \equiv -V \, \mathrm{d}\tau$ and ranges from $\tau = 0$ to τ_* during $N = N_0$ to N_*. Moreover, since the potential is sum-separable ($V = \sum W_i(\phi_i)$) using the slow roll equations of motion (8.2) the number of e-folds can be calculated as [126]

$$N = -\sum_i \int \mathrm{d}\phi_i \frac{W_i}{\partial_i W_i} \,. \tag{8.2}$$

Thus, field values happen to satisfy a so-called hypersphere constraint at all times during the evolution

$$\sum_i \Phi_i^2 = -4N \,, \tag{8.3}$$

---

[2]In our analysis the fields' masses are taken constant with $\mathcal{N}$, but some models (e.g. those based on random matrix theory), have taken the fields' masses to grow like $\sqrt{\mathcal{N}}$. In these cases, the n_s we compute depends on ratios of masses to equal powers, so is identical in the many-field limit.

[3]Although $\mathcal{N}$-flation was introduced as a model with sufficiently large number of fields, here $\mathcal{N}$ is arbitrary.

where the field values are evaluated at $|N|$ e-folds before the end of inflation.

The previous sums can be rewritten in a convenient way by introducing the *sample average*. For an arbitrary random variable A we define the sample average as

$$\langle A \rangle_{\mathrm{s}} \equiv \frac{\sum A_i}{\mathcal{N}} \,, \tag{8.4}$$

which is also a random variable. In the limit $\mathcal{N} \to \infty$, if the conditions of the central limit theorem are satisfied, then the sample average converges to the *expectation value* $\langle A \rangle$. Moreover, we will need joint expectation values of Φ_0 and m^2 to arbitrary powers k and l respectively

$$\langle \Phi_0^k (m^2)^l \rangle \equiv \int \mathrm{d}\Phi_0 \, \mathrm{d}(m^2) \, \Phi_0^k (m^2)^l P(\Phi_0, m^2) \,, \tag{8.5}$$

where $P(\Phi_0, m^2)$ is the joint distribution of fields and masses. When the two random variables are independent, the probability distribution becomes product-separable and the average value splits into product of averages $\langle \Phi_0^k (m^2)^l \rangle = \langle \Phi_0^k \rangle \langle (m^2)^l \rangle$.

According to the δN formalism, if the gradient-flow approximation is valid then the power spectrum at the end of inflation is given by [110]

$$P_{\mathcal{R}}^2 = \frac{H^2}{(2\pi)^2} \partial_i N \partial^i N \Big|_{N=N_*} \,, \tag{8.6}$$

and for monomial potentials in general the spectral index is given by

$$n_{\mathrm{s}} = 1 - 2\epsilon_* + \frac{1}{N_*} \,. \tag{8.7}$$

It will prove convenient to rescale the initial values of the fields $\Phi_{i,0} = 2\sqrt{N_0/\mathcal{N}} \phi_i$ to obtain the normalisation $\langle \phi^2 \rangle_{\mathrm{s}} = 1$. The spectral index at horizon crossing in this notation is given by

$$n_{\mathrm{s}} = 1 + \frac{1}{N_*} \left(1 + \frac{\langle e^{-2m^2\tau_*} \phi^2 \rangle_{\mathrm{s}} \langle m^4 e^{-2m^2\tau_*} \phi^2 \rangle_{\mathrm{s}}}{\langle m^2 e^{-2m^2\tau_*} \phi^2 \rangle_{\mathrm{s}}^2} \right) \,, \tag{8.8}$$

where the sample averages are calculated for a specific realization of the fields and masses, and we used

$$N_0 \langle e^{-2m^2\tau_*} \phi^2 \rangle_{\mathrm{s}} = N_* \,. \tag{8.9}$$

For a choice of masses (drawn from a given mass distribution) the numerical value of the previous equation depends on the fields' realization, leading

to an intrinsic initial conditions dependence.[4] In the following we will discuss two physically well-motivated priors that have been considered in the literature and examine how time evolution affects predictions.[5]

N_0-*prior* [132]: Every vector $\vec{\phi}$ corresponds to a point of the $\mathcal{N}$-dimensional hypersphere with radius 1. The method to obtain a random point includes sampling from the multi-variate distribution $N_{\mathrm{GS}}(\mathbb{0}, \mathbb{1})$ and then dividing by the norm of the vector. Assuming that the ϕ_i's are uncorrelated with the masses and employing similar techniques as in Refs. [190, 193], one can show that at the limit of infinite number of fields Eq. (8.8) is normally distributed with mean

$$
n_{\mathrm{s}} \xrightarrow[\mathcal{N} \to \infty]{} 1 + \frac{1}{N_*} \left(1 + \frac{\langle e^{-2m^2 \tau_*}\rangle \langle m^4 e^{-2m^2 \tau_*}\rangle}{\langle m^2 e^{-2m^2 \tau_*}\rangle^2} \right) , \tag{8.10}
$$

and standard deviation that scales as $1/\sqrt{\mathcal{N}}$; thus, we find sharp many-field predictions. The expectation values are integrals over the mass distribution that should be evaluated at τ_*, the latter given as a solution of the integral equation

$$
\langle e^{-2m^2 \tau_*}\rangle \equiv \int \mathrm{d}m^2 P(m^2) e^{-2m^2 \tau_*} = \frac{N_*}{N_0} . \tag{8.11}
$$

Thus, this choice of prior results in a spectral index that is given by a specific time-dependent combination of the moments of the mass distribution: at $\tau = 0$, i.e. starting at a random point on N_*, this is given by the variance of the distribution, while starting at a random point at a higher N_0 there will also be higher-order moments that contribute.

E_0-*prior* [194]: Instead, one can start with a fixed initial energy E_0, and assume the energy per field to be uncorrelated with the mass distribution. Defining initial energies as $2E_i = m_i^2 \phi_i^2$ its sample average is $\langle E \rangle = -E_0/(4N_0)$. The central limit theorem implies that, at large $\mathcal{N}$, (8.8) becomes

$$
n_{\mathrm{s}} \xrightarrow[\mathcal{N} \to \infty]{} 1 + \frac{1}{N_*} \left(1 + \frac{\langle m^{-2} e^{-2m^2 \tau_*}\rangle \langle m^2 e^{-2m^2 \tau_*}\rangle}{\langle e^{-2m^2 \tau_*}\rangle^2} \right) . \tag{8.12}
$$

The initial energy and the number of e-folds are related by $E_0 = -2N_0/\langle m^{-2}\rangle$ while τ_* is calculated by Eq. (8.11). Hence, for this initial conditions prior,

---

[4]Recall that n_{s} is strictly bounded $n_{\mathrm{s}} \in [n_{\mathrm{s,min}}, 1 + 2/N_*]$, with the lower bound corresponding to a configuration where only the heaviest and lightest fields are non-zero and contribute with equal energies.

[5]Hartle-Hawking based priors (e.g. [191, 192]) are also a physically well-motivated choice, and lead to motion in purely the smallest-mass direction and observables identical to single-field inflation.

the spectral index is given by a different time-dependent combination[6] of the moments of $P(m^2)$.

The asymptotic behaviour (for either prior) can be inferred as follows: at sufficiently large time $\tau_* \gg 1$, the lightest field ϕ_1 (provided its mass is non-zero) will dominate the numerator and denominator in Eq. (8.8) and the ratio asymptotes to $\langle e^{-2m^2\tau_*}\rangle_s/(\phi_1^2 e^{-2m_1^2\tau_*})$. Using Eq. (8.11) this term is equal to 1 and so $n_s \to 1 + 2/N_*$, the single field result. On the contrary, if the mass distribution is gapless (i.e. the lightest field is massless) the previous ratio becomes undefined and the asymptotic value only depends on the behaviour of the mass spectrum around the massless point. Precisely, for a mass spectrum with lowest order term $P(m^2) \propto m^{2\alpha} + \mathcal{O}(m^{2(1+\alpha)})$, applying (8.5) and taking the asymptotic limit gives

$$n_s \xrightarrow[N_0 \to -\infty]{} 1 + \frac{1}{N_*}\left(2 + \frac{1}{\gamma + \alpha}\right), \qquad (8.13)$$

where $\gamma = 1$ for the N_0-prior, $\gamma = 0$ for the E_0-prior and $\gamma + \alpha > 0$.

Finally, the above formalism allows for a straightforward calculation of the running, by differentiating Eq. (8.8) with respect to N_*. This results again in specific combinations of the time-dependent averages $q_k \equiv \langle e^{-2m^2\tau_*}m^k\phi^2\rangle$:

$$\alpha_s = \frac{1}{N_*^2 q_2^3}(q_2^3 + 2q_0 q_2 q_4^2 - q_0^2 q_6), \qquad (8.14)$$

at lowest order in slow-roll.

8.3 Numerical results

The above approximations and trends are confirmed by full numerical simulations. We use the `Inflation.jl` transport code,[7] which is capable of solving the perturbations' equations of motion for $\mathcal{N} \sim 100$ using the transport method. We take the mass distribution to be Marcenko-Pastur [144]

$$p(\lambda) = \frac{1}{2\pi\lambda\beta\sigma^2}\sqrt{(b - \lambda)(\lambda - a)}, \qquad (8.15)$$

where $a = \sigma^2(1 - \sqrt{\beta})^2$ and $b = \sigma^2(1 + \sqrt{\beta})^2$. The overall normalization σ^2 drops out of the spectral index, and β sets the width of the distribution.

---

[6]For quadratic inflation and these two priors (or any prior for the quantity $m^p\phi$), the distribution $P(\phi)$ is not necessary for the calculation of $\langle n_s \rangle$ since the field- or energy-dependent terms decouple from masses.

[7]The code Inflation.jl has been developed by Robert Rosati and is publicly available. There also exist other codes in the literature that are capable of solving the perturbations' equations for $\mathcal{O}(100)$ fields, e.g. [195–197].

With these mass distributions and a horizon-crossing surface at $N_* = -55$, we have taken 200 samples per prior and plotted the spectral index in Figs. 8.1, 8.2 and 8.4.

There are a number of striking results that follow from our general analysis. First of all, for a given initial hypersphere of the N_0-prior, the probability distribution has a clear peak in the many-field limit. Secondly, this peak value depends on the radius of the initial hypersphere. The peaked distribution was already found in [142] but not the dependence on the initial hypersurface. Instead, we see a clear trend: starting at $N_0 = -55$ the spectral index is set by the variance of the mass distribution, the peak value first goes down and reaches a minimum around $N_0 \sim -160$ for the specific mass distribution [8] of Fig. 8.1. Starting at yet larger radii, the heavier fields have more time to decay and this will eventually result in the single-field prediction in the large N_0 limit.

Next, we examine the gapless Marcenko-Pastur distribution with $\beta = 1$ in Fig. 8.1 for the N_0-prior. Instead of converging to the single-field result, we instead find $n_\mathrm{s} \to 1 + 4/N_\star \sim 0.927$. This asymptotic value only depends on the behavior of the mass spectrum around the massless point $p(m^2) \sim m^{-1}$, in accordance to the discussion in the previous section.

---

[8]A minimum in n_s as a function of N_0 will be present when $n_\mathrm{s}(N_*)$ is lower than its asymptotic value and $dn_\mathrm{s}/d\tau|_{\tau=\tau_*} < 0$. For a mass distribution with $\langle m^2 \rangle = 1$ and an asymptotic relation $n_\mathrm{s} \to 1 + c/N_*$, these conditions imply a minimum will occur whenever $\langle m^4 \rangle > c - 1$ and $\langle m^6 \rangle < 2c(c-1)$. For Marcenko-Pastur, the expectation values for the quartic and sextic moments are given by $1+\beta$ and $1+3\beta+\beta^2$, respectively. The gapped case that we consider has $\beta = 1/2$ and asymptotes to $c = 2$ and therefore satisfies both conditions.
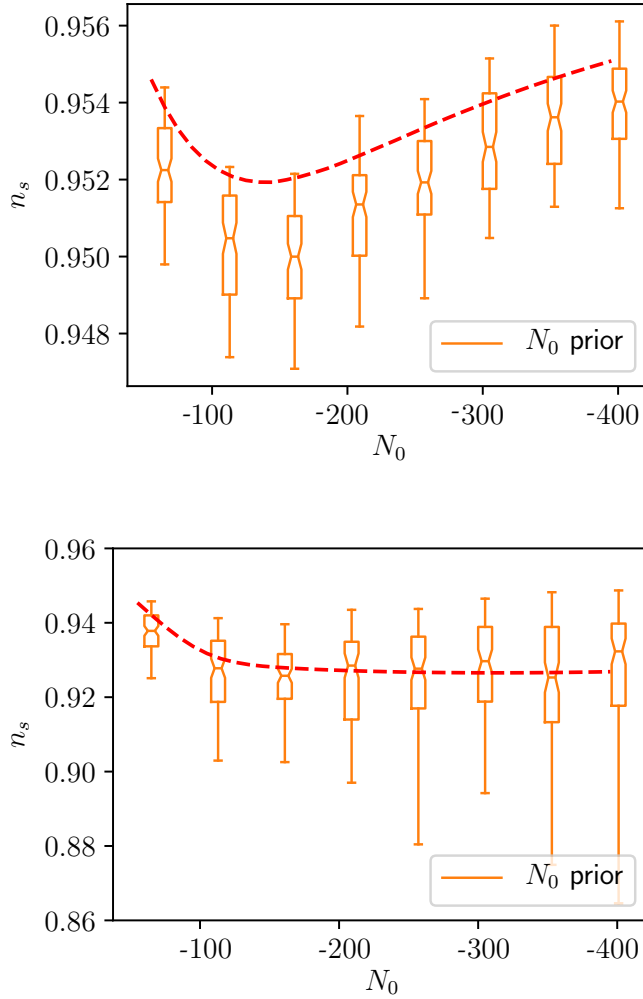
Transport method simulations of many-field $\mathcal{N}$-flation with 100 fields and initial conditions set to a fixed radius (i.e. a fixed number of e-folds) and masses drawn from the Marcenko-Pastur distribution with $\beta = 1/2$ (upper panel) and for $\beta = 1$ describing a gapless spectrum (lower panel). We compare the transport method (orange) and our analytic result (dashed, red) for initial conditions drawn uniformly over the hypersphere. At each radius, the numerical data are binned into a box and whiskers marking the 50% and 95% confidence intervals respectively. Agreement is at the per mil level.
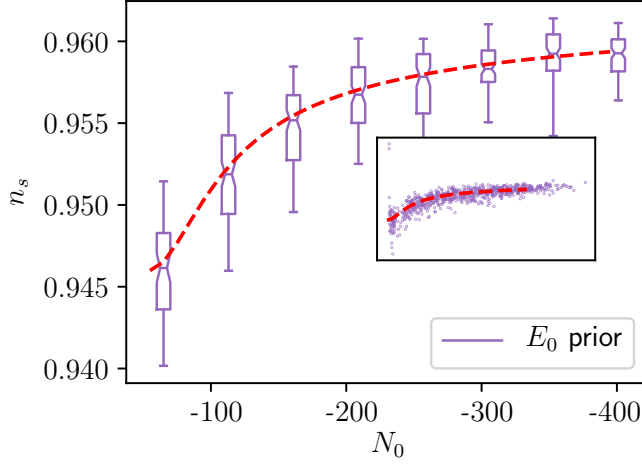
FIGURE 8.2

Transport method simulations of many-field $\mathcal{N}$-flation with 100 fields and initial conditions set to a fixed energy (i.e. constrained to a hyper-ellipse) and masses drawn from the Marcenko-Pastur distribution with $\beta = 1/2$. The data are binned by e-folds, using the number of e-folds the realization would have if its energy were equipartitioned. The number of e-folds varies by as much as $\pm 30\%$ from equipartitioned energies. At each energy, the data are binned into a box similarly to Fig 8.1, or alternatively the unbinned data are displayed in the inset. The dashed red line marks our corresponding many-field analytic result. Agreement is at least at the per mil level.

Finally, we examine the E_0-prior, which corresponds to selecting random field values that have a fixed energy, forming a hyper-ellipse. When starting at CMB horizon crossing, this will lead to the spectral index determined by the moments $\langle m^{-2} \rangle$ and $\langle m^2 \rangle$. For higher energies the resulting spectral index at CMB horizon crossing can be easily calculated from the time-dependent moments, and is illustrated in Fig. 8.2. We provide a similar numerical analysis that confirms the trend in this evolution.

8.4 Higher monomials

For higher monomials of degree n with

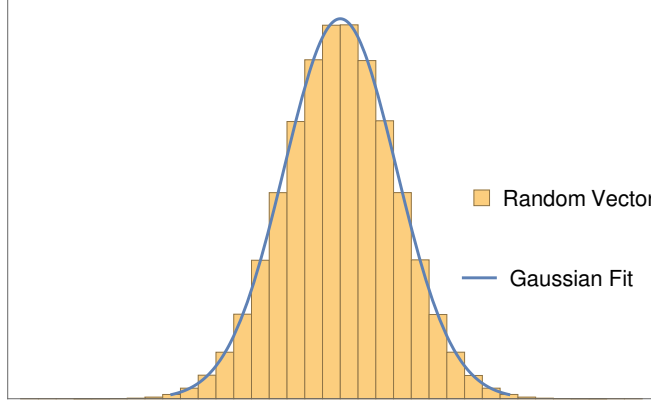$$V = \sum_i \frac{1}{n} \lambda_i \Phi_i^n \,, \tag{8.16}$$

FIGURE 8.3
Probability density of the components of a random vector for $\mathcal{N} = 10^7$ and the corresponding analytically estimated Gaussian distribution. Agreement is perfect.

the number of *e*-folds as a function of the fields is given by $\sum_i \Phi_{i,0}^2 = -2nN_0$. Specializing to $n > 2$, the slow-roll equations imply

$$\Phi_{i,*} = \left(\Phi_{i,0}^{2-n} + (n-2)\lambda_i \tau_* \right)^{\frac{1}{2-n}} , \tag{8.17}$$

where τ has mass dimension $2 - n$. Using e.g. the N_0-prior introducing normalised fields $\Phi_{i,0} = 2n\sqrt{-N_0/\mathcal{N}}\phi_i$ and the rescaled time $\xi = \tau \left(-2nN_0/\mathcal{N}\right)^{n/2-1}$, the moment of CMB horizon crossing is given by

$$\langle \left(\phi_i^{2-n} + (n-2)\lambda\xi_* \right)^{\frac{2}{2-n}} \rangle_{\mathrm{s}} = \frac{N_*}{N_0} . \tag{8.18}$$

The horizon-crossing formula is similarly

$$n_{\mathrm{s}} = 1 + \frac{1}{N_*} + \frac{n}{2N_0} \frac{\langle \lambda^2 \left(\phi_i^{2-n} + (n-2)\lambda\xi_* \right)^{\frac{2n-2}{2-n}} \rangle_{\mathrm{s}}}{\langle \lambda \left(\phi_i^{2-n} + (n-2)\lambda\xi_* \right)^{\frac{n}{2-n}} \rangle_{\mathrm{s}}^2} . \tag{8.19}$$

For $\mathcal{N} \to \infty$ sample averages can be calculated from expectation values if the distribution of ϕ_i is known.

Because of the hypersphere constraint, the distribution $P(\Phi_0)$ is not a Gaussian for finite $\mathcal{N}$ (for instance, the distribution for one field is a sum of two delta's located at ± 1). However, when $\mathcal{N} \to \infty$ the distribution $P(\Phi_0)$, which can be seen as the distribution of the components of a random vector on the $\mathcal{N}$-sphere, asymptotes to a Gaussian distribution with zero mean and standard deviation $1/\sqrt{\mathcal{N}}$ (see Fig. 8.3). For the rescaled fields ϕ their
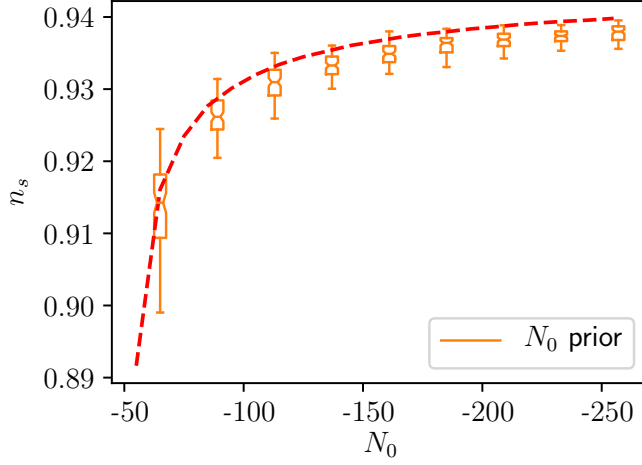
FIGURE 8.4
Transport method simulations of many-field quartic monomial inflation with 100 fields and initial conditions set to a fixed radius (i.e. a fixed number of e-folds) and 'masses' drawn from the Marcenko-Pastur distribution with $\beta = 1/2$. Transport numerics are in yellow and our horizon-crossing prediction in red. Agreement is at the per mil level.

statistical moments[9] for $\mathcal{N} \to \infty$ can be reproduced by the expectation values $\langle \phi^n \rangle$ using $P(\phi) = e^{-\phi^2/2}/\sqrt{2\pi}$. With the distribution of the fields known, expectation values correspond to double integrals over fields and 'masses' λ.

In Fig. 8.4 we depict numerical simulations for quartic fields using the N_0-prior. In contrast to the quadratic case, there is no minimum, since the conditions for its existence are not satisfied, and instead we observe a monotonic increase towards the asymptotic value. The horizon-crossing formula is again in a good agreement with the numerical results.

8.5 Discussion

In this chapter we have examined inflationary observables of sum-separable monomial potentials in the horizon-crossing approximation and provided elegant analytical expressions. Although for a chosen prior there are in principle infinite different field and mass realizations (parameterized as random

---

[9]These can be calculated independently as integrals over the $\mathcal{N}$-sphere $\langle \psi_i^n \rangle = \int d\Omega \psi_i^n / \int d\Omega$, expressing fields in spherical coordinates.

variables), the computed distribution of the spectral index in the many-field limit has a sharp peak. This universality can be attributed to the central limit theorem, since the analytical formulae include sums of random variables.

While this theorem guarantees that sample averages will converge to expectation values $\langle A \rangle_s \to \int d\phi\, d\lambda P(\phi, \lambda) A$, the latter will depend on the joint probability distribution $P(\phi, \lambda)$, i.e. the prior. Different priors, as seen in Figs. 8.1-8.2, can lead to different predictions, both in the spectral index and its running. Specifically for a gapped mass spectrum, the predictions range from variance-dominated to the single-field limit. Instead, for gapless mass distributions, the behaviour of the probability distribution for the lightest masses determines its asymptotic behaviour at high N_0, as seen in Fig. 8.1.

We have compared our analytical predictions with numerical simulations. The excellent agreement between both approaches also confirms the validity of the horizon-crossing approximation. Moreover, it shows that 100 fields suffices to reach the universal many-field regime.

In the absence of a non-trivial scalar-field geometry, our results for quadratic potentials can be seen as generic: the large-$\mathcal{N}$ limit pushes the horizon-crossing point towards the minimum in field space, where more complicated models can be approximated with a quadratic potential. This suggests that the universality and prior dependence identified in this paper should apply to a range of more general models as well. It would be interesting to investigate the scope of our results in this direction, as well as the effects of scalar geometry in the many-field limit.

9
Summary and conclusions

"We live on an island surrounded by a sea of ignorance. As our island of knowledge grows, so does the shore of our ignorance", J. A. Wheeler, Scientific American (1992), Vol. 267.

Multi-field models with a non-trivial field metric parameterization have been under scrutiny over the last years [101, 106, 146–148, 154, 167–169]. They introduce several new features, such as non-trivial dynamics, the enhancement of the power spectrum due to rapid turns [91–93], while at the same time these models are phenomenologically viable [94,95,198]. This thesis was a step towards a better understanding of multi-field dynamics and the investigation of predictions at the many-field limit.

In Chapters 2 and 3 we introduced the basic elements of modern cosmology and the inflationary theory. We discussed the observational evidence for cosmic isotropy that supports the FLRW universe and the hot Big-Bang scenario. Our current best understanding of the large-scale observable universe includes an isotropic and homogeneous universe composed of dust, radiation and a cosmological constant. Even though this model fits observations to a great accuracy, several philosophically-based objections have been posed, leading to extensions of the standard picture and the introduction of inflation. One of the major phenomenological successes of inflation is the existence of a mechanism that accounts for structure formation, through the exponential stretching of primordial quantum fluctuations in an FLRW background.

Later in Chapter 4 we studied in depth the multi-field dynamics. Following the literature, we started with the adiabatic/entropic split of background dynamics and calculated sufficient conditions for the existence of slow-roll solutions ($\epsilon, \eta \ll 1$). Then we discussed the evolution of curvature and isocurvature perturbations at the previous limit arguing that the superhorizon evolution can be calculated in the same way for all slow-roll models. Specifically for models following the gradient flow, one can show that the amplitude of quantum fluctuations at horizon crossing is the same as in single-field models and therefore the power spectra at the end of inflation can be calculated analytically. We used the double quadratic potential as an example where observables can be calculated analytically, demonstrating the initial conditions dependence of multi-field models.

Having set the basic theory, in Chapter 5 we presented a two-field generalization of single-field α-attractors. The model consists of two quadratic fields and the hyperbolic field space in Poincaré coordinates. We showed the existence of a novel attractor solution that succeeds the previously found gradient flow phase for appropriate values of the model's parameters. In particular, the number of *e*-folds spent during this phase is proportional to the curvature of the hyperbolic space and the mass ratio between the fields. If fluctuations cross the horizon during the 'radial phase' then predictions are altered simply by taking into account the time spent on the

new (angular) phase.

In Chapter 6 we presented a classification of various two-field scaling solutions with non-trivial field space parameterization. We explained why it is natural to search for "frozen" type solutions, i.e. those with one non-dynamical, in addition to the inflaton, field. Then, we performed a detailed stability analysis and derived the stability criteria in the general case and several examples followed to clarify the conditions for stable solutions. We argued that scaling solutions are relevant in inflationary model building because they approximate various proposals in the literature that display non-trivial dynamics. In addition, we explained that studying background stability with the adiabatic/entropic equations for perturbations does not always lead to the correct conclusions, but only when there exists a coordinate system in which the orthogonal field is canonically normalized.

In Chapter 7 we proposed a coordinate construction that provides an intuitive way to understand the late-time attractor solutions. In this picture, orthogonal fields are stabilized at the minima of an effective potential which takes into account contributions from the field metric. Performing calculations in that particular coordinate system and using some reasonable assumptions allowed us to derive a coordinate-independent solution, which as we showed, describes all novel solutions that do not follow the gradient flow. Using the results from the previous chapter, we derived the stability criteria with emphasis on bifurcations. We used several examples from the literature to demonstrate the unified perspective of our approach and, in particular, we found that the hyperinflation model belongs to the sidetracked family.

Finally, in Chapter 8 we examined predictions at the many-field limit. We utilized the horizon-crossing approximation to derive analytical formulae and investigate the initial conditions dependence. Assuming a random initial configuration on a reduced $\mathcal{N} - 1$ hypersurface, we demonstrated the convergence of observables to specific values due to the central limit theorem. However, we also found that different initial hypersurfaces result in different central-limit values for the observables. Therefore, we conclude that, contrary to various claims in the literature, many-field inflation remains inherently non-predictive.

Future directions

In this thesis we were mostly concerned with the dynamics and observational signatures of two-field models. A natural step forward, is the extension of our analysis to $\mathcal{N}$ fields in order to quantify the effects of extra fields

on the curvature perturbation (as for instance in the recent works [199–201]) and to investigate whether the strong attractor behaviour for two fields persists in the presence of more. Furthermore, the scaling solutions presented in Ch. 6 have the potential to describe late universe as well. It would be interesting to explore the dynamics and observational viability of these multi-field models in the presence of matter (e.g. [159, 202, 203]) and in the light of the Hubble tension.

The results from the previous chapters will have the potential to be applied in more general contexts, such as black-hole physics. Although connections between the inflationary paradigm and the generation of black holes have been known since the early days of the theory, the recent data from gravitational waves interferometers have sparked renewed interest on primordial black holes [204, 205]. Recent works have pointed out that the steep growth of the power spectrum, necessary to produce regions with large inhomogeneity, has a natural mechanism in multi-field models with large or sudden turns in field space [96, 97]. It still remains unanswered whether there is a limit on the rate of growth of the power spectrum, over a sustained period of time, for multi-field models with non-canonical kinetic terms. It would be interesting to explore this idea further, building on the results of [96, 97] and extend the framework of [205] for non-trivial field manifolds. In this way, these models can be used as high-energy probes for new physics, such as dark matter, covering a broader area in theoretical physics.

A
Cosmological perturbation theory

A.1 Some remarks on general relativity

A fundamental difference between Newtonian (or special relativistic) physics and general relativity is the a priori existence of inertial observers who are essential in defining the laws of physics. These observers move at constant velocity and all agree on the form of Newton's laws, i.e. they are equivalent. On the contrary, accelerated observers have to introduce fictitious forces in order to stay at rest in their reference frame. It should be stressed that the existence of these observers is a build-in feature of the theory.

From a mathematical point of view, an observer induces a coordinate system defined on a spacetime manifold. These coordinate systems can be chosen cleverly to reflect the equivalence class between observers of the theory, namely isometries of the spacetime. Even though any coordinate system can be used in principle, the laws of Newtonian physics (or special relativity) admit simpler forms when written in Cartesian (or Lorentz) coordinates. The situation is drastically different for general relativity because it does not build on a specific isometry structure of a given spacetime manifold; Einstein's field equations have the same form in every coordinate system. One can only generalize the notion of inertial observers, whose motion lies along the geodesics of the spacetime. Therefore, there are no intrinsic observers for a generic gravitational problem and in order to do physics one needs to specify the observers of the theory. The definition

of an observer is by means of a timelike unit vector that is tangent to its worldline u^μ. Every tensor of the theory can be decomposed into parts parallel and orthogonal to the vector, yielding the 3+1 decomposition (or $(d-1)+1$ for a space of d dimensions.[1]) Then, the energy-momentum tensor is constructed from the matter content of the spacetime and one can attempt to calculate the metric tensor.

Even with the energy-momentum tensor fully specified the metric can not be determined uniquely from the Einstein's field equations for the following reason. Any metric in d dimensions is defined up to d coordinate transformations that could simplify its form; stated differently, one is able to perform d arbitrary coordinate transformations, which manifest as d relations on the components of the metric, to further reduce the independent components by d. Therefore, the total number of independent components for the metric is $d(d-1)/2$ instead. However, this would indicate a problem with Einstein's equations. Since the Einstein's tensor contains $d(d+1)/2$ independent components, for the $d(d-1)/2$ independent components of the metric it appears as overdetermined. Nevertheless, $G_{\mu\nu}$ is subject to the constraint $G^{\mu\nu}_{\;;\nu} = 0$ (the contracted Bianchi identities) which cuts d equations and the number of equations becomes the same as the number of the unknowns.

It becomes clear from the above considerations that in order to solve the Einstein's field equations one has to make a coordinate choice that would remove the four unphysical degrees of freedom. What remains unclear is whether the remaining six degrees of freedom will all be propagating, i.e. they satisfy second order differential equations in time. What one finds in practice is that for every gauge choice (without imposing equations of motion) the field equations with appropriate boundary conditions remove another one degree of freedom and in a loose sense the gauge hits twice (we will demonstrate this in the case of cosmological perturbation theory in Sec. A.3). Combining the previous together the metric tensor in Einstein's

---

[1]See also [206] for an overview of the 3+1 or 2+1+1 kinematical and dynamical analysis of general relativity.

gravity has $d(d-3)/2$ true propagating degrees of freedom.[2]

A.2   Scalar-vector-tensor decomposition

We assume the following form of the perturbed metric

$$\mathrm{d}s^2 = -(1+hA)\,\mathrm{d}t^2 + haC_i\,\mathrm{d}x^i\,\mathrm{d}t + a^2(\delta_{ij} + he_{ij})\,\mathrm{d}x^i\,\mathrm{d}x^j\,, \qquad \text{(A.3)}$$

where h is the expansion parameter, A is the lapse function, C_i is the shift (co-)vector and e_{ij} is the three-metric of the ADM decomposition [207]. First, we will decompose every component into scalar, vector and tensor components applying Helmhotz's theorem: vectors are split into a gradient (curl-free) part and a divergence-less part as follows

$$C^i = \partial^i B + v^i\,, \qquad \text{(A.4)}$$

with $b^i_{,i} = 0$. Tensors are decomposed into tracefull, traceless (scalar), transverse and the remaining tensor parts

$$e_{ij} = 2\psi\delta_{ij} + \partial_i\partial_j\chi + w_{i,j} + w_{j,i} + \gamma_{ij}\,, \qquad \text{(A.5)}$$

where $w^i_{,i} = 0$, $\gamma^i_i = \gamma^{ij}_{,j} = 0$. The metric now becomes

$$\begin{aligned}
\mathrm{d}s^2 = -\,&(1+hA)\,\mathrm{d}t^2 + ha(\partial^i B + v^i)\,\mathrm{d}x^i\,\mathrm{d}t + a^2(\delta_{ij} + 2\psi\delta_{ij})\,\mathrm{d}x^i\,\mathrm{d}x^j \\
&+ a^2(\partial_i\partial_j\chi w_{i,j} + w_{j,i} + \gamma_{ij})\,\mathrm{d}x^i\,\mathrm{d}x^j\,.
\end{aligned} \qquad \text{(A.6)}$$

Note that the 3-vectors and 3×3 tensors defined above are raised/lowered with the Euclidean metric to lowest order, so we will not distinguish between upper/lower indices. Second, we will examine how the different components of the metric transform under an infinitesimal diffeomorphism

$$\tilde{x}^\mu = x^\mu + h\xi^\mu\,, \qquad \text{(A.7)}$$

---

[2]An analogous problem exists in electromagnetism. In terms of the four-potential, $A^\mu \equiv (A^0, \boldsymbol{A})$ Maxwell's equations in vacuum are

$$(\partial^\mu\partial_\mu\eta_{\nu k} - \partial_\nu\partial_k)\,A^k = 0\,. \qquad \text{(A.1)}$$

We observe that A^0 does not obey an evolution equation but instead

$$\nabla^2 A^0 - \partial_t(\boldsymbol{\nabla}\cdot\boldsymbol{A}) = 0\,, \qquad \text{(A.2)}$$

and therefore A^0 is completely fixed from $\boldsymbol{A}$. Choosing e.g. the Coulomb gauge $\boldsymbol{\nabla}\cdot\boldsymbol{A} = 0$ (without imposing equations of motion) gives $\nabla^2 A^0 = 0$, and with the boundary condition $A^0(\Omega) = 0$ the Laplace equation forces A^0 to be zero everywhere in space. Thus, the off-shell gauge-fixing $\boldsymbol{\nabla}\cdot\boldsymbol{A} = 0$ removes one degree and using this in combination to the equations of motion $\nabla^2 A^0 = 0$ removes another one, leaving the two physical degrees of freedom of the photon.

using the transformation properties of rank-two tensors

$$\tilde{g}_{\mu\nu}(\tilde{x}) = g_{\kappa\lambda}(x)\frac{\partial x^{\kappa}}{\partial x^{\mu}}\frac{\partial x^{\lambda}}{\partial x^{\nu}} \Rightarrow \tilde{g}_{\mu\nu}(x) = g_{\mu\nu}(x) - \mathcal{L}_{\xi}g_{\mu\nu}\,. \qquad \text{(A.8)}$$

Decomposing the generator vector ξ as

$$\tilde{x}^0 = x^0 + h\xi^0\,, \qquad\qquad\qquad\qquad\qquad \text{(A.9)}$$

$$\tilde{x}^i = x^i + h\partial^i\xi_s + b^i\,, \qquad\qquad\qquad\quad \text{(A.10)}$$

we obtain the following transformations

$$\tilde{A} = A + 2\dot{\xi}^0\,, \qquad\qquad\qquad\qquad\qquad \text{(A.11)}$$

$$\tilde{B} = B + \frac{1}{a}(\xi^0 - 2H\xi_s + \dot{\xi}_s)\,, \qquad\qquad \text{(A.12)}$$

$$\tilde{\psi} = \psi - H\xi_s\,, \qquad\qquad\qquad\qquad\qquad \text{(A.13)}$$

$$\tilde{\chi} = \chi + \frac{2}{\alpha^2}\xi_s\,, \qquad\qquad\qquad\qquad\quad \text{(A.14)}$$

$$\tilde{\varphi}^{(1)} = \varphi^{(1)} - \xi^0\dot{\phi}\,, \qquad\qquad\qquad\qquad \text{(A.15)}$$

$$\tilde{v}_i = v_i + \frac{1}{a}(\dot{b}_i - 2Hb_i)\,, \qquad\qquad\qquad \text{(A.16)}$$

$$\tilde{w}_i = w_i + \frac{1}{a^2}b_i\,, \qquad\qquad\qquad\qquad\quad \text{(A.17)}$$

$$\tilde{\gamma}_{ij} = \gamma_{ij}\,. \qquad\qquad\qquad\qquad\qquad\qquad \text{(A.18)}$$

We observe that the tensor part is invariant under the diffeomorphism, which is expected as there is no tensor part in Eqs. (A.9)-(A.10). Using linear combinations of the previous quantities one can construct the Bardeen's variables [65]

$$\Psi = \psi + aHB - \frac{1}{2}H\dot{\chi}\,, \qquad\qquad\qquad \text{(A.19)}$$

$$\Phi = \frac{1}{2}A - 2\frac{\mathrm{d}}{\mathrm{d}t}(aB) + \frac{\mathrm{d}}{\mathrm{d}t}(a^2\chi)\,, \qquad\quad \text{(A.20)}$$

$$\delta\phi = \varphi^{(1)} + a\dot{\phi}\left(B - \frac{1}{2}a\dot{\chi}\right)\,, \qquad\qquad \text{(A.21)}$$

$$V_i = v_i - a\dot{w}_i\,, \qquad\qquad\qquad\qquad\qquad \text{(A.22)}$$

$$\gamma_{ij}\,. \qquad\qquad\qquad\qquad\qquad\qquad\quad \text{(A.23)}$$

Note that we obtain 3 scalar, 1 vector and 1 tensor variables with a total number of $3+2+2 = 7$ independent components, which amounts to four less components than the original problem. These are exactly the redundant

degrees of the metric which need to be fixed before we attempt to solve the Einstein's equations. To proceed we have two options: either express the action or the Einstein's equations in terms of these variables or choose an appropriate gauge; we will do the latter.

A.3 Evolution of perturbations

We will work in the gauge with $B = \chi = w_i = 0$, which is known as the Newtonian gauge. This can be achieved by choosing the vector ξ to satisfy

$$\xi_s = -\frac{a^2}{2}\chi, \tag{A.24}$$

$$\xi^0 = 2H\xi_s - \dot{\xi}_s, \tag{A.25}$$

$$b_i = -a^2 w_i, \tag{A.26}$$

and the off-shell gauge-fixed metric becomes

$$\mathrm{d}s^2 = -(1 + 2h\Phi)\,\mathrm{d}t^2 + haV_i\,\mathrm{d}x^i\,\mathrm{d}t + a^2\left[\delta_{ij}(1 + 2h\Psi) + h\gamma_{ij}\right]\mathrm{d}x^i\,\mathrm{d}x^j. \tag{A.27}$$

Now we will expand the gamma-gamma action [208]

$$S = \int \mathrm{d}^4 x \sqrt{-g} \left[\frac{1}{2}g^{\mu\nu}\left(\Gamma^\lambda_{\mu\kappa}\Gamma^\kappa_{\nu\lambda} - \Gamma^\lambda_{\lambda\kappa}\Gamma^\kappa_{\mu\nu}\right) - \frac{1}{2}g^{\mu\nu}\partial_\mu\varphi\partial_\nu\varphi - V\right], \tag{A.28}$$

to second order. The zeroth and first order terms in the Lagrangian are

$$-3a\dot{a}^2 + a^3\left(\frac{1}{2}\dot{\phi}^2 - V\right), \tag{A.29}$$

$$h\left[6\left(a^2\Psi V + \dot{\Psi}\dot{a}\right) + a^3\left(\dot{\delta\phi}\dot{\phi} - \delta\phi\frac{\mathrm{d}V}{\mathrm{d}\phi}\right)\right]. \tag{A.30}$$

The first order term is a 'boundary term' in the sense that its variation with respect to Ψ and $\delta\phi$ gives terms proportional to the background equations of motion, and hence zero. The second order part contains four parts:

1. The vector part,

$$S_{\mathrm{vector}} = \int \mathrm{d}^4 x \frac{1}{4}a(\boldsymbol{\nabla} \times V) \cdot (\boldsymbol{\nabla} \times V). \tag{A.31}$$

   After integration by parts, the previous can also be written as

$$S_{\mathrm{vector}} = -\int \mathrm{d}^4 x \frac{1}{4}aV_{i,k}V_{i,k} + \int \mathrm{d}^4 x \frac{1}{4}a(V_{i,k}V_i)_{,k}. \tag{A.32}$$

With the boundary condition $V_i(\partial\Omega) = 0$ application of Stoke's theorem makes the second term zero. Therefore, vector perturbations satisfy constraint equations

$$\nabla^2 V_i = 0\,, \tag{A.33}$$

which yield $V_i = 0$, given the boundary conditions of the problem.

2. The scalar part,

$$
\begin{aligned}
S_{\text{scalar}} = \int \mathrm{d}^4 x a^3 \Big(& \frac{1}{2}\dot{\delta\phi}^2 - \frac{1}{2a^2}\delta\phi_{,k}\delta\phi_{,k} - \frac{1}{2}V_{,\phi\phi}\delta\phi^2 - 3\dot{\Psi}^2 \\
& + \frac{1}{a^2}\Psi_{,k}\Psi_{,k} + V(\Phi^2 - 3\Psi^2) + (3\Psi - \Phi)V_{,\phi}\delta\phi \\
& - 6H(\Phi + \Psi)\dot{\Psi} - (3\Psi + \Phi)\dot{\phi}\dot{\delta\phi} - \frac{2}{a^2}\Phi_{,k}\Psi_{,k}\Big)\,.
\end{aligned}
\tag{A.34}
$$

3. The tensor part,

$$S_{\text{tensor}} = \int \mathrm{d}^4 x \left(\frac{1}{8}a^3\dot{\gamma}_{ij}\dot{\gamma}^{ij} + \frac{1}{2}a^3 V\gamma_{ij}\gamma^{ij} + F(\gamma_{ij,k}) + a^2\dot{a}\gamma_{ij}\dot{\gamma}^{ij}\right)\,, \tag{A.35}$$

where F contains only spatial derivatives of the metric. Integrating by parts the last terms we obtain

$$\int \mathrm{d}^4 x \frac{1}{2}\frac{\mathrm{d}}{\mathrm{d}t}\left(a^2\dot{a}\gamma_{ij}\gamma^{ij}\right) - \int \mathrm{d}^4 x \frac{1}{2}\gamma_{ij}\gamma^{ij}a^3 V\,, \tag{A.36}$$

where in the latter we used the background equation of motion $2a\dot{a}^2 + a^2\ddot{a} = a^3 V$. Similarly, integrating by parts F and discarding all boundary terms[3] we have

$$S_{\text{tensor}} = \int \mathrm{d}^4 x \frac{1}{8}a^3\left(\dot{\gamma}_{ij}\dot{\gamma}^{ij} - \frac{1}{a^2}\boldsymbol{\nabla}\gamma_{ij}\cdot\boldsymbol{\nabla}\gamma^{ij}\right)\,. \tag{A.38}$$

4. Finally, the mixing terms,

$$
\begin{aligned}
S_{\text{mix}} = \int \mathrm{d}^4 x a^2 \frac{1}{2}[& V_{i,j}(\gamma^{ij}H + \dot{\gamma}^{ij}) - \dot{V}^i(3\Psi_{,i} + \Phi_{,i}) \\
& + V^i(H\Phi_{,i} - 7H\Psi_{,i} - 2V^i\delta\phi_i\dot{\phi})]\,.
\end{aligned}
\tag{A.39}
$$

---

[3]Variation of the first term, denoted by $\dot{A}$, in Eq. (A.36) yields

$$\partial_\mu\left(\frac{\partial\dot{A}}{\partial(\gamma_{ij,\mu})}\right) = \frac{\partial}{\partial t}\frac{\partial\dot{A}}{\partial\dot{\gamma}_{ij}} = \frac{\partial}{\partial t}\frac{\partial A}{\partial\gamma_{ij}} = \frac{\partial\dot{A}}{\partial\gamma_{ij}}\,, \tag{A.37}$$

and so it satisfies the Euler-Lagrange equations identically.

Integrating by parts and using the divergenceless-transverse proper-ties of V_i and γ_{ij} only boundary terms are left which can be set to zero with Stoke's theorem. Thus, with appropriate boundary condi-tions at infinity the mixing terms can be set to zero and the different modes evolve independently to first order in h.

B

Dynamical systems, isometries and stability

B.1 Dynamical systems analysis

In Ch. 6 we derived exact solutions which are valid only for specific initial conditions. In order to include them in the inflationary framework it is necessary to demonstrate that solutions for arbitrary initial conditions will converge towards them and so they will capture the late-time evolution of the system. We will demonstrate this attracting behaviour using concepts from the theory of dynamical systems.

B.1.1 Allowed critical points

Even without knowledge of the exact solution general properties of the solutions can be deduced using the theory of dynamical systems (see also [209,210] for a review of the theory and techniques applied to cosmology and [211–213] for more specialized applications to inflation and quintessence). With the aid of an auxiliary variable u we can transform the system into

first order form

$$\dot{\phi} = u \,, \tag{B.1}$$

$$\dot{u} = -3Hu - V_{,\phi} \,, \tag{B.2}$$

$$\dot{H} = -\frac{1}{2}u^2 \,, \tag{B.3}$$

along with the Friedmannian constraint. In order to use the latter to eliminate the dependence on H and reduce the problem's dimensionality we need to ensure that the root does not change sign (H being a monotonically decreasing function is not guaranteed to remain non-zero at any time). Because of the Friedman constraint not all initial data for H are allowed but only those lying on the hypersurface $6H^2 - \dot{\phi}^2 - 2V = 0$. If H starts at a negative value, $H(0) < 0$, then it will remain negative describing a contracting universe.Contracting universes lie outside the scope of this work and in the following we focus only on the case where $H(0) > 0$.

The asymptotic behaviour of the system can be determined by the form of its critical points. For a dynamical system of the form

$$\dot{\boldsymbol{x}} = \boldsymbol{f}(\boldsymbol{x}) \,, \tag{B.4}$$

where $\boldsymbol{x} \equiv \boldsymbol{x}(t) : \boldsymbol{R} \to \boldsymbol{R}^n$ and $\boldsymbol{f} : \boldsymbol{R}^n \to \boldsymbol{R}^n$ a critical point denoted by $\boldsymbol{x}_{\mathrm{cr}}$[1] marks steady-state solutions $\boldsymbol{f}(\boldsymbol{x}_{\mathrm{cr}}) = \boldsymbol{0}$; if the system (B.4) is non-singular then the initial value problem with $\boldsymbol{x}(0) = \boldsymbol{x}_{\mathrm{cr}}$ has a unique solution $\boldsymbol{x}(t) = \boldsymbol{x}_{\mathrm{cr}}$. The behaviour of the system near its critical points can provide information about qualitative features of solutions.

A critical point is called **stable** if trajectories that begin at a small distance $|\boldsymbol{\delta x}(t_0)|$ away from it remain bounded $|\boldsymbol{\delta x}(t)| \leq |\boldsymbol{\delta x}(t_0)|$ for $t > t_0$, while **asymptotically stable** if trajectories are bounded and converge to the critical value $|\boldsymbol{x}(t)| \to |\boldsymbol{x}_{\mathrm{cr}}|$. Two methods are widely used to determine stability: the linearization (or indirect method of stability) and Lyapunov's functions (or direct method of stability). In the former a Taylor expansion around $\boldsymbol{x}_{\mathrm{cr}}$ yields

$$\dot{\boldsymbol{x}} = \boldsymbol{Df}|_{\boldsymbol{x}=\boldsymbol{x}_{\mathrm{cr}}} \cdot (\boldsymbol{x} - \boldsymbol{x}_{\mathrm{cr}}) + \cdots \,, \tag{B.5}$$

where the first term in the expansion $\boldsymbol{f}(\boldsymbol{x}_{\mathrm{cr}})$ vanishes at the critical point and $\boldsymbol{Df}$ is the Jacobian or derivative matrix. The Hartman-Grobman theorem (see references above) allows deduction about local stability of the

---

[1]When a critical point is the $\boldsymbol{0}$ element of $\boldsymbol{R}^n$ it is also called fixed-point because it satisfies $\boldsymbol{f}(\boldsymbol{x}) = \boldsymbol{x}$. If $\boldsymbol{x}_{\mathrm{cr}}$ is finite it is always possible to perform a linear coordinate transformation to move the critical point at the origin.

non-linear dynamical system (B.4) around the critical point by studying its simplified linearisation (B.5) if the eigenvalues of the derivative matrix evaluated at that point have non-zero real part.

For the system of equations (B.1)-(B.3) if a critical point exists[2] it is necessary that $u = 0$ which implies that $\dot{u}$ can be zero only if $V' = 0$. Moreover, H is set by the constraint and its critical value is $\pm|\frac{1}{\sqrt{3}}V(\phi_{\rm cr})|$, depending on the sign of the potential. If $V_{\rm cr} < 0$ a critical point makes the Hamiltonian constraint inconsistent because at that point u satisfies

$$u_{\rm cr}^2 - 2|V_{\rm cr}| = 6H_{\rm cr}^2 \geq 0 \,, \tag{B.6}$$

which in turn requires $u_{\rm cr} \neq 0$. Thus, if the potential has critical points at negative values they do not satisfy the Friedman constraint. For $V_{\rm cr} \geq 0$ the linearized matrix evaluated at the critical point $(\phi_{\rm cr}, 0, H_{\rm cr})$ gives

$$\begin{pmatrix} 0 & 1 & 0 \\ -V_{,\phi\phi}(\phi_{\rm cr}) & -3H_{\rm cr} & 0 \\ 0 & 0 & 0 \end{pmatrix} \,. \tag{B.7}$$

The eigenvalue equation of this matrix is

$$-\lambda^2(\lambda + 3H_{\rm cr}) - \lambda V_{,\phi\phi}(\phi_{\rm cr}) = 0 \,, \tag{B.8}$$

with eigenvalues

$$\lambda = 0 \ \ \text{and} \ \ \lambda = -\frac{1}{2}\left(3H_{\rm cr} \pm \sqrt{9H_{\rm cr}^2 - 4V_{,\phi\phi}(\phi_{\rm cr})}\right) \,. \tag{B.9}$$

Now it is clear that when $H_{\rm cr}$ is negative at least one of the eigenvalues has positive real part and the critical point will be unstable. When $H_{\rm cr}$ is non-negative since there exists one eigenvalue with zero real part the theorem can not be used. However, in the Klein-Gordon equation we can eliminate the dependence on H by substituting its value using the Friedman constraint. When $V_{\rm min} \geq 0$ the Hubble parameter at the critical point will satisfy $H_{\rm min} \geq 0$ and so H will be given by the positive root of Eq. (3.7). The reduced system reads

$$\ddot{\phi} + \sqrt{3}\dot{\phi}\sqrt{\frac{1}{2}\dot{\phi}^2 + V} + V_{,\phi} = 0 \,, \tag{B.10}$$

---

[2]Strictly speaking the full problem does not admit critical points, because the Liouville measure is conserved, but for flat spatial curvature the problem can be reduced to the study of $\phi - \dot{\phi}$ subspace [214].

or transforming it into first order form

$$\dot{\phi} = u \,, \tag{B.11}$$

$$\dot{u} = -\sqrt{\frac{3}{2}} u \sqrt{u^2 + 2V} - V_{,\phi} \,. \tag{B.12}$$

The derivative matrix becomes

$$\begin{pmatrix} 0 & 1 \\ -V_{,\phi\phi}(\phi_{\mathrm{cr}}) & -\sqrt{3V_{\mathrm{cr}}} \end{pmatrix} \,, \tag{B.13}$$

with eigenvalues

$$\lambda_{\pm} = -\frac{1}{2} \left(\sqrt{3V_{\mathrm{cr}}} \pm \sqrt{3V_{\mathrm{cr}} - 4V_{,\phi\phi}(\phi_{\mathrm{cr}})} \right) \,. \tag{B.14}$$

Stability is determined by the sign of the discriminant; potentials with a maximum result into strictly positive discriminant and one of the eigenvalues will be positive (unstable critical point). In the case of a saddle at least one eigenvalue will be zero and there is no conclusion about stability. However, the u-equation indicates that a small perturbation on the negative axis will result into negative u that will increase indefinitely; the critical point is overall unstable. We conclude that only potentials with a non-negative global minimum admit **physically acceptable solutions** with a stable critical point.

In the case of a positive local minimum $V_{\mathrm{cr}}, V_{,\phi\phi}(\phi_{\mathrm{cr}}) > 0$ and irrespective of the discriminant's sign the critical point will be stable; this solution describes an eternally inflating universe. Usually, we demand a Minkowski space after inflation and so $V_{\mathrm{cr}} = 0$. The two eigenvalues become imaginary $\lambda = \pm i \sqrt{V_{,\phi\phi}(\phi_{\mathrm{cr}})}$ and linearized analysis fails. It is clear, though, that oscillations around the minimum will be damped, because Hubble friction forces the energy of the system to decrease, so one expects that the system will eventually settle down to its minimum. This physical argument naturally suggests the use of Lyapunov's second theorem to determine stability [215] and it will be the subject of the next subsection.

B.1.2 Lyapunov's theorem and LaSalle's principle

If there exists a scalar function $L(\boldsymbol{x})$ with continuous first partial derivatives which satisfies the following properties

1. positive definite for $\boldsymbol{x} \neq \boldsymbol{x}_{\mathrm{cr}}$ and $L(\boldsymbol{x}_{\mathrm{cr}}) = 0$,

2. decreasing function of time $\dot{L} \leq 0$,

then $\boldsymbol{x}_{\mathrm{cr}}$ is stable. If additionally

3. $\dot{L} < 0$ for $\boldsymbol{x} \neq \boldsymbol{x}_{\mathrm{cr}}$ and $\dot{L}(\boldsymbol{x}_{\mathrm{cr}}) = 0$,

4. L is radially unbounded: $L \to +\infty$ for $|\boldsymbol{x}| \to \infty$,

then $\boldsymbol{x}_{\mathrm{cr}}$ is globally asymptotically stable. For spatially flat scalar field models $3H^2$ seems a suitable Lyapunov's function [216] because it satisfies properties (1),(2) and (4). Its vanishes when $\dot{\phi} = 0$, leaving ϕ unspecified, and applying Lyapunov's theorem we can only conclude that the critical point is stable. To prove global asymptotic stability we need LaSalle's theorem [217] which states that whenever the time derivative of the Lyapunov's function is negative semidefinite, $\dot{L} \leq 0$, then the ω-limit set of every trajectory (the set of accumulation points of $\boldsymbol{x}(t)$ for $t \to \infty$) will be contained in the set $\{\boldsymbol{x} : \dot{L}(\boldsymbol{x}) = 0\}$. In our case by assumption there is only one critical point and application of the theorem proves asymptotic stability. Therefore for potentials with a global minimum that take zero value at the minimum the origin is globally asymptotically stable

$$\lim_{t \to +\infty} (\phi(t), \dot{\phi}(t)) = (\phi_{\mathrm{cr}}, 0) \,, \tag{B.15}$$

and the generalization for multiple fields is straightforward.

B.2 Hurwitz-Routh stability criterion

A polynomial of degree n is called stable if all roots have negative real part. The relevance to the stability of dynamical systems is clear: the characteristic equation of the $N \times N$ Jacobian matrix is an nth order polynomial

$$\lambda^n + a_{n-1}\lambda^{n-1} + \cdots + a_0 = 0 \,, \tag{B.16}$$

and if every root has negative real part the dynamical system is called (asymptotically) stable. Analytical formulae for the roots of Eq. (B.16) exist up to 4th order so it is necessary to develop tools to infer stability without finding the roots. One method is the Hurwitz-Routh theorem [218]: a polynomial will be stable if every coefficient is positive $a_n > 0$ and if every principal Hurwitz determinant is also positive. The latter is the determinant of a matrix constructed as follows: the first elements are $\{a_{n-1}, 1\}$ while the rest are zeros. In the second row the first elements are $\{a_{n-3}, a_{n-2}, a_{n-3}, 1\}$

and the rest zero. Similarly, the i-th row is constructed using the a_{n-i} coefficient

$$\Delta_k = \begin{pmatrix} a_{n-1} & 1 & \cdots & 0 \\ a_{n-3} & a_{n-2} & \cdots & 0 \\ \cdots & \cdots & \cdots & 0 \\ a_{n-k} & \cdots & a_{k+1} & a_k \end{pmatrix}. \tag{B.17}$$

The criterion is formulated as follows: $|\Delta_k| > 0$, for all $k < n$.

For a quadratic equation the criterion reduces to positivity of every coefficient, while for a cubic equation we obtain the additional condition $a_2 a_1 > a_0$.

B.3   Coordinate transformations and isometries

A metric with an isometry possesses a Killing vector $\vec{\xi} = \xi^I \partial_I$. Under a coordinate change $x^I \equiv \{\chi, \psi\} \to \tilde{x}^I \equiv \{\rho, \phi\}$ the components of the vector transform according to

$$\tilde{\xi}^I = \frac{\partial \tilde{x}^I}{\partial x^K} \xi^K. \tag{B.18}$$

Therefore, it is possible to set the first component to zero which is equivalent to solving the advection equation with variable coefficients

$$\frac{\partial \rho}{\partial \chi} \xi^\chi + \frac{\partial \rho}{\partial \psi} \xi^\psi = 0. \tag{B.19}$$

With appropriate boundary conditions this can always be solved, e.g. by the method of characteristics. Thus, in the new coordinate system the Killing vector points along the second basis vector $\vec{\xi} = \tilde{\xi}^\phi \partial_\phi$ and so the new metric is independent of that coordinate. Any remaining off-diagonal terms can be absorbed through a redefinition of the variable ϕ, whereas $G_{\rho\rho}$ can be set to one by an appropriate redefinition of ρ

$$\tilde{\phi} = -\int \frac{G_{\rho\phi}}{G_{\phi\phi}} \, d\rho + c_1(\phi) \qquad \tilde{\rho} = \int \sqrt{G_{\rho\rho}} \, d\rho + c_2(\phi). \tag{B.20}$$

As a side note, 2D metrics can have 0, 1 or 3 isometries, where the latter case describes a maximally symmetric space of constant curvature (flat, hyperbolic or spherical).

Bibliography

[1] Wayne Horowitz. *Mesopotamian Cosmogony and Cosmology*, pages 1823–1827. Springer New York, New York, NY, 2015.

[2] V.J. Katz. *A History of Mathematics: An Introduction*. Addison-Wesley, 2009.

[3] B. L. van der Waerden. *Science awakening. English translation by Arnold Dresden, with additions of the author*. P. Noordhoff Groningen, 1954.

[4] H. van der Waerden. *Science Awakening II*. Science awakening. Springer Netherlands, 1973.

[5] T.S. Kuhn and J.B. Conant. *The Copernican Revolution: Planetary Astronomy in the Development of Western Thought*. A Harvard Paperback. Harvard University Press, 1957.

[6] Miguel A. Granada. Aristotle, copernicus, bruno: centrality, the principle of movement and the extension of the universe. *Studies in History and Philosophy of Science Part A*, 35(1):91–114, 2004.

[7] Stephen G. Brush. The nebular hypothesis and the evolutionary worldview. *History of Science*, 25(3):245–278, 1987.

[8] E. R. Harrison. Olbers' Paradox and the Background Radiation Density in an Isotropic Homogeneous Universe. *Monthly Notices of the Royal Astronomical Society*, 131(1):1–12, 12 1965.

[9] Edward Harrison. The dark night-sky riddle, "olbers's paradox". *Symposium - International Astronomical Union*, 139:3–17, 1990.

[10] A. Friedman. On the Curvature of space. *Z. Phys.*, 10:377–386, 1922.

[11] Georges Lemaitre. A Homogeneous Universe of Constant Mass and Growing Radius Accounting for the Radial Velocity of Extragalactic Nebulae. *Gen. Rel. Grav.*, 45(8):1635–1646, 2013.

[12] M. A. Hoskin. The 'Great Debate': What Really Happened. *Journal for the History of Astronomy*, 7:169, January 1976.

[13] Edwin Hubble. A relation between distance and radial velocity among extra-galactic nebulae. *Proceedings of the National Academy of Sciences*, 15(3):168–173, 1929.

[14] Ruth Durrer. The cosmic microwave background: the history of its experimental investigation and its significance for cosmology. *Class. Quant. Grav.*, 32(12):124007, 2015.

[15] Adam G. Riess et al. Observational evidence from supernovae for an accelerating universe and a cosmological constant. *Astron. J.*, 116:1009–1038, 1998.

[16] S. Perlmutter et al. Measurements of Ω and Λ from 42 high redshift supernovae. *Astrophys. J.*, 517:565–586, 1999.

[17] Volker Springel, Carlos S. Frenk, and Simon D.M. White. The large-scale structure of the Universe. *Nature*, 440:1137, 2006.

[18] H.P. Robertson. Kinematics and World-Structure. *Astrophys. J.*, 82:284–301, 1935.

[19] H.P. Robertson. Kinematics and World-Structure. 2. *Astrophys. J.*, 83:187–201, 1935.

[20] A. G. Walker. On Milne's Theory of World-Structure. *Proceedings of the London Mathematical Society*, 42:90–127, January 1937.

[21] C. Marinoni, J. Bel, and A. Buzzi. The Scale of Cosmic Isotropy. *JCAP*, 10:036, 2012.

[22] C.L. Bennett, A. Banday, K.M. Gorski, G. Hinshaw, P. Jackson, P. Keegstra, A. Kogut, George F. Smoot, D.T. Wilkinson, and E.L. Wright. Four year COBE DMR cosmic microwave background observations: Maps and basic results. *Astrophys. J. Lett.*, 464:L1–L4, 1996.

[23] C. L. Bennett, D. Larson, J. L. Weiland, N. Jarosik, G. Hinshaw, N. Odegard, K. M. Smith, R. S. Hill, B. Gold, M. Halpern, and et al. Nine-year wilkinson microwave anisotropy probe (wmap) observations: Final maps and results. *The Astrophysical Journal Supplement Series*, 208(2):20, Sep 2013.

[24] P. A. R. Ade et al. Planck 2013 results. I. Overview of products and scientific results. *Astron. Astrophys.*, 571:A1, 2014.

[25] N. Aghanim et al. Planck 2018 results. I. Overview and the cosmological legacy of Planck. *Astron. Astrophys.*, 641:A1, 2020.

[26] Charles W. Misner. The Isotropy of the universe. *Astrophys. J.*, 151:431–457, 1968.

[27] Jacques Colin, Roya Mohayaee, Mohamed Rameez, and Subir Sarkar. Evidence for anisotropy of cosmic acceleration. *Astron. Astrophys.*, 631:L13, 2019.

[28] K. Migkas, G. Schellenberger, T.H. Reiprich, F. Pacaud, M.E. Ramos-Ceja, and L. Lovisari. Probing cosmic isotropy with a new X-ray galaxy cluster sample through the $L_{\mathrm{X}} - T$ scaling relation. *Astron. Astrophys.*, 636:A15, 2020.

[29] Roy Maartens. Is the Universe homogeneous? *Phil. Trans. Roy. Soc. Lond. A*, 369:5115–5137, 2011.

[30] B. Ryden. *Introduction to cosmology*. Cambridge University Press, 11 2016.

[31] Sean M. Carroll. *Spacetime and Geometry*. Cambridge University Press, 7 2019.

[32] Willem de Sitter. On the relativity of inertia. Remarks concerning Einstein's latest hypothesis. *Koninklijke Nederlandse Akademie van Wetenschappen Proceedings Series B Physical Sciences*, 19:1217–1225, March 1917.

[33] W. de Sitter. On the curvature of space. *Koninklijke Nederlandse Akademie van Wetenschappen Proceedings Series B Physical Sciences*, 20:229–243, January 1918.

[34] P.A. Zyla et al. Review of Particle Physics. *PTEP*, 2020(8):083C01, 2020.

[35] N. Aghanim et al. Planck 2018 results. VI. Cosmological parameters. 7 2018.

[36] David N. Spergel and Paul J. Steinhardt. Observational evidence for self-interacting cold dark matter. *Phys. Rev. Lett.*, 84:3760–3763, 2000.

[37] Lars Bergström. Nonbaryonic dark matter: Observational evidence and detection methods. *Rept. Prog. Phys.*, 63:793, 2000.

[38] W. Rindler. Visual horizons in world-models. *Gen. Rel. Grav.*, 34:133–153, 2002.

[39] C.B. Collins and S.W. Hawking. Why is the Universe isotropic? *Astrophys. J.*, 180:317–334, 1973.

[40] S.W. Hawking and W. Israel. *General Relativity: An Einstein Centenary Survey*. Univ. Pr., Cambridge, UK, 1979.

[41] Alan H. Guth. The Inflationary Universe: A Possible Solution to the Horizon and Flatness Problems. *Adv. Ser. Astrophys. Cosmol.*, 3:139–148, 1987.

[42] Stefan Hollands and Robert M. Wald. An Alternative to inflation. *Gen. Rel. Grav.*, 34:2043–2055, 2002.

[43] Sean M. Carroll. *In What Sense Is the Early Universe Fine-Tuned?* 6 2014.

[44] C.D. McCoy. Does inflation solve the hot big bang model's fine-tuning problems? *Studies in History and Philosophy of Science Part B: Studies in History and Philosophy of Modern Physics*, 51:23 – 36, 2015.

[45] Marc Holman. How Problematic is the Near-Euclidean Spatial Geometry of the Large-Scale Universe? *Found. Phys.*, 48(11):1617–1647, 2018.

[46] H.E.S. Velten, R.F. vom Marttens, and W. Zimdahl. Aspects of the cosmological "coincidence problem". *Eur. Phys. J. C*, 74(11):3160, 2014.

[47] L. Verde, T. Treu, and A.G. Riess. Tensions between the Early and the Late Universe. 7 2019.

[48] Adam G. Riess, Stefano Casertano, Wenlong Yuan, Lucas M. Macri, and Dan Scolnic. Large Magellanic Cloud Cepheid Standards Provide a 1% Foundation for the Determination of the Hubble Constant and Stronger Evidence for Physics beyond ΛCDM. *Astrophys. J.*, 876(1):85, 2019.

[49] S. Birrer et al. H0LiCOW - IX. Cosmographic analysis of the doubly imaged quasar SDSS 1206+4332 and a new measurement of the Hubble constant. *Mon. Not. Roy. Astron. Soc.*, 484:4726, 2019.

[50] Wendy L. Freedman et al. The Carnegie-Chicago Hubble Program. VIII. An Independent Determination of the Hubble Constant Based on the Tip of the Red Giant Branch. 7 2019.

[51] G. Efstathiou. A Lockdown Perspective on the Hubble Tension (with comments from the SH0ES team). 7 2020.

[52] Eleonora Di Valentino et al. Cosmology Intertwined II: The Hubble Constant Tension. 8 2020.

[53] Alexei A. Starobinsky. Spectrum of relict gravitational radiation and the early state of the universe. *JETP Lett.*, 30:682–685, 1979.

[54] Alexei A. Starobinsky. A New Type of Isotropic Cosmological Models Without Singularity. *Adv. Ser. Astrophys. Cosmol.*, 3:130–133, 1987.

[55] K. Sato. Cosmological Baryon Number Domain Structure and the First Order Phase Transition of a Vacuum. *Adv. Ser. Astrophys. Cosmol.*, 3:134–138, 1987.

[56] D. Kazanas. Dynamics of the Universe and Spontaneous Symmetry Breaking. *Astrophys. J. Lett.*, 241:L59–L63, 1980.

[57] Alan H. Guth and S.H.H. Tye. Phase Transitions and Magnetic Monopole Production in the Very Early Universe. *Phys. Rev. Lett.*, 44:631, 1980. [Erratum: Phys.Rev.Lett. 44, 963 (1980)].

[58] John Preskill. Cosmological Production of Superheavy Magnetic Monopoles. *Phys. Rev. Lett.*, 43:1365, 1979.

[59] Lev Kofman, Andrei D. Linde, and Alexei A. Starobinsky. Towards the theory of reheating after inflation. *Phys. Rev. D*, 56:3258–3295, 1997.

[60] Daniel Baumann and Liam McAllister. *Inflation and String Theory.* Cambridge Monographs on Mathematical Physics. Cambridge University Press, 5 2015.

[61] D.S. Salopek and J.R. Bond. Nonlinear evolution of long wavelength metric fluctuations in inflationary models. *Phys. Rev. D*, 42:3936–3962, 1990.

[62] Perseas Christodoulidis. General solutions to $\mathcal{N}$-field cosmology with exponential potentials. *Eur. Phys. J. C*, 81(5):471, 2021.

[63] Andrew R. Liddle, Paul Parsons, and John D. Barrow. Formalizing the slow roll approximation in inflation. *Phys. Rev. D*, 50:7222–7232, 1994.

[64] John Joseph M. Carrasco, Simon Foreman, Daniel Green, and Leonardo Senatore. The Effective Field Theory of Large Scale Structures at Two Loops. *JCAP*, 07:057, 2014.

[65] James M. Bardeen. Gauge Invariant Cosmological Perturbations. *Phys. Rev. D*, 22:1882–1905, 1980.

[66] Viatcheslav F. Mukhanov, H.A. Feldman, and Robert H. Brandenberger. Theory of cosmological perturbations. Part 1. Classical perturbations. Part 2. Quantum theory of perturbations. Part 3. Extensions. *Phys. Rept.*, 215:203–333, 1992.

[67] Viatcheslav F. Mukhanov. Quantum Theory of Gauge Invariant Cosmological Perturbations. *Sov. Phys. JETP*, 67:1297–1302, 1988.

[68] Karim A. Malik and David R. Matravers. Comments on gauge-invariance in cosmology. *Gen. Rel. Grav.*, 45:1989–2001, 2013.

[69] Antonio Riotto. Inflation and the theory of cosmological perturbations. *ICTP Lect. Notes Ser.*, 14:317–413, 2003.

[70] T.S. Bunch and P.C.W. Davies. Quantum Field Theory in de Sitter Space: Renormalization by Point Splitting. *Proc. Roy. Soc. Lond. A*, A360:117–134, 1978.

[71] David H. Lyth, Karim A. Malik, and Misao Sasaki. A General proof of the conservation of the curvature perturbation. *JCAP*, 05:004, 2005.

[72] Y. Akrami et al. Planck 2018 results. X. Constraints on inflation. 7 2018.

[73] M.C. Guzzetti, N. Bartolo, M. Liguori, and S. Matarrese. Gravitational waves from inflation. *Riv. Nuovo Cim.*, 39(9):399–495, 2016.

[74] Daniel Baumann. Inflation. In *Theoretical Advanced Study Institute in Elementary Particle Physics: Physics of the Large and the Small*, pages 523–686, 2011.

[75] Misao Sasaki. Large Scale Quantum Fluctuations in the Inflationary Universe. *Prog. Theor. Phys.*, 76:1036, 1986.

[76] Claus Kiefer and David Polarski. Why do cosmological perturbations look classical to us? *Adv. Sci. Lett.*, 2:164–173, 2009.

[77] Claus Kiefer, David Polarski, and Alexei A. Starobinsky. Quantum to classical transition for fluctuations in the early universe. *Int. J. Mod. Phys. D*, 7:455–462, 1998.

[78] Juan Martin Maldacena. Non-Gaussian features of primordial fluctuations in single field inflationary models. *JHEP*, 05:013, 2003.

[79] Paolo Creminelli and Matias Zaldarriaga. Single field consistency relation for the 3-point function. *JCAP*, 10:006, 2004.

[80] Rafael Bravo and Gonzalo A. Palma. Unifying attractor and non-attractor models of inflation under a single soft theorem. 9 2020.

[81] Oliver Friedrich, Cora Uhlemann, Francisco Villaescusa-Navarro, Tobias Baldauf, Marc Manera, and Takahiro Nishimichi. Primordial non-Gaussianity without tails – how to measure fNL with the bulk of the density PDF. *Mon. Not. Roy. Astron. Soc.*, 498(1):464–483, 2020.

[82] Abraham Loeb and Matias Zaldarriaga. Measuring the small - scale power spectrum of cosmic density fluctuations through 21 cm tomography prior to the epoch of structure formation. *Phys. Rev. Lett.*, 92:211301, 2004.

[83] Viatcheslav Mukhanov. Quantum Cosmological Perturbations: Predictions and Observations. *Eur. Phys. J. C*, 73:2486, 2013.

[84] Diederik Roest. Universality classes of inflation. *JCAP*, 01:007, 2014.

[85] P. A. R. Ade et al. Joint Analysis of BICEP2/*KeckArray* and *Planck* Data. *Phys. Rev. Lett.*, 114:101301, 2015.

[86] Edmund J. Copeland, Andrew R. Liddle, David H. Lyth, Ewan D. Stewart, and David Wands. False vacuum inflation with Einstein gravity. *Phys. Rev. D*, 49:6410–6433, 1994.

[87] Sébastien Renaux-Petel and Krzysztof Turzyński. Geometrical Destabilization of Inflation. *Phys. Rev. Lett.*, 117(14):141301, 2016.

[88] Ana Achucarro, Jinn-Ouk Gong, Sjoerd Hardeman, Gonzalo A. Palma, and Subodh P. Patil. Features of heavy physics in the CMB power spectrum. *JCAP*, 01:030, 2011.

[89] Ana Achucarro, Jinn-Ouk Gong, Sjoerd Hardeman, Gonzalo A. Palma, and Subodh P. Patil. Effective theories of single field inflation when heavy fields matter. *JHEP*, 05:066, 2012.

[90] Ana Achucarro, Vicente Atal, Sebastian Cespedes, Jinn-Ouk Gong, Gonzalo A. Palma, and Subodh P. Patil. Heavy fields, reduced speeds of sound and decoupling during inflation. *Phys. Rev. D*, 86:121301, 2012.

[91] Sebastian Garcia-Saenz and Sébastien Renaux-Petel. Flattened non-Gaussianities from the effective field theory of inflation with imaginary speed of sound. *JCAP*, 11:005, 2018.

[92] Jacopo Fumagalli, Sebastian Garcia-Saenz, Lucas Pinol, Sébastien Renaux-Petel, and John Ronayne. Hyper-Non-Gaussianities in Inflation with Strongly Nongeodesic Motion. *Phys. Rev. Lett.*, 123(20):201302, 2019.

[93] Sebastian Garcia-Saenz, Lucas Pinol, and Sébastien Renaux-Petel. Revisiting non-Gaussianity in multifield inflation with curved field space. *JHEP*, 01:073, 2020.

[94] Theodor Bjorkmo, Ricardo Z. Ferreira, and M.C. David Marsh. Mild Non-Gaussianities under Perturbative Control from Rapid-Turn Inflation Models. *JCAP*, 12:036, 2019.

[95] Ricardo Z. Ferreira. Non-Gaussianities in models of inflation with large and negative entropic masses. *JCAP*, 08:034, 2020.

[96] Gonzalo A. Palma, Spyros Sypsas, and Cristobal Zenteno. Seeding primordial black holes in multifield inflation. *Phys. Rev. Lett.*, 125(12):121301, 2020.

[97] Jacopo Fumagalli, Sébastien Renaux-Petel, John W. Ronayne, and Lukas T. Witkowski. Turning in the landscape: a new mechanism for generating Primordial Black Holes. 4 2020.

[98] Ana Achúcarro and Gonzalo A. Palma. The string swampland constraints require multi-field inflation. *JCAP*, 02:041, 2019.

[99] Theodor Bjorkmo and M.C. David Marsh. Hyperinflation generalised: from its attractor mechanism to its tension with the 'swampland conditions'. *JHEP*, 04:172, 2019.

[100] Theodor Bjorkmo. Rapid-Turn Inflationary Attractors. *Phys. Rev. Lett.*, 122(25):251301, 2019.

[101] Vikas Aragam, Sonia Paban, and Robert Rosati. Multi-field Inflation in High-Slope Potentials. *JCAP*, 04:022, 2020.

[102] Shuntaro Mizuno, Shinji Mukohyama, Shi Pi, and Yun-Long Zhang. Hyperbolic field space and swampland conjecture for DBI scalar. *JCAP*, 09:072, 2019.

[103] Rafael Bravo, Gonzalo A. Palma, and Simón Riquelme. A Tip for Landscape Riders: Multi-Field Inflation Can Fulfill the Swampland Distance Conjecture. *JCAP*, 02:004, 2020.

[104] E. Kreyszig. *Differential Geometry*. Dover Books on Mathematics. Dover Publications, 2013.

[105] Alexander Hetz and Gonzalo A. Palma. Sound Speed of Primordial Fluctuations in Supergravity Inflation. *Phys. Rev. Lett.*, 117(10):101301, 2016.

[106] Perseas Christodoulidis, Diederik Roest, and Evangelos I. Sfakianakis. Angular inflation in multi-field α-attractors. *JCAP*, 11(11):002, 2019.

[107] Dibya Chakraborty, Roberta Chiovoloni, Oscar Loaiza-Brito, Gustavo Niz, and Ivonne Zavala. Fat inflatons, large turns and the η-problem. *JCAP*, 2001(01):020, 2020.

[108] David H. Lyth and Andrew R. Liddle. *The primordial density perturbation: Cosmology, inflation and the origin of structure.* 2009.

[109] I-Sheng Yang. The Strong Multifield Slowroll Condition and Spiral Inflation. *Phys. Rev. D*, 85:123532, 2012.

[110] Misao Sasaki and Ewan D. Stewart. A General analytic formula for the spectral index of the density perturbations produced during inflation. *Prog. Theor. Phys.*, 95:71–78, 1996.

[111] David I. Kaiser, Edward A. Mazenc, and Evangelos I. Sfakianakis. Primordial Bispectrum from Multifield Inflation with Nonminimal Couplings. *Phys. Rev. D*, 87:064004, 2013.

[112] Christopher Gordon, David Wands, Bruce A. Bassett, and Roy Maartens. Adiabatic and entropy perturbations from inflation. *Phys. Rev. D*, 63:023506, 2000.

[113] Karim A. Malik and David Wands. Cosmological perturbations. *Phys. Rept.*, 475:1–51, 2009.

[114] Luca Amendola, Christopher Gordon, David Wands, and Misao Sasaki. Correlated perturbations from inflation and the cosmic microwave background. *Phys. Rev. Lett.*, 88:211302, 2002.

[115] David Wands, Nicola Bartolo, Sabino Matarrese, and Antonio Riotto. An Observational test of two-field inflation. *Phys. Rev. D*, 66:043520, 2002.

[116] Christian T. Byrnes and David Wands. Curvature and isocurvature perturbations from two-field inflation in a slow-roll expansion. *Phys. Rev. D*, 74:043529, 2006.

[117] David H. Lyth and Yeinzon Rodriguez. The Inflationary prediction for primordial non-Gaussianity. *Phys. Rev. Lett.*, 95:121302, 2005.

[118] David Seery and James E. Lidsey. Primordial non-Gaussianities from multiple-field inflation. *JCAP*, 09:011, 2005.

[119] Filippo Vernizzi and David Wands. Non-gaussianities in two-field inflation. *JCAP*, 05:019, 2006.

[120] Christian T. Byrnes, Ki-Young Choi, and Lisa M. H. Hall. Conditions for large non-Gaussianity in two-field slow-roll inflation. *JCAP*, 10:008, 2008.

[121] Christian T. Byrnes and Ki-Young Choi. Review of local non-Gaussianity from multi-field inflation. *Adv. Astron.*, 2010:724525, 2010.

[122] Sera Cremonini, Zygmunt Lalak, and Krzysztof Turzynski. Strongly Coupled Perturbations in Two-Field Inflationary Models. *JCAP*, 03:016, 2011.

[123] Andrew J. Tolley and Mark Wyman. The Gelaton Scenario: Equilateral non-Gaussianity from multi-field dynamics. *Phys. Rev. D*, 81:043502, 2010.

[124] Nima Arkani-Hamed and Juan Maldacena. Cosmological Collider Physics. 3 2015.

[125] Dong-Gang Wang. On the inflationary massive field with a curved field manifold. *JCAP*, 01:046, 2020.

[126] Alexei A. Starobinsky. Multicomponent de Sitter (Inflationary) Stages and the Generation of Perturbations. *JETP Lett.*, 42:152–155, 1985.

[127] Ross N. Greenwood, David I. Kaiser, and Evangelos I. Sfakianakis. Multifield Dynamics of Higgs Inflation. *Phys. Rev. D*, 87:064021, 2013.

[128] Matthew P. DeCross, David I. Kaiser, Anirudh Prabhu, C. Prescod-Weinstein, and Evangelos I. Sfakianakis. Preheating after Multifield Inflation with Nonminimal Couplings, I: Covariant Formalism and Attractor Behavior. *Phys. Rev. D*, 97(2):023526, 2018.

[129] Dhimiter D. Canko, Ioannis D. Gialamas, and George P. Kodaxis. A simple $F(\mathcal{R}, \phi)$ deformation of Starobinsky inflationary model. *Eur. Phys. J. C*, 80(5):458, 2020.

[130] Evan McDonough, Alan H. Guth, and David I. Kaiser. Nonminimal Couplings and the Forgotten Field of Axion Inflation. 10 2020.

[131] Sebastien Renaux-Petel and Krzysztof Turzynski. On reaching the adiabatic limit in multi-field inflation. *JCAP*, 06:010, 2015.

[132] Jonathan Frazer. Predictions in multifield models of inflation. *JCAP*, 01:028, 2014.

[133] Yun-Song Piao. On perturbation spectra of N-flation. *Phys. Rev. D*, 74:047302, 2006.

[134] P.A.R. Ade et al. Planck 2013 results. XXII. Constraints on inflation. *Astron. Astrophys.*, 571:A22, 2014.

[135] Ana Achúcarro, Vicente Atal, Cristiano Germani, and Gonzalo A. Palma. Cumulative effects in inflation with ultra-light entropy modes. *JCAP*, 02:013, 2017.

[136] Renata Kallosh, Andrei Linde, and Diederik Roest. Superconformal Inflationary α-Attractors. *JHEP*, 11:198, 2013.

[137] Renata Kallosh, Andrei Linde, and Diederik Roest. Universal Attractor for Inflation at Strong Coupling. *Phys. Rev. Lett.*, 112(1):011303, 2014.

[138] David I. Kaiser and Evangelos I. Sfakianakis. Multifield Inflation after Planck: The Case for Nonminimal Couplings. *Phys. Rev. Lett.*, 112(1):011302, 2014.

[139] Mario Galante, Renata Kallosh, Andrei Linde, and Diederik Roest. Unity of Cosmological Inflation Attractors. *Phys. Rev. Lett.*, 114(14):141302, 2015.

[140] John Joseph M. Carrasco, Renata Kallosh, Andrei Linde, and Diederik Roest. Hyperbolic geometry of cosmological attractors. *Phys. Rev. D*, 92(4):041301, 2015.

[141] S. Dimopoulos, S. Kachru, J. McGreevy, and Jay G. Wacker. N-flation. *JCAP*, 08:003, 2008.

[142] Richard Easther, Jonathan Frazer, Hiranya V. Peiris, and Layne C. Price. Simple predictions from multifield inflationary models. *Phys. Rev. Lett.*, 112:161302, 2014.

[143] Mafalda Dias, Jonathan Frazer, and M. C. David Marsh. Simple emergent power spectra from complex inflationary physics. *Phys. Rev. Lett.*, 117(14):141303, 2016.

[144] Richard Easther and Liam McAllister. Random matrices and the spectrum of N-flation. *JCAP*, 05:018, 2006.

[145] Mafalda Dias, Jonathan Frazer, and M. c. David Marsh. Seven Lessons from Manyfield Inflation in Random Potentials. *JCAP*, 01:036, 2018.

[146] Ana Achúcarro, Renata Kallosh, Andrei Linde, Dong-Gang Wang, and Yvette Welling. Universality of multi-field α-attractors. *JCAP*, 04:028, 2018.

[147] Adam R. Brown. Hyperbolic Inflation. *Phys. Rev. Lett.*, 121(25):251601, 2018.

[148] Shuntaro Mizuno and Shinji Mukohyama. Primordial perturbations from inflation with a hyperbolic field-space. *Phys. Rev. D*, 96(10):103533, 2017.

[149] Juan Garcia-Bellido and David Wands. Metric perturbations in two field inflation. *Phys. Rev. D*, 53:5437–5445, 1996.

[150] Mafalda Dias, Jonathan Frazer, and David Seery. Computing observables in curved multifield models of inflation—A guide (with code) to the transport method. *JCAP*, 12:030, 2015.

[151] Pedro Carrilho, David Mulryne, John Ronayne, and Tommi Tenkanen. Attractor Behaviour in Multifield Inflation. *JCAP*, 06:032, 2018.

[152] Katelin Schutz, Evangelos I. Sfakianakis, and David I. Kaiser. Multifield Inflation after Planck: Isocurvature Modes from Nonminimal Couplings. *Phys. Rev. D*, 89(6):064044, 2014.

[153] Perseas Christodoulidis, Diederik Roest, and Evangelos I. Sfakianakis. Scaling attractors in multi-field inflation. *JCAP*, 12:059, 2019.

[154] Sebastian Garcia-Saenz, Sébastien Renaux-Petel, and John Ronayne. Primordial fluctuations and non-Gaussianities in sidetracked inflation. *JCAP*, 07:057, 2018.

[155] Karim A. Malik and David Wands. Dynamics of assisted inflation. *Phys. Rev. D*, 59:123501, 1999.

[156] Federico Piazza and Shinji Tsujikawa. Dilatonic ghost condensate as dark energy. *JCAP*, 07:004, 2004.

[157] Andrew J. Tolley and Daniel H. Wesley. Scale-invariance in expanding and contracting universes from two-field models. *JCAP*, 05:006, 2007.

[158] N. Dimakis, A. Paliathanasis, Petros A. Terzis, and T. Christodoulakis. Cosmological Solutions in Multiscalar Field Theory. *Eur. Phys. J. C*, 79(7):618, 2019.

[159] Michele Cicoli, Giuseppe Dibitetto, and Francisco G. Pedro. New accelerating solutions in late-time cosmology. *Phys. Rev. D*, 101(10):103524, 2020.

[160] Andronikos Paliathanasis and Genly Leon. Dynamics of a two scalar field cosmological model with phantom terms. *Class. Quant. Grav.*, 38(7):075013, 2021.

[161] Andrew R. Liddle, Anupam Mazumdar, and Franz E. Schunck. Assisted inflation. *Phys. Rev. D*, 58:061301, 1998.

[162] Lilia Anguelova, Elena Mirela Babalic, and Calin Iuliu Lazaroiu. Two-field Cosmological α-attractors with Noether Symmetry. *JHEP*, 04:148, 2019.

[163] Steven H. Strogatz. *Nonlinear Dynamics and Chaos: With Applications to Physics, Biology, Chemistry and Engineering*. Westview Press, 2000.

[164] Gregory Faye. An introduction to bifurcation theory, oct 2011.

[165] Michele Cicoli, Veronica Guidetti, and Francisco G. Pedro. Geometrical Destabilisation of Ultra-Light Axions in String Inflation. *JCAP*, 05:046, 2019.

[166] Michele Cicoli, Veronica Guidetti, Francisco G. Pedro, and Gian Paolo Vacca. A geometrical instability for ultra-light fields during inflation? *JCAP*, 12:037, 2018.

[167] Ana Achúcarro, Vicente Atal, and Yvette Welling. On the viability of $m^2\phi^2$ and natural inflation. *JCAP*, 07:008, 2015.

[168] Ana Achúcarro and Yvette Welling. Orbital Inflation: inflating along an angular isometry of field space. 7 2019.

[169] Ana Achúcarro, Edmund J. Copeland, Oksana Iarygina, Gonzalo A. Palma, Dong-Gang Wang, and Yvette Welling. Shift-Symmetric Orbital Inflation: single field or multi-field? 1 2019.

[170] Ana Achúcarro, Gonzalo A. Palma, Dong-Gang Wang, and Yvette Welling. Origin of ultra-light fields during inflation and their suppressed non-Gaussianity. *JCAP*, 10:018, 2020.

[171] Perseas Christodoulidis, Diederik Roest, and Evangelos I. Sfakianakis. Attractors, Bifurcations and Curvature in Multi-field Inflation. *JCAP*, 08:006, 2020.

[172] Sébastien Renaux-Petel, Krzysztof Turzyński, and Vincent Vennin. Geometrical destabilization, premature end of inflation and Bayesian model selection. *JCAP*, 11:006, 2017.

[173] Oskar Grocholski, Marcin Kalinowski, Maciej Kolanowski, Sébastien Renaux-Petel, Krzysztof Turzyński, and Vincent Vennin. On backreaction effects in geometrical destabilisation of inflation. *JCAP*, 05:008, 2019.

[174] Andrei Linde, Dong-Gang Wang, Yvette Welling, Yusuke Yamada, and Ana Achúcarro. Hypernatural inflation. *JCAP*, 07:035, 2018.

[175] P.K. Townsend. Positive Energy and the Scalar Potential in Higher Dimensional (Super)gravity Theories. *Phys. Lett. B*, 148:55–59, 1984.

[176] Kostas Skenderis and Paul K. Townsend. Gravitational stability and renormalization group flow. *Phys. Lett. B*, 468:46–51, 1999.

[177] Ana Achúcarro, Sebastián Céspedes, Anne-Christine Davis, and Gonzalo A. Palma. Constraints on Holographic Multifield Inflation and Models Based on the Hamilton-Jacobi Formalism. *Phys. Rev. Lett.*, 122(19):191301, 2019.

[178] Andrei D. Linde. Hybrid inflation. *Phys. Rev. D*, 49:748–754, 1994.

[179] Perseas Christodoulidis, Diederik Roest, and Robert Rosati. Many-field Inflation: Universality or Prior Dependence? *JCAP*, 04:021, 2020.

[180] Soo A. Kim and Andrew R. Liddle. Nflation: Non-Gaussianity in the horizon-crossing approximation. *Phys. Rev. D*, 74:063522, 2006.

[181] David Seery, David J. Mulryne, Jonathan Frazer, and Raquel H. Ribeiro. Inflationary perturbation theory is geometrical optics in phase space. *JCAP*, 09:010, 2012.

[182] David J. Mulryne, David Seery, and Daniel Wesley. Moment transport equations for the primordial curvature perturbation. *JCAP*, 04:030, 2011.

[183] Sonia Paban and Robert Rosati. Inflation in Multi-field Modified DBM Potentials. *JCAP*, 09:042, 2018.

[184] Theodor Bjorkmo and M. C. David Marsh. Manyfield Inflation in Random Potentials. *JCAP*, 02:037, 2018.

[185] Cody Long, Liam McAllister, and John Stout. Systematics of Axion Inflation in Calabi-Yau Hypersurfaces. *JHEP*, 02:014, 2017.

[186] Thomas C. Bachlechner, Kate Eckerle, Oliver Janssen, and Matthew Kleban. Axion Landscape Cosmology. *JCAP*, 09:062, 2019.

[187] Thomas C. Bachlechner, Kate Eckerle, Oliver Janssen, and Matthew Kleban. The Axidental Universe. 2 2019.

[188] Laila Alabidi and David H. Lyth. Inflation models and observation. *JCAP*, 05:016, 2006.

[189] Soo A Kim and Andrew R Liddle. Nflation: multi-field inflationary dynamics and perturbations. *Phys. Rev. D*, 74:023513, 2006.

[190] Layne C. Price, Hiranya V. Peiris, Jonathan Frazer, and Richard Easther. Gravitational wave consistency relations for multifield inflation. *Phys. Rev. Lett.*, 114(3):031301, 2015.

[191] Thomas Hertog. Predicting a Prior for Planck. *JCAP*, 02:043, 2014.

[192] James Hartle and Thomas Hertog. One Bubble to Rule Them All. *Phys. Rev. D*, 95(12):123502, 2017.

[193] Zhong-Kai Guo. Large number limit of multifield inflation. *Phys. Rev. D*, 96(12):123521, 2017.

[194] Richard Easther and Layne C. Price. Initial conditions and sampling for multifield inflation. *JCAP*, 07:027, 2013.

[195] Mafalda Dias, Jonathan Frazer, David J. Mulryne, and David Seery. Numerical evaluation of the bispectrum in multiple field inflation—the transport approach with code. *JCAP*, 12:033, 2016.

[196] David J. Mulryne and John W. Ronayne. PyTransport: A Python package for the calculation of inflationary correlation functions. *J. Open Source Softw.*, 3(23):494, 2018.

[197] John W. Ronayne and David J. Mulryne. Numerically evaluating the bispectrum in curved field-space— with PyTransport 2.0. *JCAP*, 01:023, 2018.

[198] Marios Bounakis, Ian G. Moss, and Gerasimos Rigopoulos. Observational constraints on Hyperinflation. *JCAP*, 02:006, 2021.

[199] Vikas Aragam, Sonia Paban, and Robert Rosati. The Multi-Field, Rapid-Turn Inflationary Solution. *JHEP*, 03:009, 2021.

[200] Lucas Pinol. Multifield inflation beyond $N_{\mathrm{field}} = 2$: non-Gaussianities and single-field effective theory. *JCAP*, 04:002, 2021.

[201] Lilia Anguelova. On Primordial Black Holes from Rapid Turns in Two-field Models. 12 2020.

[202] Michele Cicoli, Giuseppe Dibitetto, and Francisco G. Pedro. Out of the Swampland with Multifield Quintessence? *JHEP*, 10:035, 2020.

[203] Perseas Christodoulidis and Andronikos Paliathanasis. $\mathcal{N}$-field cosmology in hyperbolic field space: stability and general solutions. *Journal of Cosmology and Astroparticle Physics*, 2021(05):038, may 2021.

[204] Misao Sasaki, Teruaki Suyama, Takahiro Tanaka, and Shuichiro Yokoyama. Primordial Black Hole Scenario for the Gravitational-Wave Event GW150914. *Phys. Rev. Lett.*, 117(6):061101, 2016. [Erratum: Phys.Rev.Lett. 121, 059901 (2018)].

[205] Pedro Carrilho, Karim A. Malik, and David J. Mulryne. Dissecting the growth of the power spectrum for primordial black holes. *Phys. Rev. D*, 100(10):103529, 2019.

[206] Michael Tsamparlis and Andronikos Paliathanasis. The generic model of General Relativity. *Arab. J. Math.*, 8(3):201–254, 2019.

[207] Richard L. Arnowitt, Stanley Deser, and Charles W. Misner. The Dynamics of general relativity. *Gen. Rel. Grav.*, 40:1997–2027, 2008.

[208] E.T. Tomboulis. On the 'simple' form of the gravitational action and the self-interacting graviton. *JHEP*, 09:145, 2017.

[209] Christian G. Boehmer and Nyein Chan. Dynamical systems in cosmology. 9 2014.

[210] Sebastian Bahamonde, Christian G. Böhmer, Sante Carloni, Edmund J. Copeland, Wei Fang, and Nicola Tamanini. Dynamical systems applied to cosmology: dark energy and modified gravity. *Phys. Rept.*, 775-777:1–122, 2018.

[211] John Miritzis. Scalar field cosmologies with an arbitrary potential. *Class. Quant. Grav.*, 20:2981–2990, 2003.

[212] Luca Salasnich. Instabilities, point attractors and limit cycles in an inflationary universe. *Mod. Phys. Lett. A*, 10:3119–3128, 1995.

[213] A. de la Macorra and G. Piccinelli. General scalar fields as quintessence. *Phys. Rev. D*, 61:123503, 2000.

[214] Grant N. Remmen and Sean M. Carroll. Attractor Solutions in Scalar-Field Cosmology. *Phys. Rev. D*, 88:083518, 2013.

[215] A. M. LYAPUNOV. The general problem of the stability of motion. *International Journal of Control*, 55(3):531–534, 1992.

[216] Valerio Faraoni and Charles S. Protheroe. Scalar field cosmology in phase space. *Gen. Rel. Grav.*, 45:103–123, 2013.

[217] J. LaSalle. Some extensions of liapunov's second method. *IRE Transactions on Circuit Theory*, 7(4):520–527, 1960.

[218] Yury S. Barkovsky. Lectures on the routh-hurwitz problem, 2008.

List of Publications

The results presented in this thesis are based on the following collaborative works:

- P. Christodoulidis, D. Roest and E. I. Sfakianakis, "Angular inflation in multi-field α-attractors," JCAP **11** (2019), 002.

- P. Christodoulidis, D. Roest and E. I. Sfakianakis, "Scaling attractors in multi-field inflation," JCAP **12** (2019), 059.

- P. Christodoulidis, D. Roest and R. Rosati, "Many-field Inflation: Universality or Prior Dependence?," JCAP **04** (2020), 021.

- P. Christodoulidis, D. Roest and E. I. Sfakianakis, "Attractors, Bifurcations and Curvature in Multi-field Inflation," JCAP **08** (2020), 006.

I have also published the following works which are not included as chapters in this thesis:

- P. Christodoulidis and A. Paliathanasis, "$\mathcal{N}$-field cosmology in hyperbolic field space: stability and general solutions," JCAP **05** (2021), 038.

- P. Christodoulidis, "General solutions to $\mathcal{N}$-field cosmology with exponential potentials," Eur. Phys. J. C 81, 471 (2021).

Samenvatting

Multi-veld modellen met een niet-triviale veldmetrische parametrisering zijn de afgelopen jaren onder de loep genomen. Ze introduceren verschillende nieuwe eigenschappen, zoals een niet-triviale dynamiek, de verbetering van het vermogensspectrum door snelle omslagen, terwijl deze modellen tegelijkertijd fenomenologisch levensvatbaar zijn. Dit proefschrift was een stap in de richting naar een beter begrip van multi-veld dynamica en het onderzoek van voorspellingen in het vele-veldenlimiet.

In de hoofdstukken 2 en 3 hebben we de basiselementen van de moderne kosmologie en de inflatoire theorie geïntroduceerd. We bespraken het observationele bewijs voor kosmische isotropie dat het FLRW-universum en het hete oerknal-scenario ondersteunt. Ons huidige beste begrip van het waarneembare universum op grote schaal omvat een isotroop en homogeen universum dat bestaat uit stof, straling en een kosmologische constante. Hoewel dit model met grote nauwkeurigheid aan de waarnemingen voldoet, zijn er verschillende filosofisch onderbouwde bezwaren naar voren gebracht, deze hebben geleid tot uitbreidingen van het standaardbeeld en de introductie van inflatie. Een van de belangrijkste fenomenologische successen van inflatie is het bestaan van een mechanisme dat verantwoordelijk is voor structuurvorming, door middel van het exponentieel uitrekken van primordiale kwantumfluctuaties in een FLRW-achtergrond.

Later in Hoofdstuk 4 hebben we de multi-veld dynamica diepgaand bestudeerd. In navolging van de literatuur zijn we begonnen met de adiabatische / entropische splitsing van de achtergronddynamica en hebben we voldoende voorwaarden berekend voor het bestaan van slow-roll-oplossingen ($\epsilon, \eta \ll 1$). Vervolgens bespraken we de evolutie van kromming en isocurvatuurverstoringen in het eerdergenoemde limiet, met het argument dat de superhorizon-evolutie op dezelfde manier kan worden berekend voor alle slow-roll-modellen. Specifiek voor modellen die de gradiëntstroom volgen, kan men aantonen dat de amplitude van kwantumfluctuaties bij horizonovergang dezelfde is als in enkelveldsmodellen en daarom kunnen de vermogensspectra aan het einde van inflatie analytisch worden berekend. We gebruikten het standaard vele-veldenmodel met kwadratische poten-

tiaal als een voorbeeld waarvan de observabelen analytisch kunnen worden berekend, hiermee wordt de afhankelijkheid van de beginvoorwaarden aangetoond.

Nadat we de basistheorie hadden opgesteld, presenteerden we in Hoofdstuk 5 een twee-velds generalisatie van α-attractoren met één veld. Het model bestaat uit twee kwadratische velden en de hyperbolische veldruimte in Poincarécoördinaten. We hebben het bestaan aangetoond van een nieuwe attractoroplossing die volgt na de gradiëntstroomfase voor een bepaald gebied van de parameterruimte. In het bijzonder is het aantal e-vemenigvuldigingen dat tijdens deze fase wordt doorgebracht evenredig met de kromming van de hyperbolische ruimte en de massaverhouding tussen de velden. Als fluctuaties de horizon kruisen tijdens de 'radiale' fase' worden voorspellingen gewijzigd door simpelweg rekening te houden met de tijd die aan de nieuwe (hoek)fase wordt besteed.

In Hoofdstuk 6 presenteerden we een classificatie van verschillende schaaloplossingen met twee velden met niet-triviale veldruimte-parametrisering. We hebben uitgelegd waarom het natuurlijk is om te zoeken naar oplossingen van het "bevroren" type, d.w.z. die met één niet-dynamisch veld, naast het inflaton-veld. Vervolgens hebben we een gedetailleerde stabiliteitsanalyse uitgevoerd en de stabiliteitscriteria in het algemene geval afgeleid en verschillende voorbeelden gevolgd om de omstandigheden te verduidelijken voor stabiele oplossingen. We voerden aan dat schaaloplossingen relevant zijn bij het bouwen van inflatoire modellen omdat ze verschillende voorstellen in de literatuur benaderen die een niet-triviale dynamiek vertonen. Bovendien hebben we uitgelegd dat het bestuderen van achtergrondsstabiliteit met de adiabatische / entropische vergelijkingen voor verstoringen niet altijd tot de juiste conclusies leidt, maar alleen als er een coördinatensysteem bestaat waarin het orthogonale veld kanoniek genormaliseerd is.

In hoofdstuk 7 hebben we een coördinatenconstructie voorgesteld die een intuïtieve manier biedt om de lange-tijd attractoroplossingen te begrijpen. Vanuit dit perspectief worden orthogonale velden gestabiliseerd op de minima van een effectieve potentiaal die rekening houdt met bijdragen van de veldmetriek. Door berekeningen in het specifieke coördinatensysteem uit te voeren en een aantal redelijke aannames te gebruiken, konden we een coördinaat-onafhankelijke oplossing afleiden, die, zoals we hebben laten zien, alle nieuwe oplossingen beschrijft die de gradiëntstroom niet volgen. Aan de hand van de resultaten uit het vorige hoofdstuk leiden we de stabiliteitscriteria af met de nadruk op vertakkingen. We gebruikten verschillende voorbeelden uit de literatuur om het uniforme perspectief van

onze aanpak te demonstreren en in het bijzonder ontdekten we dat het hyperinflatiemodel tot de zijspoorfamilie behoort.

Ten slotte onderzochten we in Hoofdstuk 8 voorspellingen op de vele-veldenlimiet. We hebben de horizonovergang-benadering gebruikt om analytische formules af te leiden en de afhankelijkheid van de beginvoorwaarden te onderzoeken. Uitgaande van een willekeurige beginconfiguratie op een gereduceerd $\mathcal{N} - 1$-hyperoppervlak, hebben we de convergentie van observabelen aangetoond, die voortkomen uit de centrale limietstelling. We ontdekten echter ook dat verschillende initiële hyperoppervlaktes resulteren in verschillende centrale grenswaarden voor de waarneembare waarden. We concluderen daarom dat, in tegenstelling tot verscheidene claims in de literatuur, inflatie op vele velden inherent niet-voorspellend blijft.

Acknowledgments

First and foremost, I would like to thank my supervisor *Diederik Roest* for providing me guidance and for developing me as a researcher. His great intuition in physics, his ability to spot interesting research topics and his optimistic approach against challenges were particularly inspiring.

Next to my supervisor, I would like to thank *Evangelos Sfakianakis* for his invaluable support and mentoring, and for everything I have learnt from him through our endless discussions. I am also indebted to my collaborators *Robert Rosati* and *Andronikos Paliathanasis* for their contribution at every stage of our research projects. Moreover, I would like to thank *David Murlyne* for enlightening discussions on numerics.

I would like to offer my special thanks to the members of the reading committee, *Ana Achúcarro, Anupam Mazumdar* and *David Wands*, for reporting several typos in the preliminary version of this thesis and suggesting useful corrections. I would also like to thank my friends *Agis, Vasilis, Nikos* and *Sara* for reading this manuscript and commenting on its clarity. Further, I would like to thank *Gideon* and *Ruud* for providing me the Dutch summary. Many thanks to the secretaries of the Van Swinderen Institute, *Annelien* and *Iris*, for dealing with all my requests during my Ph.D. years.

Life in Groningen would not have been easy without the right people keeping me company. It was a pleasure to be around *Alba, Johannes, Ceyda*, and, in particular, *Thomais*, who kept me sane during the harsh pandemic period. Last but not least, I would like to thank my parents, *Leonidas* and *Chrysanthi*, and my sister *Andria* for their emotional support during my graduate studies.